PERFORMANCE AND CHECK-OUT VERIFICATION TESTING OF A NEW TRUE TRIAXIAL APPARATUS USING PARTIALLY SATURATED SILTY SAND

by

JAE HYUN PARK

Presented to the Faculty of the Graduate School of

The University of Texas at Arlington in Partial Fulfillment

of the Requirements

for the Degree of

MASTER OF SCIENCE IN CIVIL ENGINEERING

THE UNIVERSITY OF TEXAS AT ARLINGTON

AUGUST 2005

ACKNOWLEDGEMENTS

The author would like to thank his supervising professor, Dr. Laureano R. Hoyos, for his guidance and support throughout the course of this research effort.

Thanks are also extended to the other members of his thesis committee, Drs. Anand J. Puppala and Mohamed S. Hossain, for their valuable advice and review of this manuscript. In addition, the author would like to thank the faculty and staff of the Department of Civil and Environmental Engineering at The University of Texas at Arlington for their valuable assistance during his academic studies.

The author also would like to thank all Geotechnical Engineering graduate students in this institution for their help and support. Special thanks are extended to Arthit Laikram, and Napat Intharasombat.

Finally, and most of all, the author would like to thank his family for their love, encouragement, and great support. It is the best thing in his life to be a part of this family.

July 20, 2005

ABSTRACT

PERFORMANCE AND CHECK-OUT VERIFICATION TESTING
OF A NEW TRUE TRIAXIAL APPARATUS USING
PARTIALLY SATURATED SILTY SAND

Publication No._____

Jae Hyun Park, M.S.

The University of Texas at Arlington, 2005

Supervising Professor: Laureano R. Hoyos

A stress-controlled, flexible boundary, true triaxial (cubical) testing apparatus has been developed to test 3-inch cubical specimen of partially saturated soil under different moisture contents and for a wide range of multiaxial stress paths. A series of HC, CTC, TC, TE, and SS tests were conducted in order to perform a thorough performance and check-out verification testing of the newly developed device by investigating the multiaxial stress-strain response of partially saturated silty sand specimens artificially prepared in the laboratory. The development of the apparatus, specimen preparation process, test procedure, and the corresponding validation of its suitability for testing partially saturated sandy soils are described. In this work, specimens were prepared using a dual-mesh pluviation technique at four different

moisture contents: w = 2.0, 4.5, 5.3, and 6.1%. In all cases, initial total soil suction was induced and found to exert a paramount influence on the stress-strain-strength behavior of partially saturated silty sand.

TABLE OF CONTENTS

ACKNOWLEDGEMENTS ii

ABSTRACT iii

LIST OF ILLUSTRATIONS viii

LIST OF TABLES xiii

Chapter

1. INTRODUCTION 1

1.1 Background and Importance 1

1.2 Objective and Scope 3

1.3 Organization 5

2. LITERATURE REVIEW 6

2.1 Introduction 6

2.2 Soil Suction 8

2.2.1 Extended M-C Criterion 8

2.2.2 Forces between Two Spherical Particles 10

2.2.3 Measurement of Total Suction (Filter Paper Method) 12

2.3 Previous True Triaxial Testing 14

3. FUNDAMENTALS OF TRUE TRIAXIAL TESTING AND APPARATUS DESCRIPTION 37

3.1 Introduction 37

3.2 True Triaxial Testing 38

3.2.1 Introduction 38
3.2.2 Stress Paths 40
3.3 Apparatus Description 46
3.4 Step-By-Step Assembling Process 57
4. TESTING SOIL AND EXPERIMENTAL VARIABLES 61
4.1 Introduction 61
4.2 Testing Soil 61
4.3 Pluviation Induced Densities and Moisture Contents 63
4.4 Repeatability of Specimen Preparation 63
4.5 Experimental Variables 64
4.6 Specimen Preparation Method and Placement 66
4.7 Pluviation Frame Design 67
5. ANALYSIS OF TEST RESULTS 71
5.1 Introduction 71
5.2 Specimen Notation 71
5.3 Hydrostatic Compression (HC) Test 71
5.4 Repeatability of HC Tests 74
5.5 Influence of Octahedral Stress (σ_{oct}) 76
5.5.1 Conventional Triaxial Compression (CTC) Tests 76
5.5.2 Triaxial Compression (TC) Tests 81
5.5.3 Triaxial Extension (TE) Tests 85
5.5.4 Simple Shear 90

5.6 Influence of Initial Total Suction 95

5.7 Incipient Failure Envelopes on Octahedral Plane 102

6. SUMMARY, CONCLUSIONS, AND RECOMMENDATIONS 104

6.1 Summary and Conclusions 104

6.2 Future Research Recommendation 106

REFERENCES 107

BIOGRAPHICAL INFORMATION 110

LIST OF ILLUSTRATIONS

Figure Page

1.1 Unsaturated Subgrade/Foundation Soils 3

2.1 Arid and Semi Arid Regions of the World 6

2.2 Generalized World of Soil Mechanics 7

2.3 Stress States in Saturated Soil and Unsaturated Soils 7

2.4 Extended Mohr-Coulomb Failure Surface for Unsaturated Soil 9

2.5 Air-water-solid Interaction for Two Spherical Particles and Water Meniscus 11

2.6 Calibration Curves for Whatman #42 and Schleicher and Schuell#589 filter papers 13

2.7 Photographs of Filter Paper Testing Technique 14

2.8 Deformation Measuring System 15

2.9 Stress Paths Studied 17

2.10 Hydrostatic Compression Test Results 19

2.11 Conventional Triaxial Compression Test Results 20

2.12 b = 0 Test Results 21

2.13 b = 0.25 Test Results 22

2.14 b = 0.5 Test Results 23

2.15 b = 0.75 Test Results 24

2.16 b = 1 Test Results 25

2.17 View of the Cubical Triaxial Tester 26

2.18 Load Response of Potato Starch under HTC test 27

2.19 Photograph of Cubical Base Piece 28

2.20 Hydrostatic Compression Test Results 29

2.21 Conventional Triaxial Compression Test Results 30

2.22 A Typical Multi-Stage Drained True Triaxial Tests 31

2.23 Triaxial Compression Test Results 32

2.24 Simple Shear Test Results 33

2.25 Triaxial Extension Results 34

2.26 Projection of Potential Failure Envelopes onto the Octahedral Stress Plane 35

3.1 (a) Axisymmetric ($\sigma_2 = \sigma_3$) and Hydrostatic ($\sigma_1 = \sigma_2 = \sigma_3$) Stress States; (b) True Triaxial ($\sigma_1 \neq \sigma_2 \neq \sigma_3$) Stress States 38

3.2 Representation of Stress Conditions in the Octahedral Plane 39

3.3 Hydrostatic Stress Path 41

3.4 Conventional Triaxial Compression 42

3.5 Triaxial Compression 43

3.6 Triaxial Extension 44

3.7 (a) Principal Stress Space; (b) Projection of Stress Paths on Triaxial Plane 45

3.8 Representation of Shear Stress Paths on Octahedral Planes 46

3.9 Close Photograph of Frame 47

3.10 Photograph of Frame and Mounting Support 47

3.11 Cross-Sectional View of Complete Wall Assemblies 48

3.12 Wall Assembly 49

3.13 Photograph of the Wall Assembly 50

3.14 Deformation Measuring System 51

3.15 Photograph of Calibrating 52

3.16 Example of Calibration Curve (X1(+) Face) 52

3.17 Pressure Application Process 53

3.18 Schematic of Stress Application and Control System 54

3.19 Photograph of Vacuum Chamber and Bottom Mold 55

3.20 Schematic of Data Acquisition System 56

3.21 Photograph of Bottom Wall Assembling Process 57

3.22 Photograph of Specimen Placement 58

3.23 Photograph of Lateral Wall Assembling Process 58

3.24 Photograph of Top Wall Assembling Process 59

3.25 Photograph of Pressure inlet/outlet, LVDTs, and Air Valve 59

3.26 Photograph of Complete Laboratory Setup 60

4.1 Particle Size Distribution of Artificially Prepared Silty Sand 62

4.2 Soil Water Characteristic Curve (SWCC) of Silty Sand 64

4.3 Schematic and Photograph of Specimen Preparation Mold 66

4.4 (a) Photograph of Pluviation Frame; (b) Photograph of Water Spraying 68

4.5 Schematic of Pluviation Frame Design 70

5.1 Hydrostatic Compression Test Results (p = 0 - 20 psi) 73

5.2 Hydrostatic Compression Test for repeatability (p = 0 - 20 psi) 74

5.3 Bulk Modulus as Function of Total Suction 75

5.4 CTC Results for Air-Dried Silty Sand (Ψ = 800 psi, w = 2.0%) 77

5.5 CTC Results of 85% Dry for Optimum Silty Sand
(Ψ = 365 psi, w = 4.5%) 78

5.6 CTC Results for Optimum Silty Sand (Ψ = 237 psi, w = 5.3%) 79

5.7 CTC Results of 85% Wet for Optimum Silty Sand
(Ψ = 150 psi, w = 6.1%) 80

5.8 TC Results for Air-Dried Silty Sand (Ψ = 800 psi, w = 2.0%) 81

5.9 TC Results for 85% Dry of Optimum Silty Sand
(Ψ = 365 psi, w = 4.5%) 82

5.10 TC Results for Optimum Silty Sand (Ψ = 237 psi, w =5.3 %) 83

5.11 TC Test Results of 85% Wet for Optimum Silty Sand
(Ψ = 150 psi, w = 6.1%) 84

5.12 TE Test Results for Air-Dried Silty Sand (Ψ = 800 psi, w = 2.0%) 86

5.13 TE Test Results for 85% Dry of Optimum Silty Sand
(Ψ = 365 psi, w = 4.5%) 87

5.14 TE Test Results for Optimum Silty Sand (Ψ = 237 psi, w = 5.3%) 88

5.15 TE Test Results for 85% Wet of Optimum Silty Sand
(Ψ = 150 psi, w = 6.1%) 89

5.16 SS Test Results for Air-Dried Silty Sand (Ψ = 800 psi, w = 2.0%) 91

5.17 SS Test Results for 85% Dry of Optimum Silty Sand
(Ψ = 365 psi, w = 4.5%) 92

5.18 SS Test Results for Optimum Silty Sand (Ψ = 237 psi, w = 5.3%) 93

5.19 SS Test Results for 85% Wet of Optimum Silty Sand
(Ψ = 150 psi, w = 6.1%) 94

5.20 CTC Test Results with Different Suction (σ_{oct} = 5 psi) 95

5.21 CTC Test Results with Different Suction (σ_{oct} = 10 psi, 20 psi) 96

5.22 TC Test Results with Different Suction (σ_{oct} = 20 psi)..... 97

5.23 TC Test Results with Different Suction (σ_{oct} = 30 psi, 40 psi)..... 98

5.24 TE Test Results with Different Suction (σ_{oct} = 20 psi, 30 psi) 99

5.25 TE Test Results with Different Suction (σ_{oct} = 40 psi)..... 100

5.26 SS Test Results with Different Suction (σ_{oct} = 20 psi) 100

5.27 SS Test Results with Different Suction (σ_{oct} = 30 psi, 40 psi)..... 101

5.28 Projection of Incipient Failure Envelopes
onto the Octahedral Stress Plane..... 102

LIST OF TABLES

Table Page

3.1 Value of the Slope of Calibration Curve..... 53

4.1 Basic Engineering Properties of Testing Soil 62

4.2 Initial Pluviation-Induced Soil Conditions 63

4.3 Proof of Repeatability of Specimen Preparation Process 64

4.4 Experimental Variables Used for True Triaxial Testing..... 65

4.5 Results of Density Tests of Clean Sand..... 69

5.1 Notation Symbols Used for True Triaxial Test..... 72

CHAPTER 1

INTRODUCTION

1.1 Background and Importance

In the last four decades, it has been emphasized that the intermediate principal stress plays an important role in the stress-strain behavior of soils (Ibsen and Praastrup, 2002). Moreover, most natural/compacted soils have a tendency to behave as cross-anisotropic rather than isotropic materials. This cross-anisotropic behavior of natural and compacted soils highlights the need for testing specimens under true triaxial conditions. In addition, soils in nature are often subjected to three different principal stresses (i.e., major principal stress, intermediate principal stress, and minor principal stress) inducing, correspondingly, three different principal strains (i.e., major principal strain, intermediate principal strain, and minor principal strain). In particular, true triaxial testing is critical when it comes to deriving and/or validating general constitutive models postulated for the mechanical behavior of soils along a wide range of stress paths.

The conventional (cylindrical) triaxial apparatus is a well known laboratory equipment for testing shearing resistance and deformation characteristics of soils. The effect of the intermediate stress, however, cannot be examined in the conventional triaxial apparatus since the intermediate principal stress has to be equal to at least one of the other principal stresses in the apparatus. Thus, only axisymmetric stress states ($\sigma_2 =$

σ_3) are achievable in the conventional triaxial apparatus, while true triaxial stress states ($\sigma_1 \neq \sigma_2 \neq \sigma_3$) are unachievable. The true triaxial apparatus is capable of producing independent variations of the three principal stresses and strains. Hence, testing for effects of the intermediate principal stress and cross-anisotropic behavior is possible with this equipment.

Failure mechanisms and engineering behavior of soil, rock, and cemented materials have been investigated by a considerable number of researchers using cylindrical and true triaxial testing techniques. These researchers, including Kjellman (1936), Ko and Scott (1967), Atkinson (1972), Lade and Duncan (1973), Sture (1979), Suture and Desai (1979), Arthur (1988), Reddy et al. (1992), and Callisto and Calabresi (1998), have conducted studies on the use of true triaxial devices for characterization of soil, rock, and cemented materials. These studies have outlined the benefits of the true triaxial (cubical) apparatus over the cylindrical triaxial cell for testing stress-strain-strength behavior of soils, and have contributed to the mechanical characterization of dry and saturated soils for multiaxial stress states under drained or undrained conditions. Among these research efforts, however, very few have dealt directly with the behavior of partially saturated soils with full consideration of the effect of initial total suction (negative pore-water pressure) prior to testing.

Total suction has been found to play a paramount role in partially saturated soil response under one-dimensional, isotropic, and axisymmetric loading conditions. Likewise, total suction is expected to play a critical role in the response of a partially saturated soil subjected to mutiaxial stress states, as shown in figure 1. A lack of

understating of this role among engineering graduates and practitioners has resulted in overly designed geotechnical and earth structures and increased project costs. The present instrument development and check-out verification testing program are largely motivated by the lack of experimental evidence and understanding of partially saturated soil response along mutiaxial stress states under high pluviation-induced initial suction conditions.

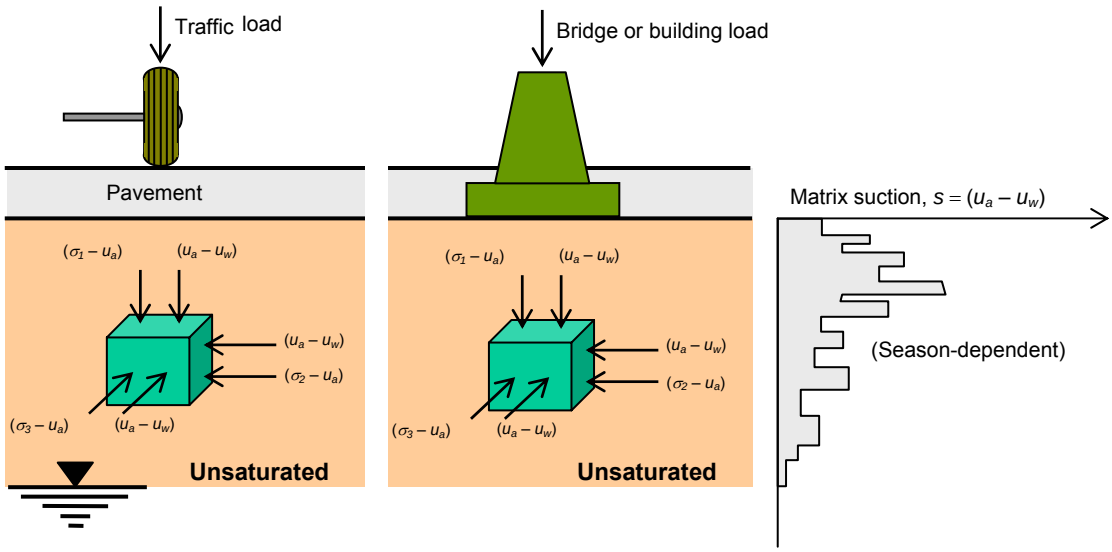

Figure 1.1 Unsaturated Subgrade/Foundation Soils

1.2 Objective and Scope

The main objective of the present thesis work is to perform a series of calibration and check-out verification tests on a newly developed true triaxial device which will be later utilized for suction-controlled true triaxial testing of unsaturated soils.

To accomplish this goal, a series of true triaxial tests was conducted on identically prepared specimens of pluviated silty sand at four different moisture

contents (w = 2.0, 4.5, 5.3, and 6.1 %) along a wide range of stress paths. Five types of stress paths were followed: hydrostatic compression (HC), conventional triaxial compression (CTC), triaxial compression (TC), triaxial extension (TE), and simple shear (SS). In the case of HC and CTC tests, initial confining pressures of 5, 10, and 20 psi were used. In the case of TC, TE, and SS tests, initial confining pressures of 20, 30, and 40 psi were used.

The soil-water characteristic curve (SWCC) of tested soil was first obtained via filter paper technique in order to assess initial values of total soil suction prior to testing at each moisture content. All 3-inch per side specimens were pluviated in five layers into a custom-made cubical preparation mold using a dual-mesh pluviation frame (Cresswell et al., 1999). The soil was artificially prepared by mixing 30% of silt (from north Arlington, Texas) and 70% of clean sand (commercially supplied from a local source). Water was evenly sprayed on each layer to achieve target moisture content. A series of repeated specimen preparation trials was conducted to ensure reproducibility of specimens prior to testing in the cubical cell. The range of low moisture contents selected in this study was intended to reproduce loose specimens with moisture contents lower than the residual gravimetric moisture content devised from the SWCC (w_r = 8%). This corresponds to soil suction values greater than the residual total suction (Ψ_r = 410 kPa).

Findings from this research effort will prove useful in certifying the correct functioning of the newly developed cubical setup using partially saturated silty sand.

Test results will also be of great value in assessing the influence of initial total suction on soil response under multiaxial stress states.

1.3 Organization

A brief summary of the content of each chapter included in this thesis document is presented in the following paragraphs.

Chapter 2 presents a brief review of soil suction concepts and recent studies reported in the literature using true triaxial testing technique, including investigation of stress-strain behavior of soils under suction controlled conditions.

Chapter 3 is devoted to describing the fundamentals of true triaxial testing techniques, main components of the newly developed apparatus, calibration of linear variable displacement transducers (LVDT), and the step-by-step assembly process.

Chapter 4 presents the basic engineering properties of the testing soil, along with a detailed description of all experimental variables, soil specimen preparation method, and design of the dual-mesh pluviation frame.

Chapter 5 presents a comprehensive analysis of results from HC, CTC, TC, TE, and SS tests, including effects of initial total suction on stress-strain behavior of pluviated silty sand and the size of incipient failure envelopes in octahedral plane (π-plane).

Chapter 6 includes the summary and conclusions of this work, as well as some key recommendations for future works.

CHAPTER 2

LITERATURE REVIEW

2.1 Introduction

The 10-40 window of the globe, which is enclosed in $+10^{o}$ and $+40^{o}$ latitude north, contains 3.1 billion people, or 60% of the world population. In this region, much of the earth is defined either arid or semi-arid, as depicted in figure 2.1. As the saturated soil mechanics and partially saturated soil mechanics compose the geotechnical world, they form a continuous profile within the 10-40 window. Due to this profile, the need for investigating the behavior of the partially saturated as well as the saturated soil increased. Accordingly, the behavior of partially saturated soil along with saturated soil has been investigated by a considerable number of researchers using a variety of laboratory and field-techniques.

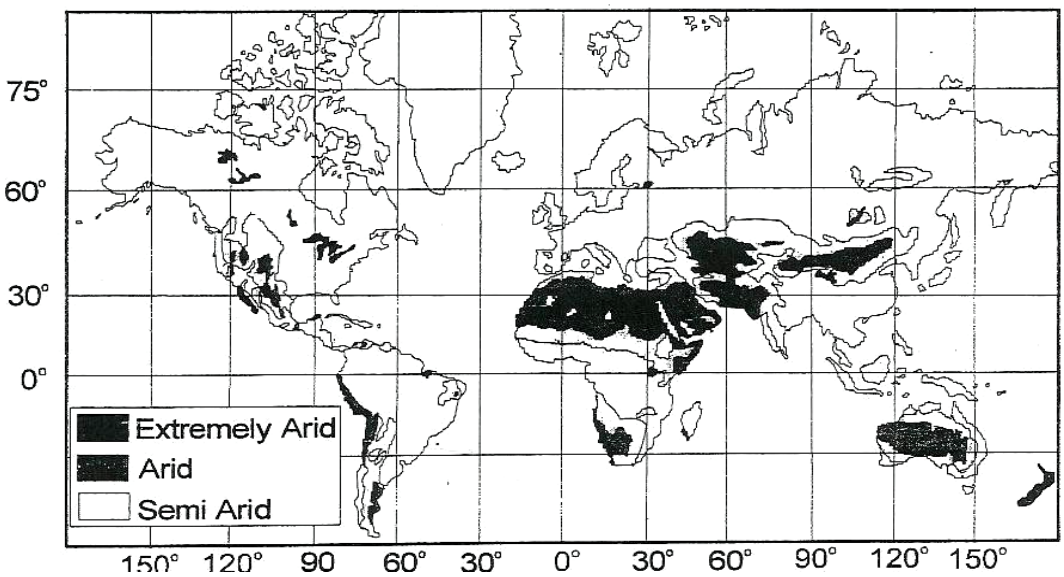

Figure 2.1 Arid and Semi Arid Regions of the World (Fredlund and Rahardjo, 1993)

Therefore, geotechnical world can be categorized into two: saturated soil mechanics and partially saturated soil mechanics. Figure 2.2 is a schematic representation of the geotechnical world visualized with the two soil mechanics.

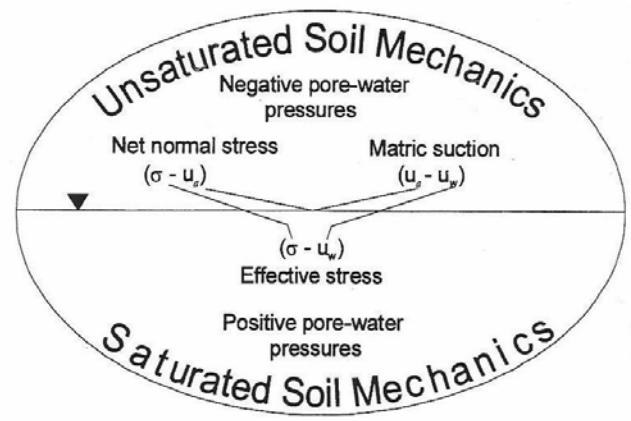

Figure 2.2 Generalized World of Soil Mechanics (Fredlund and Rahardjo, 1993)

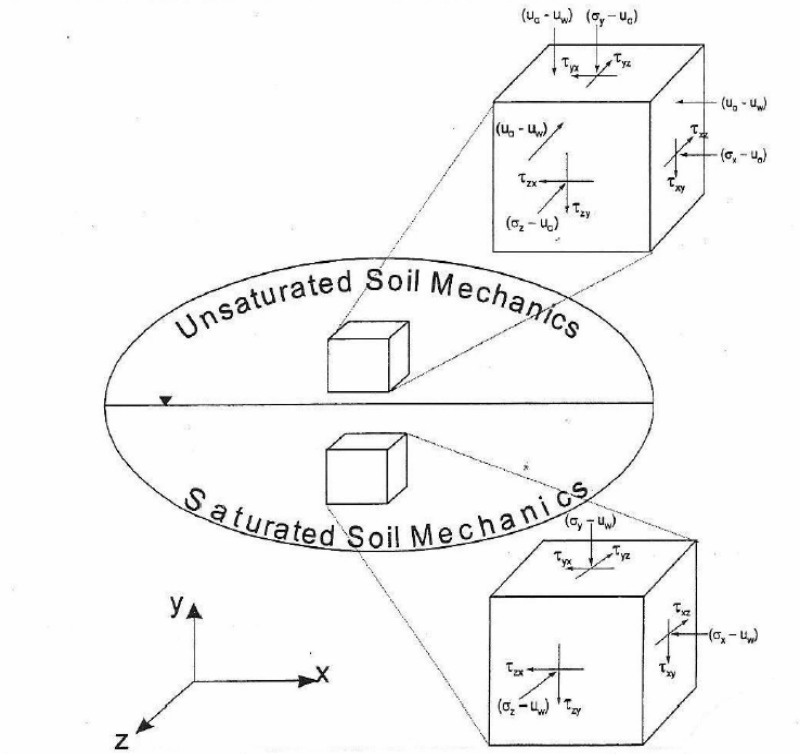

Figure 2.3 Stress States in Saturated Soil and Unsaturated Soils (Fredlund and Rahardjo, 1993)

The separation of soil mechanics in figure 2.2 is based on the pore-water pressure. Two independent stress state variables (net normal stress and matric suction) are required to describe the behavior of the soil above the water table. Net normal stress (σ-u_a) is defined as the difference between the total stress and the pore-air pressure, and matric suction (u_a-u_w) is defined as the difference between the pore-air and pore-water pressures, as shown in figure 2.3. The literatures presented in this chapter describe the stress-strain behavior of soils and particles in true triaxial devices with the view of saturated soil mechanics and/or the view of partially saturated soil mechanics. This review also focuses on the basic concept of soil suction.

2.2 Soil Suction

2.2.1 Extended M-C Criterion

In order to describe the shear strength behavior of unsaturated soil, Fredlund et al. (1978) formulated an extended M-C criterion. In the space of the stress variables: $\sigma - u_a$, $u_a - u_w$, and shear stress τ, the failure envelope is a planar surface and may be calculated as

$$\tau_f = c' + (\sigma - u_a)_f \tan\phi' + (u_a - u_w)_f \tan\phi^b \qquad (2.1)$$

Where; c' = the cohesion at zero matric suction and zero net normal stress

$(\sigma - u_a)_f$ = the net normal stress on the failure plane at failure

ϕ' = the angle of internal friction associated with net normal stress variable

$(u_a - u_w)_f$ = matric suction at failure

ϕ^b = an internal friction angle associated with matric suction that describes the rate of

increase in shear strength relative to matric suction

The first two terms on the right-hand side e.q. (2.1) present the conventional M-C criterion for the strength of saturated soil. The third term is representing the increase in shear strength along with increasing matric suction in unsaturated soil. The extended M-C criterion is illustrated in three-dimensional space as shown in figure 2.4.

In describing a projection of the failure surface to the shear stress versus net normal stress plane, the extended M-C criterion can be written as

$$\tau_f = c'_1 + (\sigma - u_a)_f \tan\phi' \qquad (2.2)$$

Where;

$$c'_1 = \tau_f|_{(\sigma - u_a)=0} = c' + (u_a - u_w)_f \tan\phi^b \qquad (2.3)$$

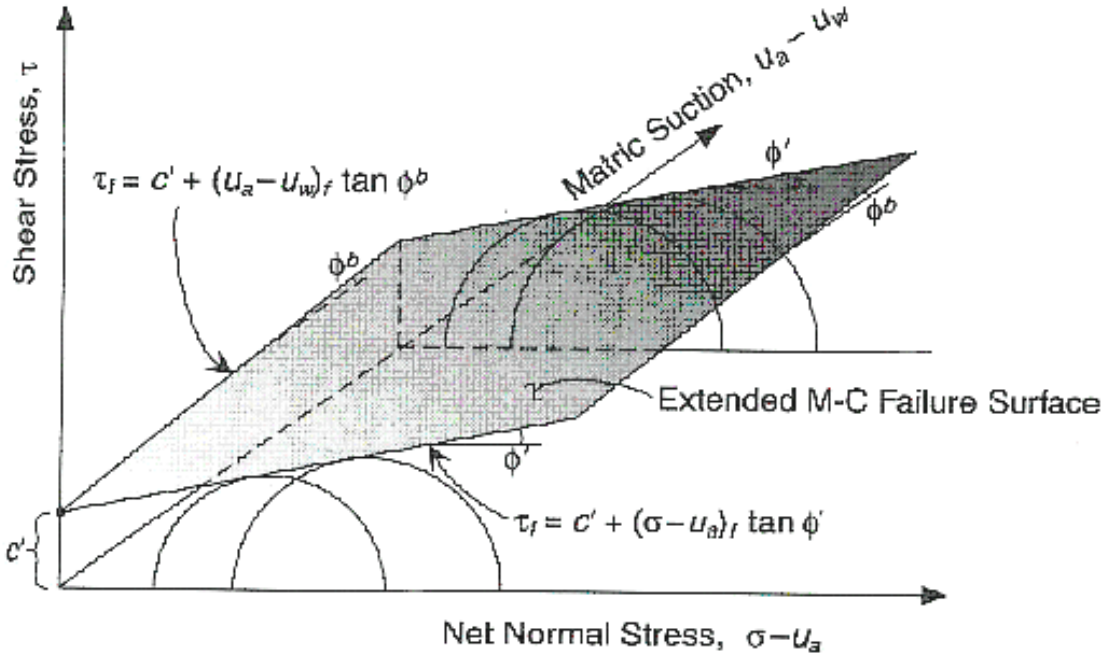

Figure 2.4 Extended Mohr-Coulomb Failure Surface for Unsaturated Soil (Fredlund and Rahardjo, 1993)

In the same way, in describing a projection of the failure surface to the shear stress versus matric suction plane, the extended M-C criterion can be expressed in the following manner

$$\tau_f = c'_2 + (u_a - u_w)_f \tan\phi^b \quad (2.4)$$

Where;

$$c'_2 = \tau_f|_{(u_a - u_w)=0} = c' + (\sigma - u_a)_f \tan\phi' \quad (2.5)$$

2.2.2 Forces between Two Spherical Particles

Lu and Likos (2004) suggested that suction stress refers to the net interparticle force generated within a matrix of unsaturated granular particles (e.g., silt or sand) due to the combined effects of negative pore water pressure and surface tension, and the macroscopic consequence of suction stress is a force that tends to pull the soil grains toward one another, similar in effect and sign convention to an overburden stress or surcharge loading. According to them, consideration of the microscale forces acting between and among idealized assemblies of spherical unsaturated soil particles is one of approaches to evaluating the magnitude of suction stress. Besides, interparticle forces arise from the presence of the air-water-solid interface defining the pore water menisci between the particles at low degrees of pore water saturation. Two particles system is shown in figure 2.5. Figure 2.5 shows that the water meniscus formed between particles may be described by two radii r_1 and r_2, the particle radius R, and a filling angle Θ . A free-body diagram for the relevant system forces, which involves contribution from air pressure u_a, pore water u_w, surface tension T_s, and applied external force of overburden F_e, is shown in figure 2.5 (Lu and Likos, 2004).

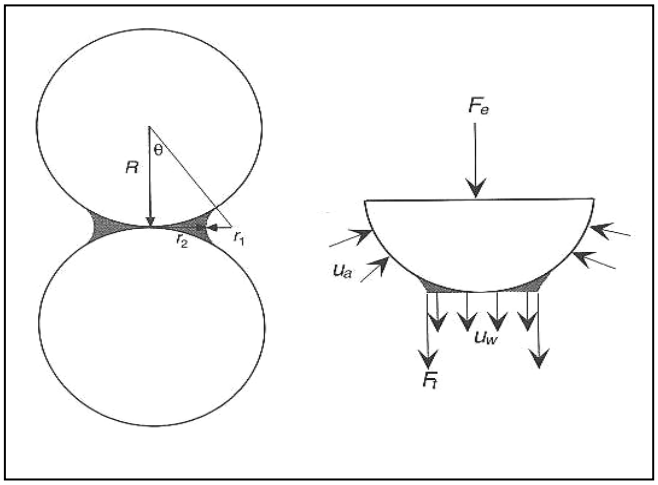

Figure 2.5 Air-water-solid Interaction for Two Spherical Particles and Water Meniscus (Lu and Likos, 2004)

A free-body diagram for the relevant system forces, which involves contribution from air pressure u_a, pore water u_w, surface tension T_s, and applied external force of overburden F_e, is shown in figure 2.5 (Lu and Likos, 2004).

A compressive force on the soil skeleton will be exerted by positive and isotropic air pressure u_a. The total force due to air pressure (F_a) is expressed as

$$F_a = u_a(\pi R^2 - \pi r_2^2) \tag{2.6}$$

F_a is equal to the product of the magnitude of the air pressure and the area of the air-solid interface over which it acts.

The total force due to surface tension (F_t) is given by

$$F_t = -T_S 2\pi r_2 \tag{2.7}$$

F_t acts along the perimeter of the water meniscus.

The projection of total force due to water pressure (F_w) is given in the following manner

$$F_W = u_W \pi r_2^2 \tag{2.8}$$

F_w acts on the water-solid interface in the vertical direction.

The sum of all three of the above forces (F_{sum}) is expressed as

$$F_{sum} = u_a \pi R^2 - u_a \pi r_2^2 - T_S 2 \pi r_2 + u_W \pi r_2^2 \tag{2.9}$$

F_{sum} is the resultant capillary force.

The net interparticle force due to the interfacial interaction (F_e) is given by

$$F_a = u_a \pi R^2 - (u_a - u_w) \pi r_2^2 - T_S 2 \pi r_2 \tag{2.10}$$

The above eq. (2.10) is based on the assumption that the air pressure is the only contribution to external force. F_e exerts a tensile stress on the soil skeleton as long as the following condition met

$$(u_a - u_w) r_2^2 + T_S 2 r_2 > u_a R^2 \tag{2.11}$$

2.2.3 Measurement of Total Suction (Filter Paper Method)

In the present thesis work, Schleicher and Schuell #589 White Hand filter papers were used to measure total suction (ASTM D5298, ASTM 2000). The sized paper is circular with a 5.5-cm diameter and weight of 0.22 g. A detailed procedure for measuring total suction using filter paper is as follows: (1) initially, filter papers were oven-dried to consistency in mass at 105^{o}C and then allowed to cool to room temperature in a desiccator; (2) a soil sample was placed in the jar; (3) a thin, light, and perforated sheet of steel mesh was trimmed to fit the inner diameter of the jar and suspended one filter paper above the soil sample; (4) carefully, filter paper was placed such that the paper did not touch top or sides of the jar where liquid water may

otherwise be adsorbed; (5) the glass jar was sealed after placing filter paper for an equilibration period of 7 to 10 days; (6) the paper was then removed from the jar and immediately weighed to the nearest 0.0001g with an electronic balance; (7) the paper was dried in the oven and weighed again to determine the filter paper water content; (8) the water content of filter paper was used to determine total suction using calibration curve (from Schleicher and Schuell Microscience) in figure 2.6; (9) the corresponding water content of the soil is gravimetrically determined to develop on point along the soil-water characteristic curve; and (10) 11 specimens prepared at different water contents were tested to generate additional points. Figure 2.7 shows a photograph of the filter paper testing setup. In this study, 20 to 40 g of 12 soil samples were used.

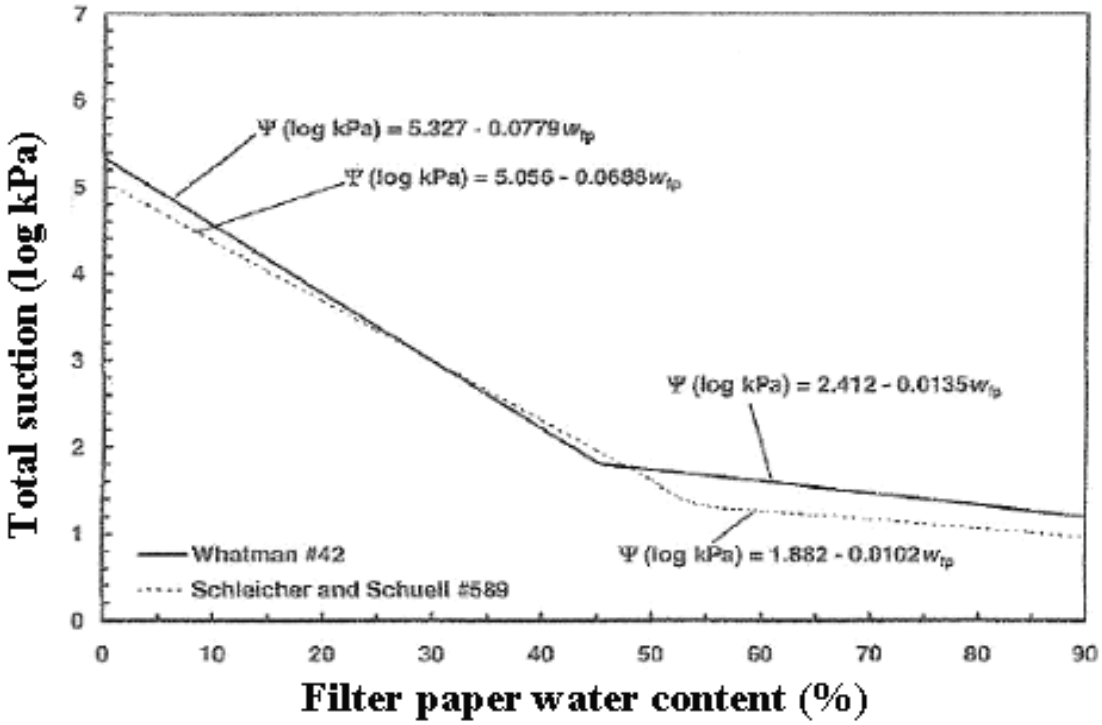

Figure 2.6 Calibration Curves for Whatman #42 and Schleicher and Schuell #589 filter papers (ASTM D5298, ASTM2000)

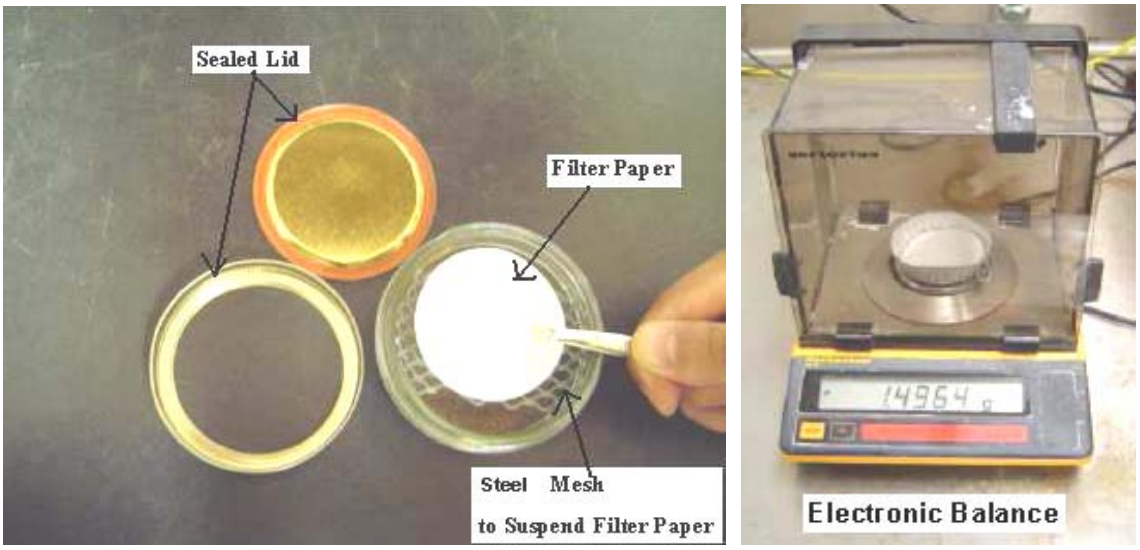

Figure 2.7 Photographs of Filter Paper Testing Technique

2.3 Previous True Triaxial Testing

Reddy et al. (1992) developed a true triaixial device that consists of the following components: a frame, six wall assemblies, a deformation measuring system, a stress application and control system, six membranes, a volume change monitoring system, a pore water pressure monitoring system, and a data acquisition system. Among components, a brief description of more important components, which are deformation measuring system and data acquisition system, is provided below.

Deformation measuring system—Four points on each of six faces using 24LVDTs were used to measure deformation. The core of each LVDT and its extension rod are thrust into contact with the specimen's membrane by a spring as depicted in figure 2.8. The excitation and output of the LVDTs are controlled and recorded by a data acquisition system.

Data acquisition system—A microcomputer equipped with a direct interface card was used for data acquisition. An analog-to-digital converter was used to convert signal. The data acquisition system can handle the 24 LVDTs for deformation and 3 pressure transducers for principal stress. In addition, a computer program was developed to calibrate the raw data (output voltages) and calculate the principal stress and principal strain.

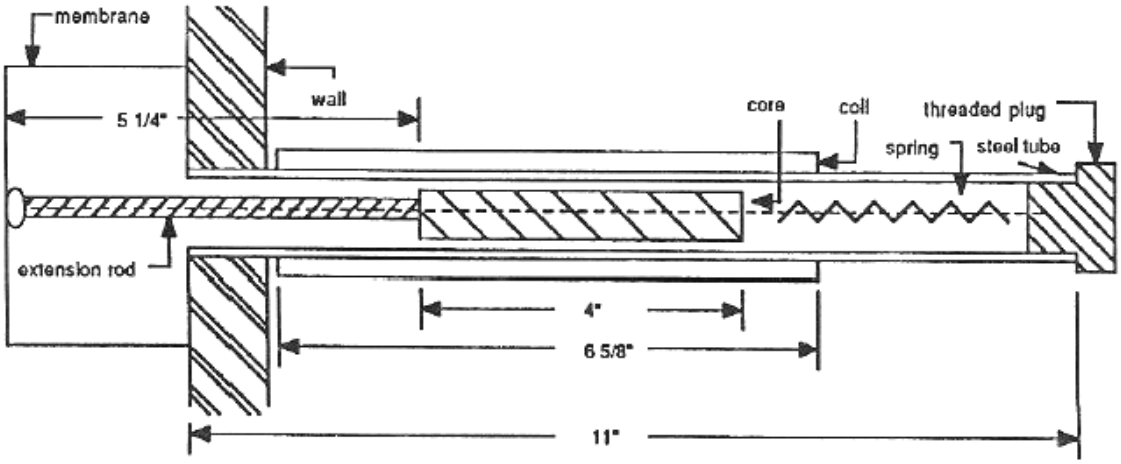

Figure 2.8 Deformation Measuring System (Reddy et al., 1992)

In the investigation conducted by Reddy et al. (1992), all the tests were performed under drained condition. The applied back-pressure remains constant during an entire test. It is assumed that no friction on the faces of the specimen is; therefore, the normal stresses (σ_x, σ_y, σ_z) and strains (ε_x, ε_y, ε_z) on the sides of the specimen are principal components of the stress and strain tensors. Hydrostatic compression tests (HC test), Conventional triaxial compression tests (CTC test), and Shear tests on octahedral planes with various b values are imposed on the specimens in this study. Stress ratio, b, is also defined as $(\sigma_2 - \sigma_1) / (\sigma_1 - \sigma_3)$. These stress paths are shown in figure 2.9.

In the case of hydrostatic compression and conventional triaxial compression tests, confining pressures were used 5,10, and 20 psi (35, 69, and 138 kPa). In the case of tests on octahedral planes were conducted by loading the specimens hydrostatically to the octahedral normal stress equal to one of three selected levels, 20, 30, 40 psi (138, 207, or 276 kPa) and then subsequently following a monotonic shear stress path to stay on the octahedral plane along different directions defined by the value of b as shown in figure 2.9. Using these results, the shape of the ultimate failure envelope could be investigated.

The results of all tests are shown in figure 2.10-2.16. Figure 2.10 shows hydrostatic compression (HC) test results. The three principal strains and volumetric strain measured are plotted against mean pressure. Figure 2.11 presents conventional triaxial compression (CTC) test results. In these tests, the results show no significant variation of ε_x and ε_y. However, the major principal strain (ε_z) is increased at all times. The volumetric strains are predominantly dilative. In b = 0 tests (shown in figure 2.12), the corresponding strains (ε_x, ε_y) were found equal and expansive as the minor and intermediate principal stresses were decreased equally. As major principal stress was increased during testing, its corresponding strain (ε_z) is compressive. The volumetric response is generally dilative. Figure 2.13 presents b = 0.25 test results. The three principal strains are different because the three principal were different during testing. The major principal strain (ε_z) is compressive, while the minor principal strain (ε_x) is expansive. Initially, the intermediate strain (ε_y) is very small during loading process and

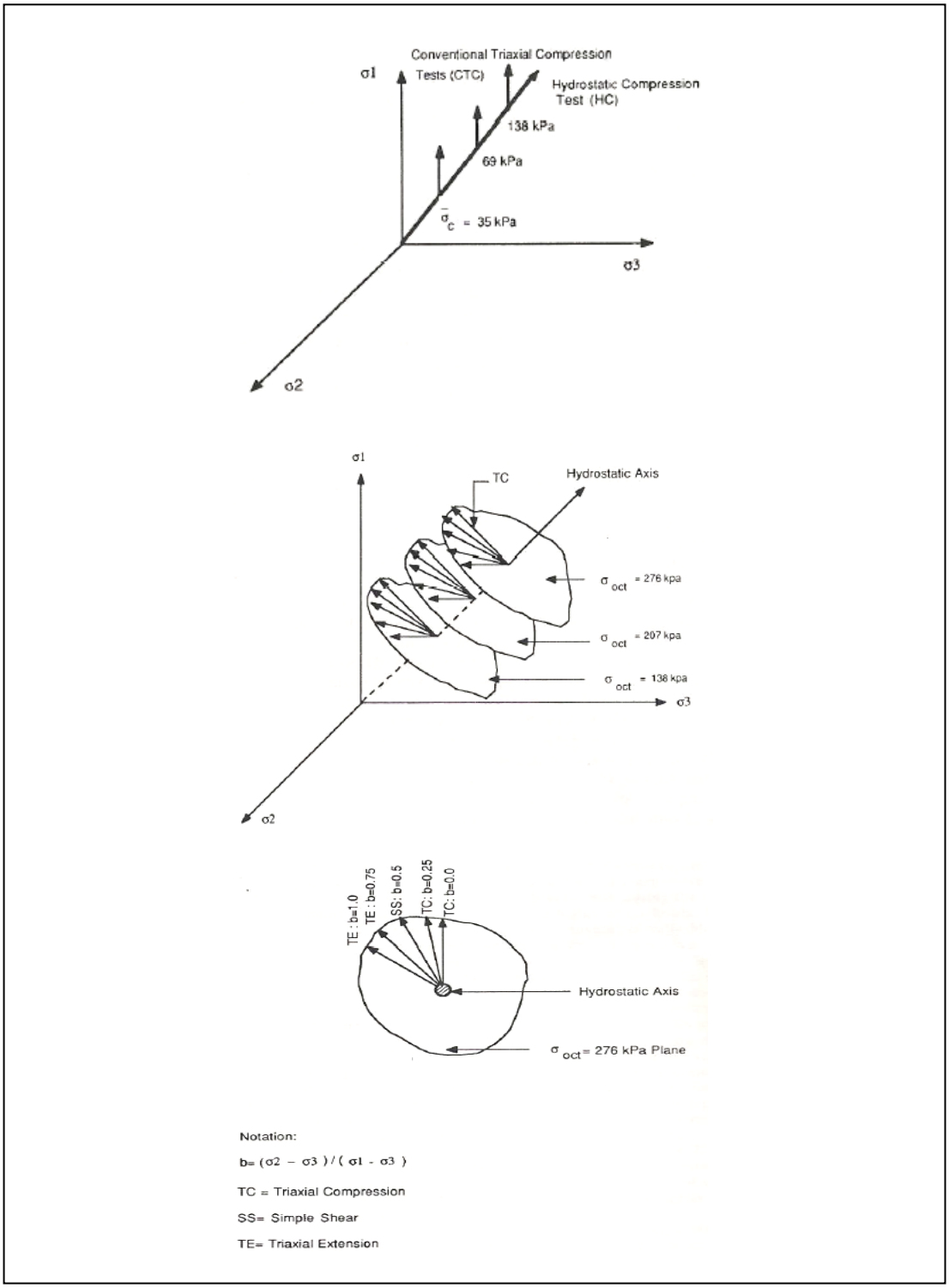

Figure 2.9 Stress Paths Studied (Reddy et al., 1992)

is expensive at higher stress level. Although the overall volumetric strains are dilative, the dilatancy in these tests are less as compared to the b = 0 tests. In b = 0.5 tests (shown in figure 2.14), the major principal strain (ε_z) is compressive, the minor strain (ε_x) is expansive, and the intermediate principal strain (ε_y) is almost zero. The dilative volumetric strain in these tests are higher than in b = 0 and b = 0.25 tests. The test results based on b = 0.75 (shown in figure 2.15) presents contraction in the direction of major principal stress and expansion in the direction of minor principal stress. In these tests, the intermediate principal strain is slightly compressive. In b = 1 tests (shown in figure 2.16), the intermediate (ε_y) and major principal (ε_z) strains are compressive and nearly equal. The minor principal strain (ε_x) is expansive. The volumetric strains are predominantly dilative. The tests results obtained by Reddy et al. (1992) indicate the following three facts: (1) cemented sand shows generally dilatant response as b value changes from 0 to 1; (2) the shape of failure envelope sand shows similar trends to the uncemented sand on triaxial and octahedral planes; and (3) contractions in the direction of major principal stress and expansions in the direction of minor principal stress were shown while changes from expansions to contractions in the direction of the intermediate principal stress were shown as b value changes from 0 to 1.

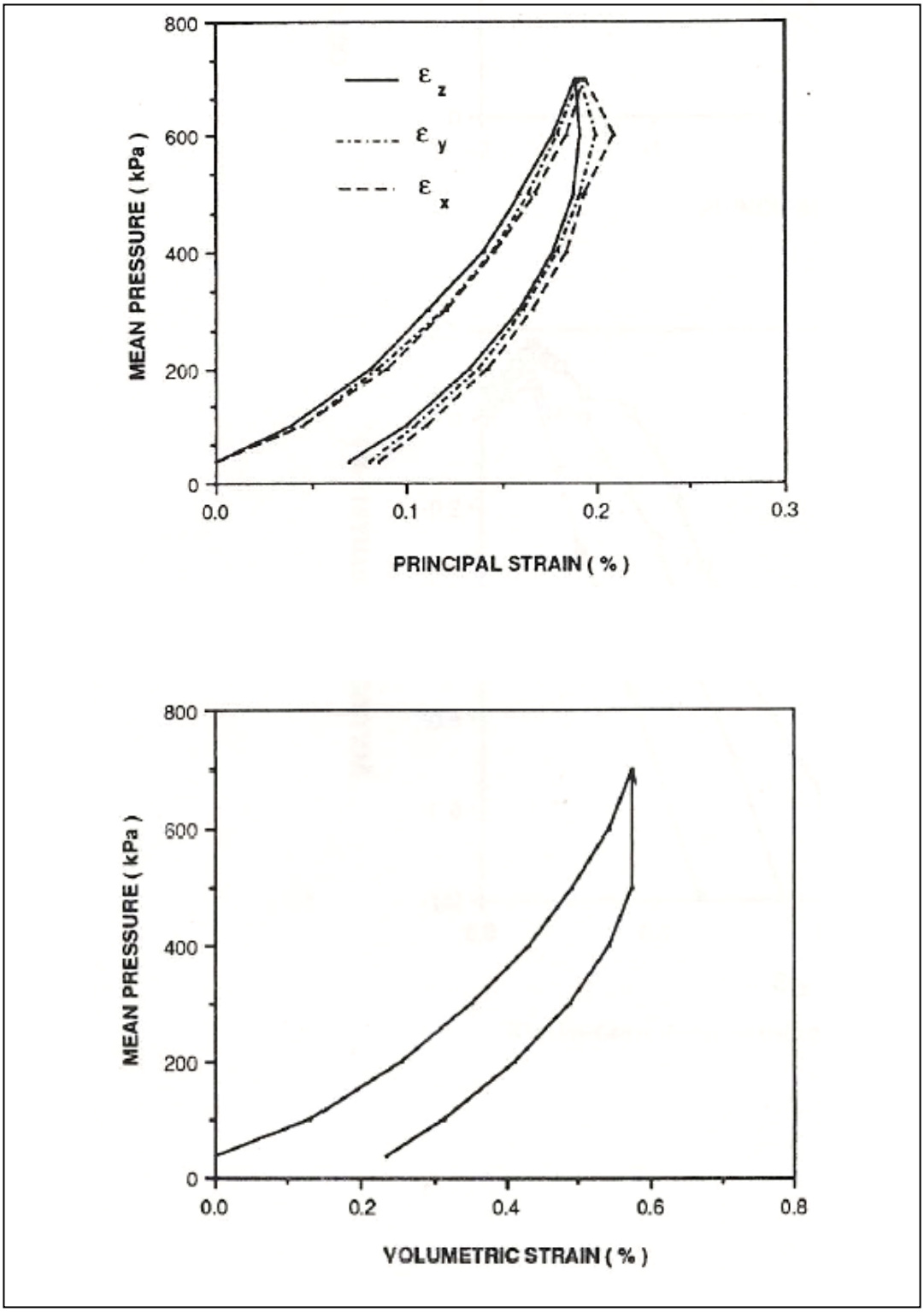

Figure 2.10 Hydrostatic Compression Test Results (Reddy et al., 1992)

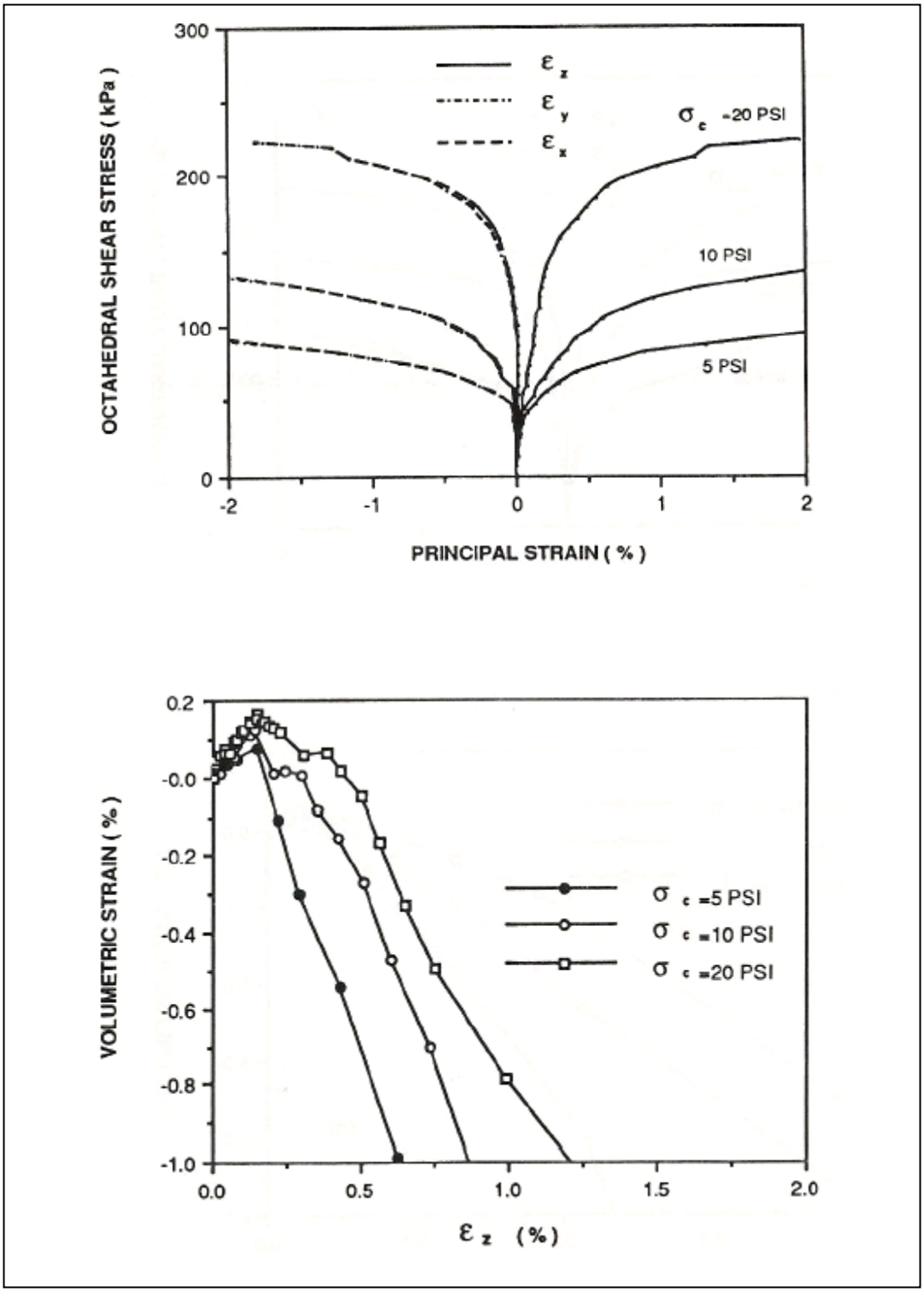

Figure 2.11 Conventional Triaxial Compression Test Results (Reddy et al., 1992)

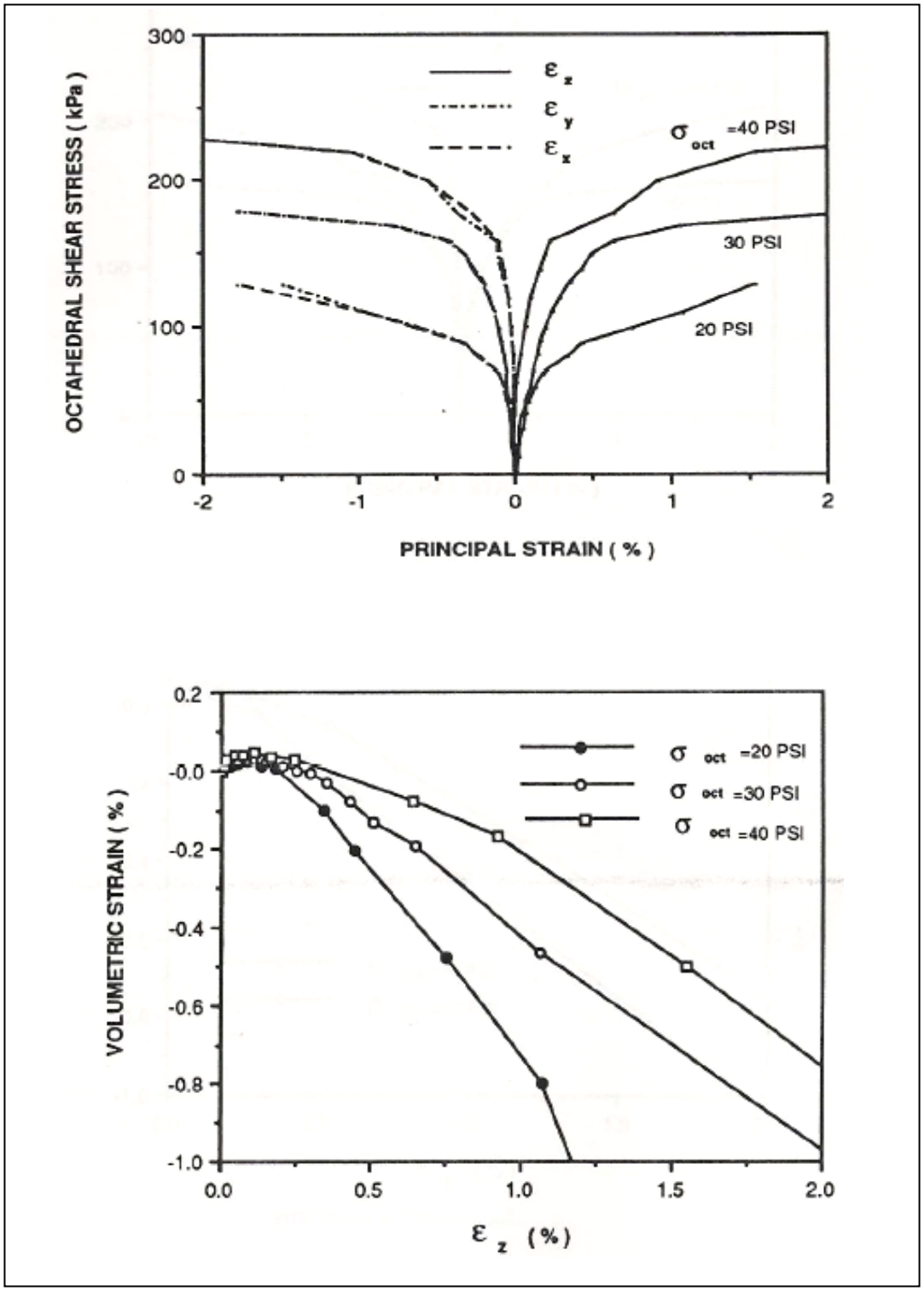

Figure 2.12 b = 0 Test Results (Reddy et al., 1992)

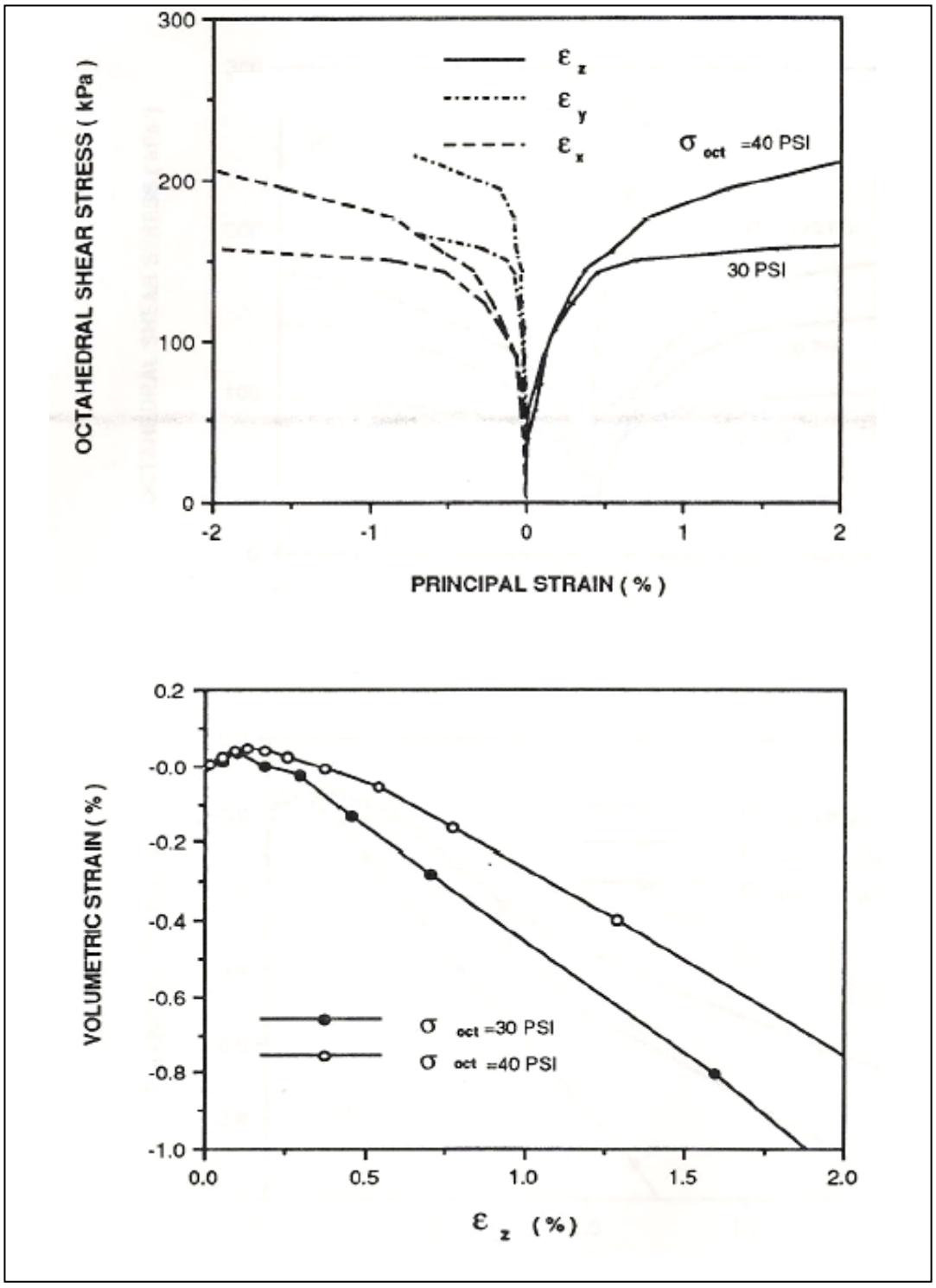

Figure 2.13 b = 0.25 Test Results (Reddy et al., 1992)

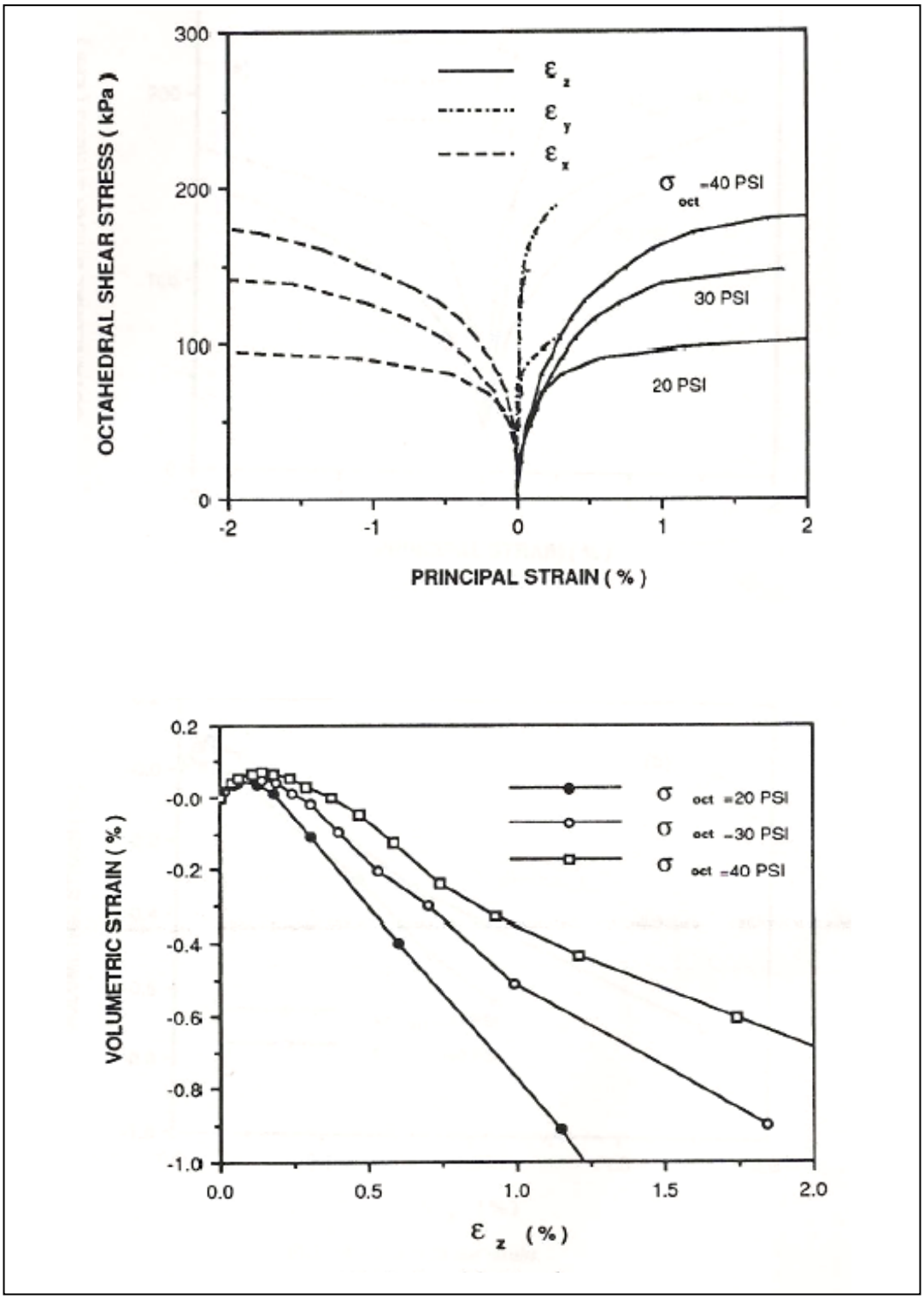

Figure 2.14 b = 0.5 Test Results (Reddy et al., 1992)

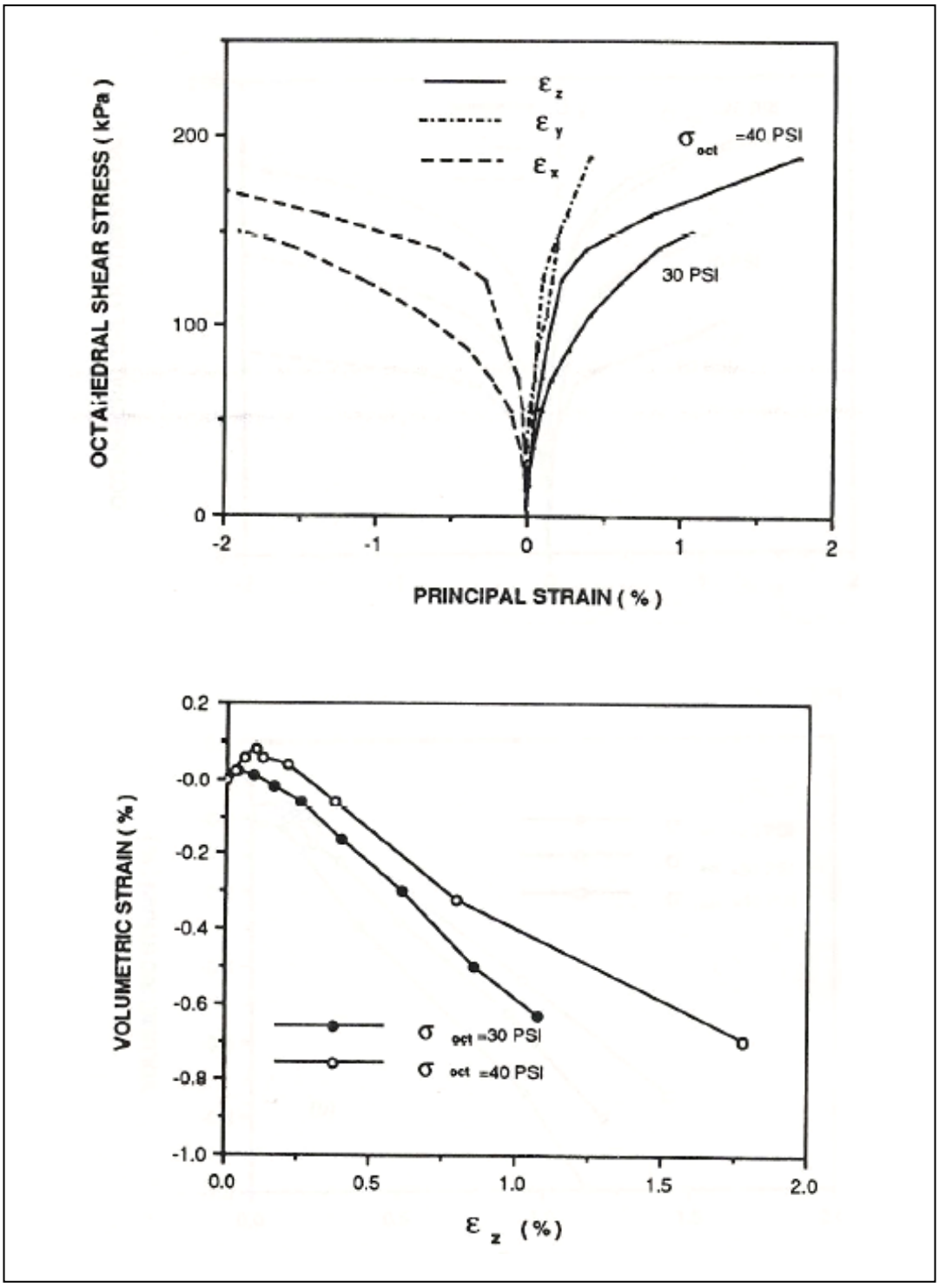

Figure 2.15 b = 0.75 Test Results (Reddy et al., 1992)

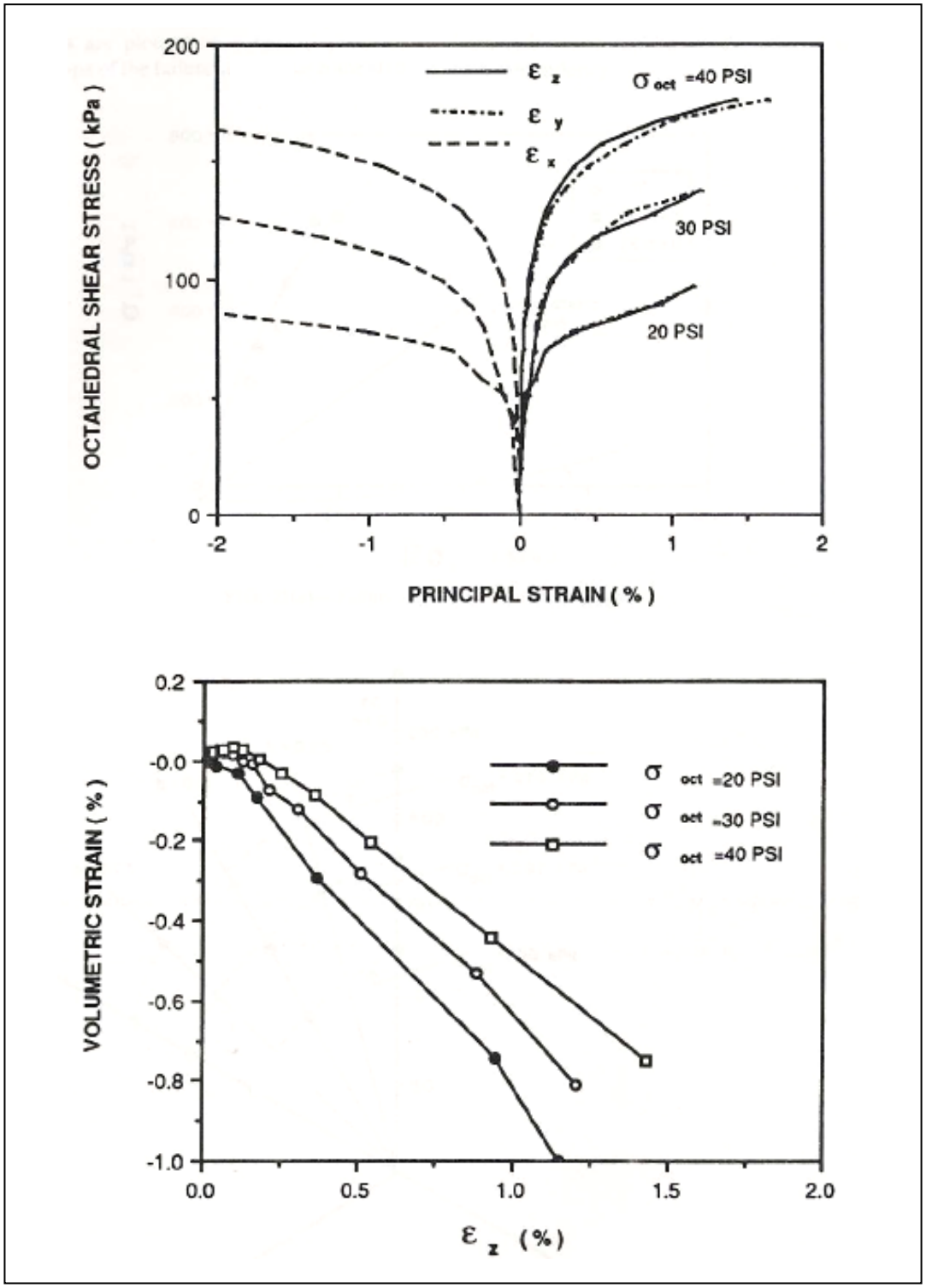

Figure 2.16 b = 1 Test Results (Reddy et al., 1992)

Li and Puri (1996) investigated anisotropy of dry cohesive and chohesionless powders and the effect of particle shape and sample deposition method on the anisotropy by using a cubical triaxial tester in figure 2.17.

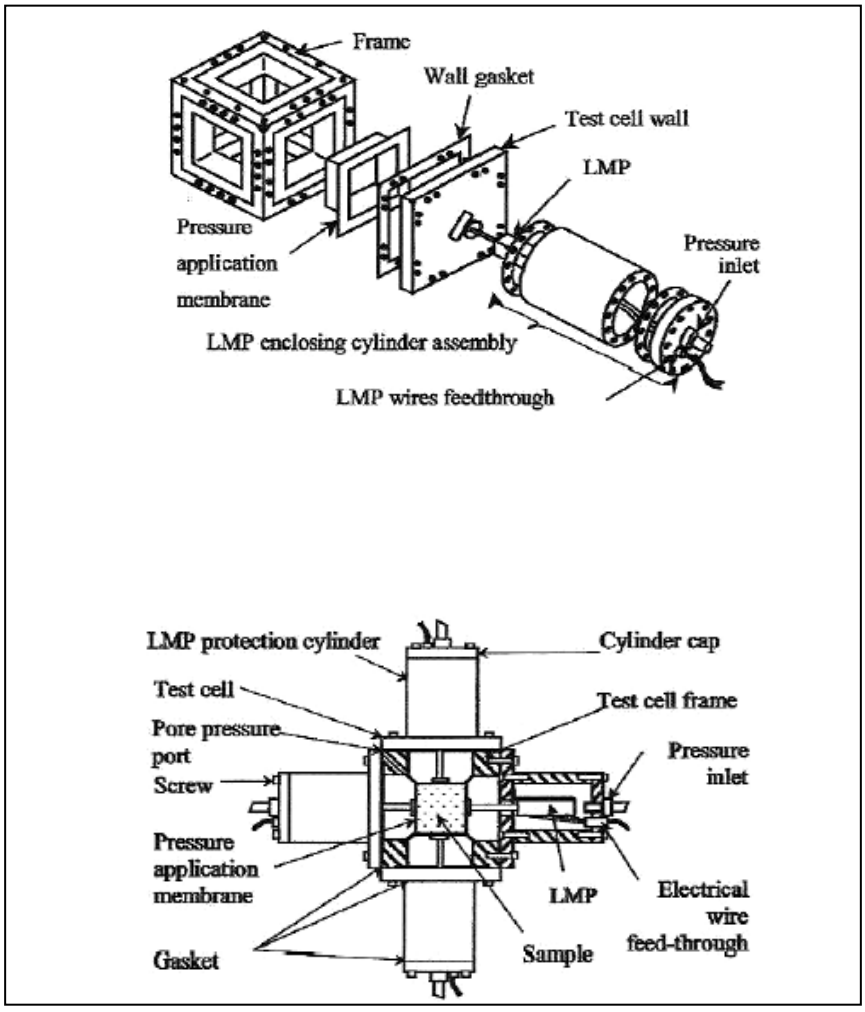

Figure 2.17 View of the Cubical Triaxial Tester (Li and Puri, 1996)

Hydrostatic triaxial compression (HTC) tests and conventional triaxial compression (CTC) tests were conducted on four powders: two cohesive, wheat flour (irregular-shaped particles) and potato starch (rounded); and two cohesionless, glass beads (spherical) and milled glass fibers (cylindrical). In order to prepare test samples,

two different deposition methods, plunging and tapping, were used. Test results showed wheat flour and glass beads were basically isotropic materials. On the contrary, potato starch showed some anisotropy that tended to increase with applied stress. In addition, significant anisotropy was observed for milled glass fibers. All test results and plots in the study presented by Li and Puri (1996) have similar trends to those of the study conducted by Reddy et al. (1992).

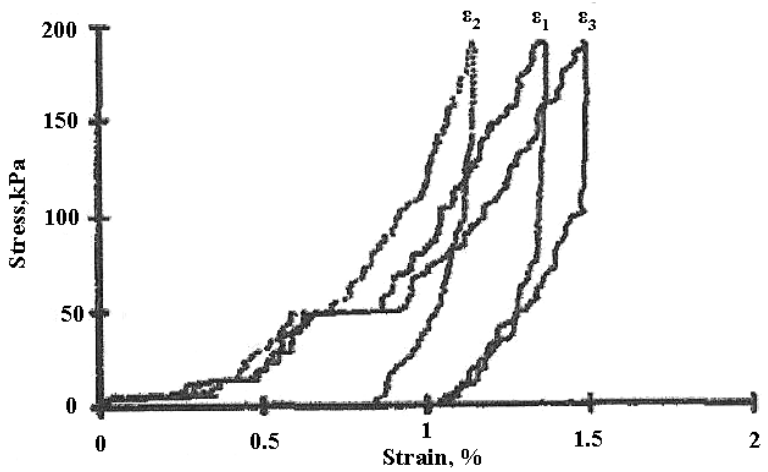

Figure 2.18 Load Response of Potato Starch under HTC test (Li and Puri, 1996)

Hoyos and Macari (2001) developed a computer driven, mixed-boundary type, and stress/suction controlled true triaxial (cubical) testing device to further investigate the influence of matric suction on the mechanical behavior of partially saturated soils under a wide range of stress paths. The device consists of nine components: (1) a steel frame, (2) a top and four lateral wall assemblies, (3) a deformation measuring system, (4) a stress application/control system, (5) five flexible membranes, (6) a pore-air pressure control/monitoring system, (7) a pore-water pressure control/monitoring system, (8) an air/water-supply pressure board, and (9) a data acquisition and process

control system. The distinctive characteristic of the device is the assembly containing the disk referred to as the *bottom wall assembly*. This assembly imposes a fixed boundary for bottom face of the specimen, as shown schematically in figure 2.19. The boundary type of this device is mixed boundary type because of a fixed boundary for bottom face of the specimen.

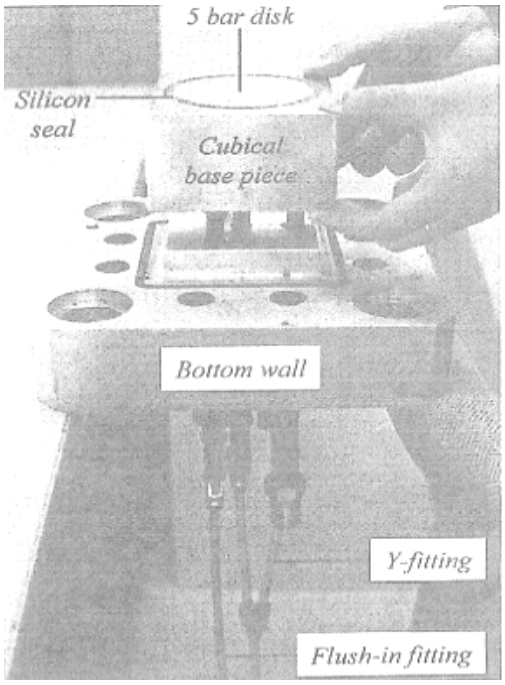

Figure 2.19 Photograph of Cubical Base Piece (Hoyos and Macari, 2001)

A series of three drained hydrostatic compression (HC) tests were conducted in this cubical setup from p (net mean pressure) = 50 kpa to p (net mean pressure) = 400 kpa under s (matric suction) = 50, 100, or 200 kpa, respectively as shown in figure 2.20. A series of six drained conventional triaxial compression (CTC) tests were conducted in this cubical set up. Prior to shearing, two different values of initial net mean stress (p =

100 and 400 kpa) were applied while matric suction (s = 50, 100, or 200 kpa) was constant, as depicted in figure 2.21).

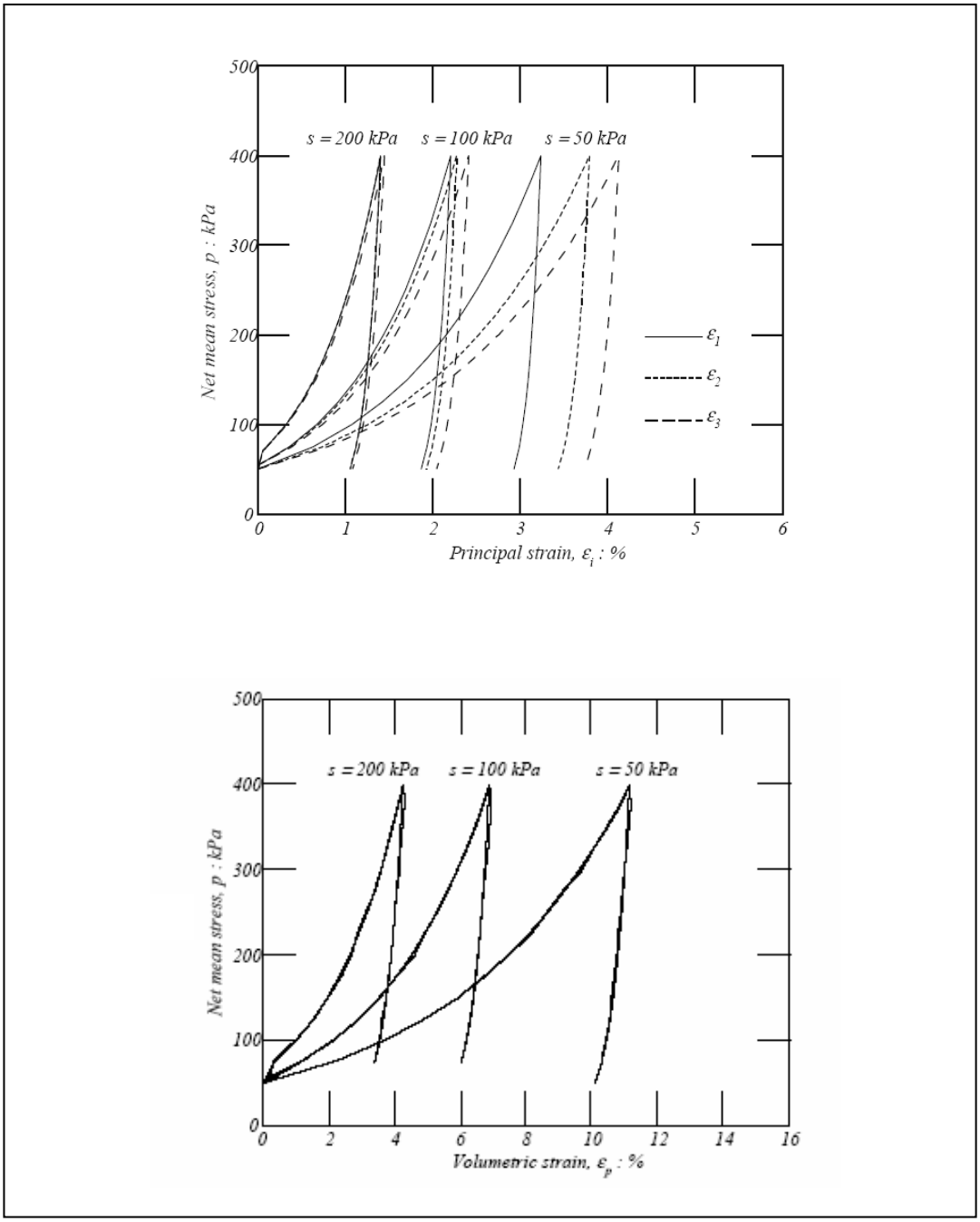

Figure 2.20 Hydrostatic Compression Test Results (Hoyos and Macari, 2001)

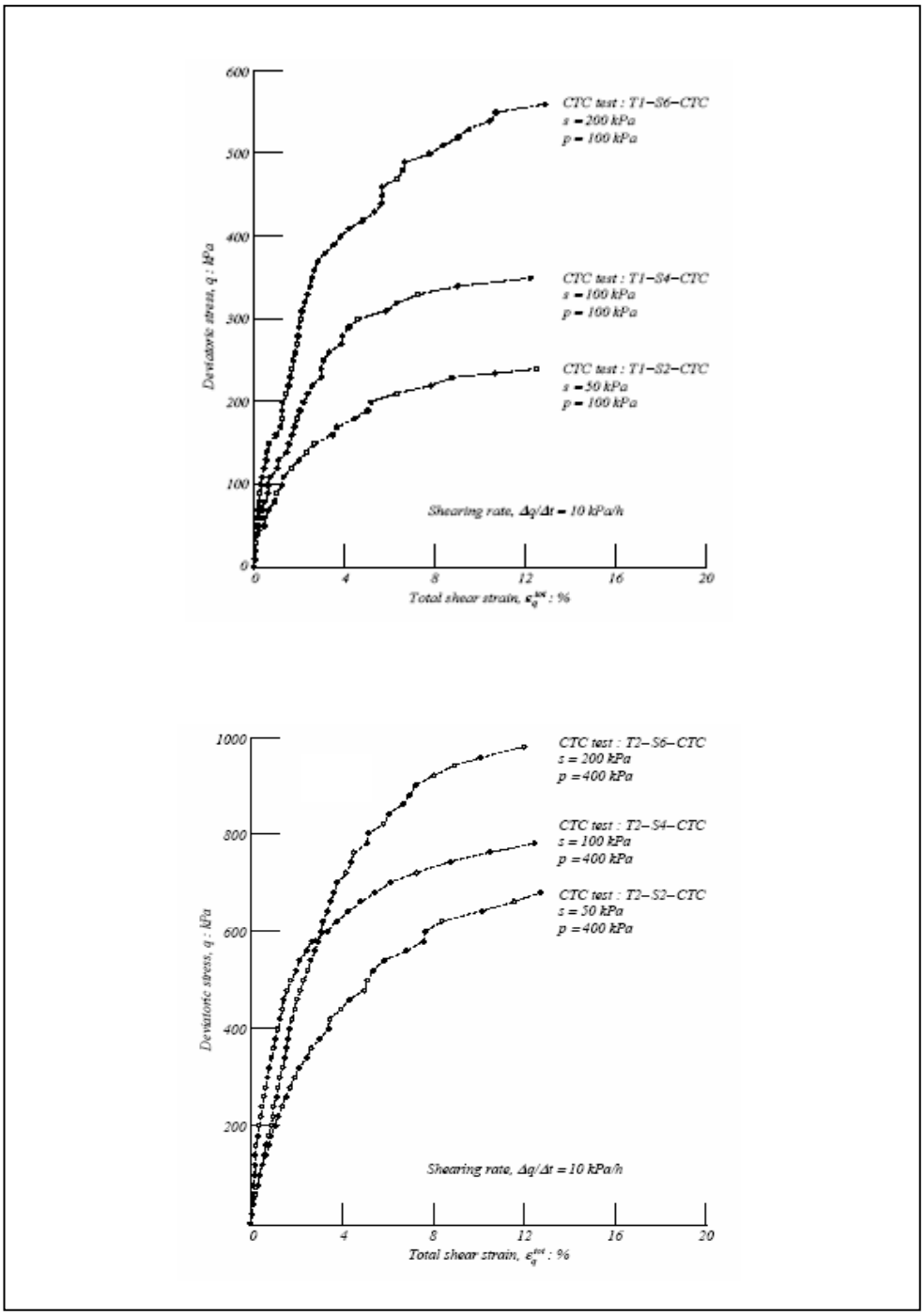

Figure 2.21 Conventional Triaxial Compression Test Results (Hoyos and Macari, 2001)

A series of nine drained triaxial compression (TC) tests, simple shear (SS) tests, and triaxial extension (TE) tests, respectively, were conducted in this cubical setup. Each specimen was tested following the muti-stage testing scheme depicted in figure 2.22, keeping constant the pre-established value of matric suction (s = 50, 100, or 200 kpa). The results of TC, SS, and TE including octahedral stress plane are shown in figure 2.23-2.26.

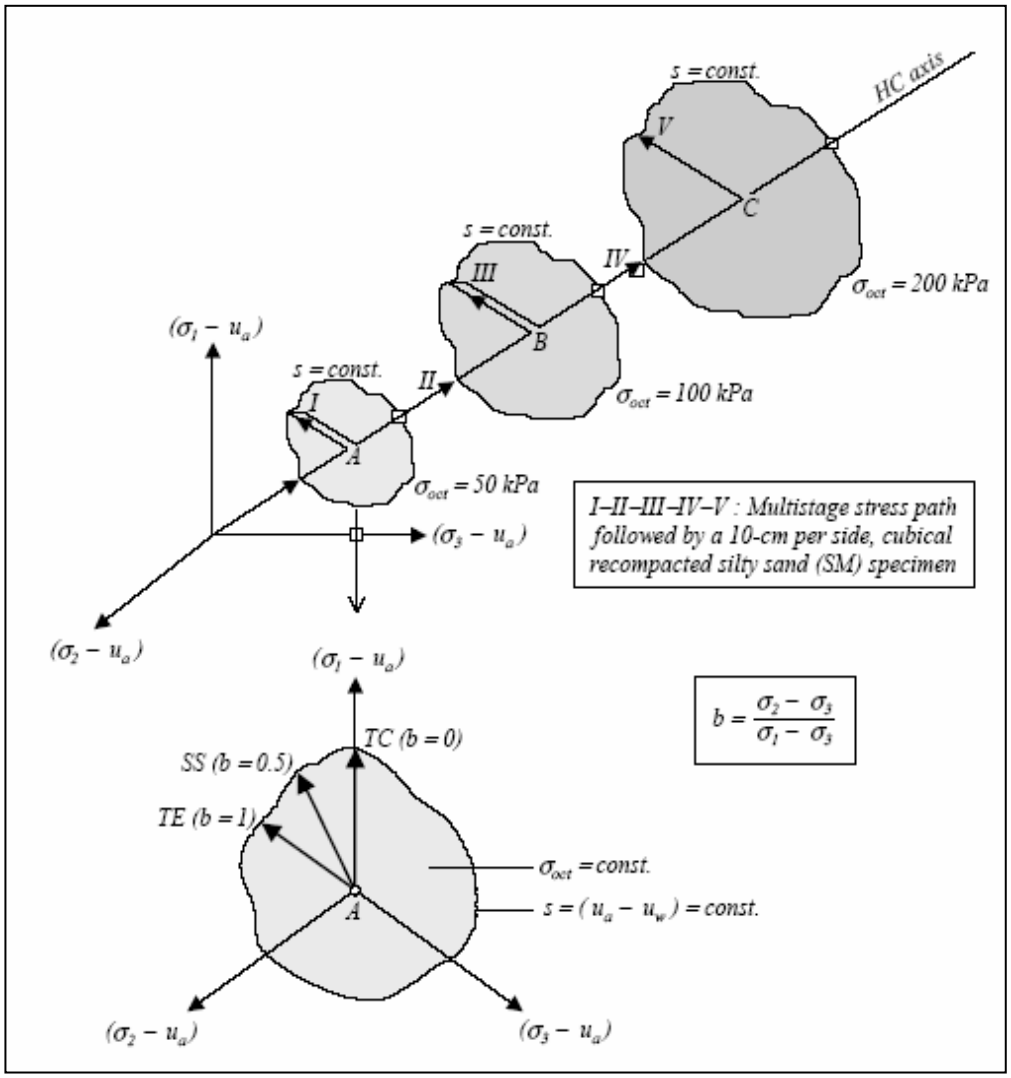

Figure 2.22 A Typical Multi-Stage Drained True Triaxial Tests (Hoyos and Macari, 2001)

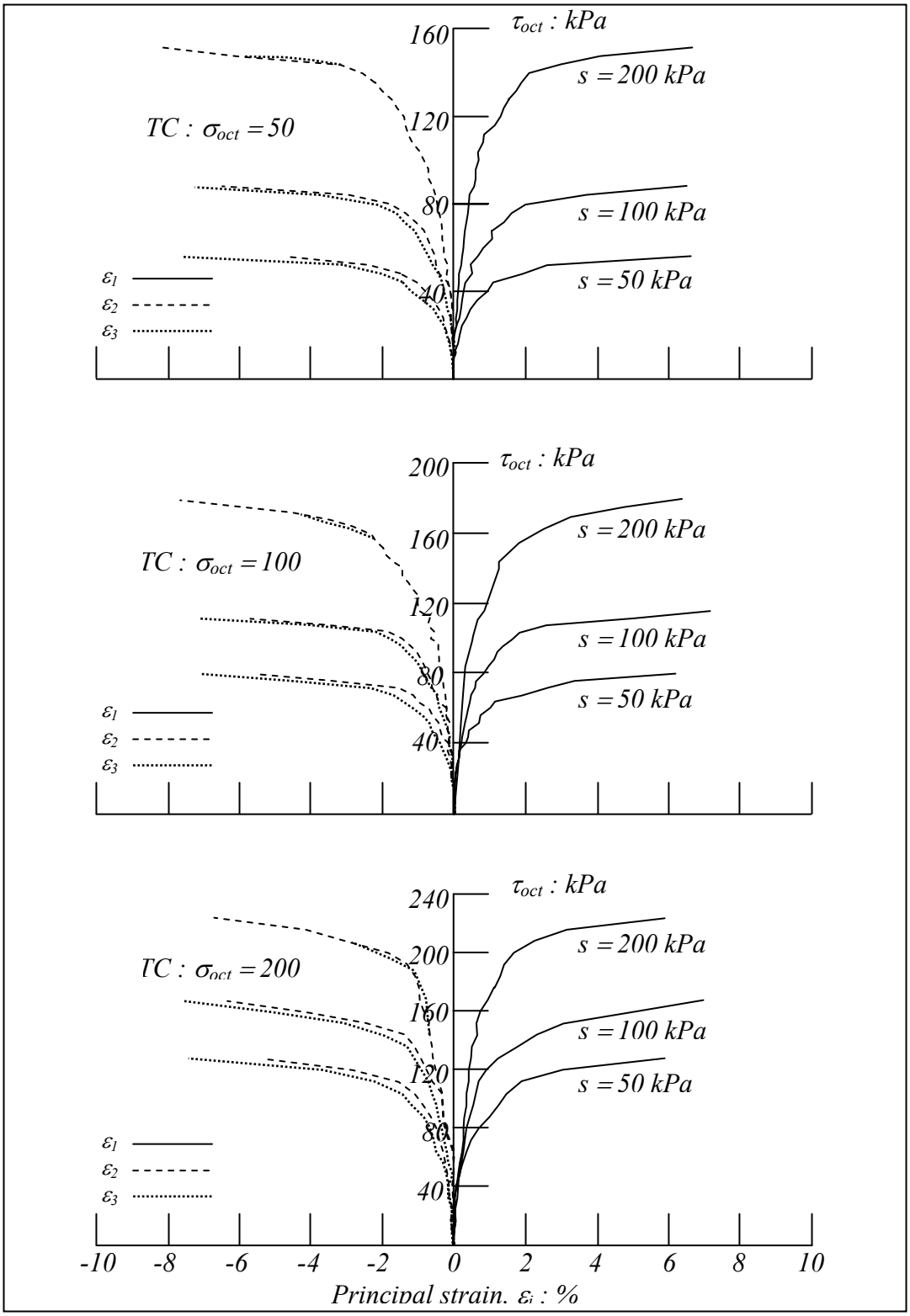

Figure 2.23 Triaxial Compression Test Results (Hoyos and Macari, 2001)

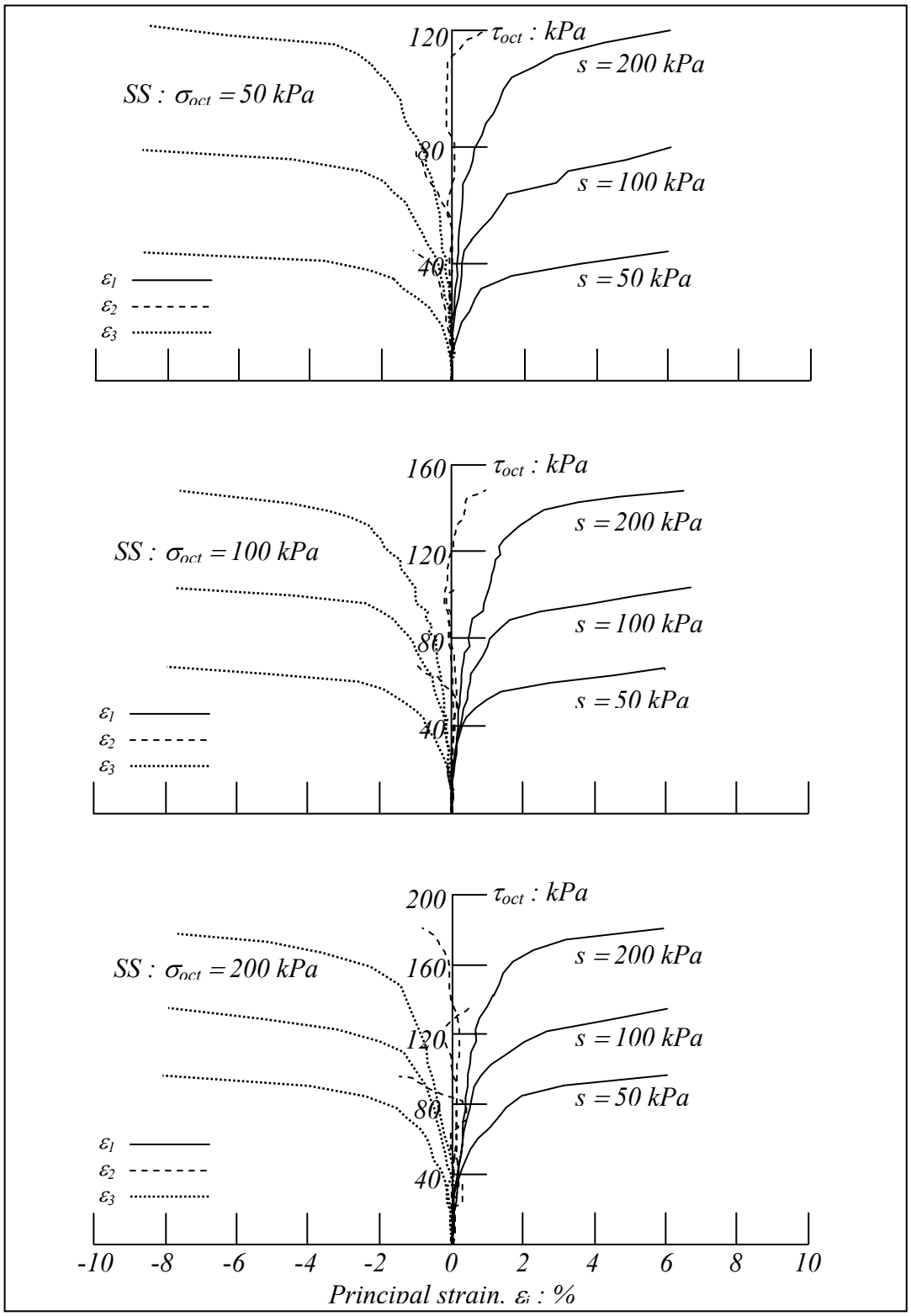

Figure 2.24 Simple Shear Test Results (Hoyos and Macari, 2001)

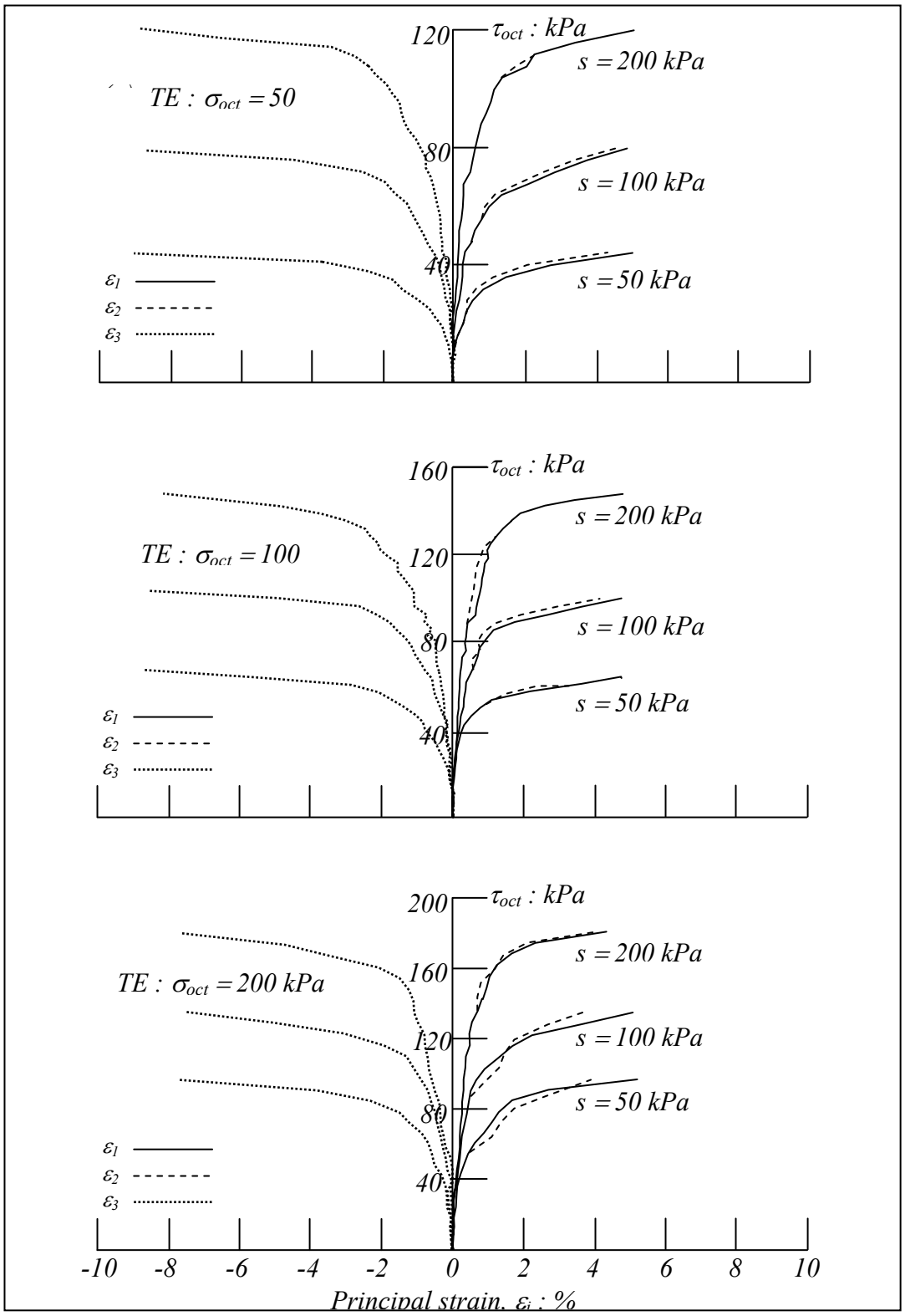

Figure 2.25 Triaxial Extension Results (Hoyos and Macari, 2001)

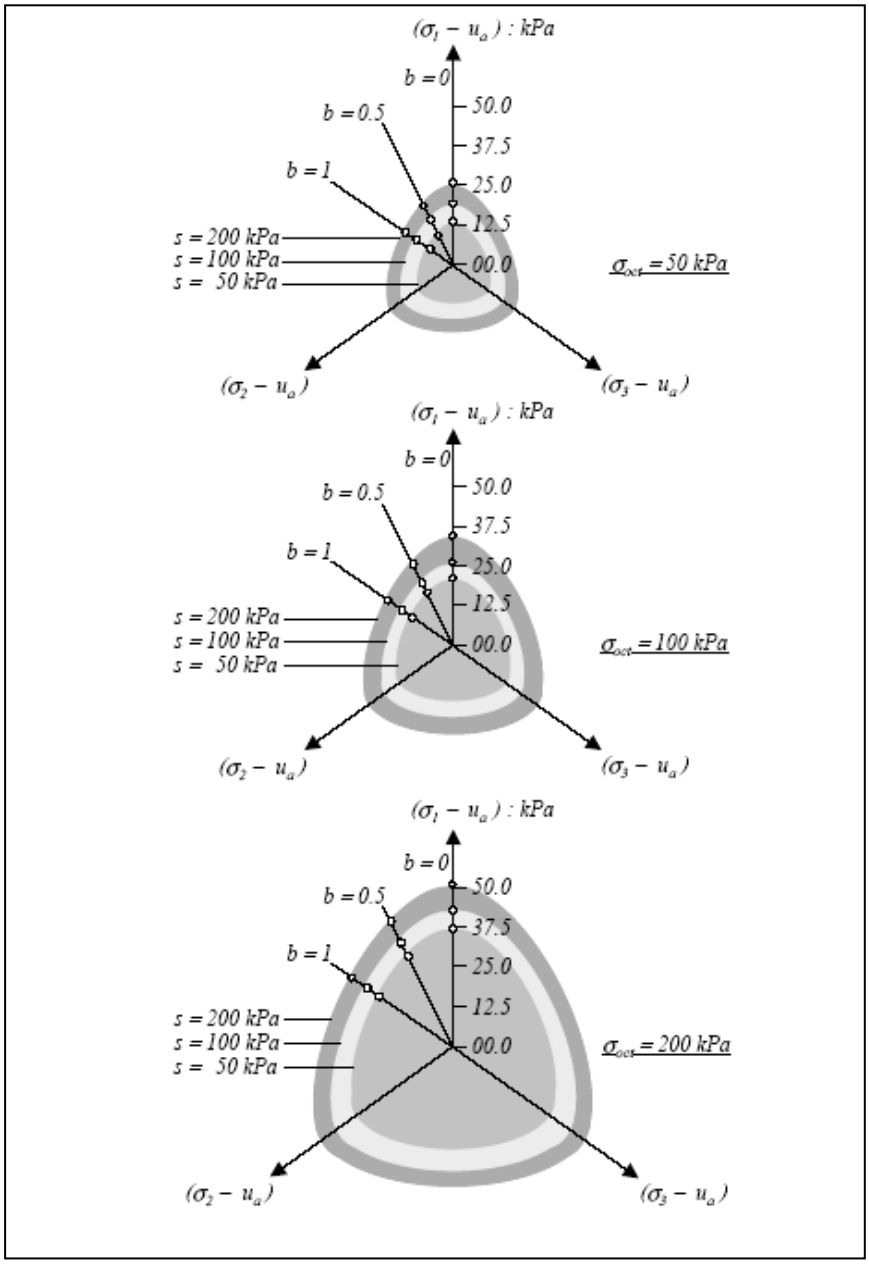

Figure 2.26 Projection of Potential Failure Envelopes onto the Octahedral Stress Plane (Hoyos and Macari, 2001)

As noticed from results reported by Hoyos and Macari (2001), matric suction was found to exert a significant influence on the stress-strain-strength behavior of

compacted silty sand as well as on the size, position, and shape of failure envelopes in octahedral plane (π-plane) for a wide variety of simple to complex stress paths.

Matsuoka et al. (2002) newly developed the existing true triaxial apparatus for sand (Matsuoka et al., 1985) by attaching a device to supply a controlled suction to the specimen. The developed true triaxial apparatus enables the specimen of unsaturated soil to be tested under a controlled constant suction. The suction applied to the specimen is produced by using negative pore-water pressure method ($s = -u_w > 0$; $u_a = 0$). The true triaxial ($\sigma_1 \geq \sigma_2 \geq \sigma_3$) and plane strain ($\varepsilon_2 = 0$; $\sigma_1 > \sigma_2 > \sigma_3$) tests were performed on an unsaturated silty soil under a constant suction and a mean pressure. It was found that true triaxial results under three different principal stresses are uniquely arranged on the extended spatially mobilized plane. Subsequently, frictional and cohesive materials are modified from the original SMP (spatially mobilized plane). It was also found that shear strengths of unsaturated silty clay obtained by the true triaxial apparatus nearly agree with the extended SMP failure criterion.

The works reported by Hoyos and Macari (2001) and Matsuoka et al. (2002) present valuable experimental evidence on multiaxial soil behavior only for suction values less than 200 kPa, mainly due to limitations in the suction-controlled techniques used in each case. In the present work, a series of tests were conducted on partially saturated silty sand in a newly developed cubical device in order to investigate the effect of initial values of suction higher than residual total suction ($\Psi_r = 410$ kPa). The next chapter describes the fundamentals of true triaxial testing and a full description of the newly developed apparatus.

CHAPTER 3

FUNDAMENTALS OF TRUE TRIAXIAL TESTING AND APPARATUS DESCRIPTION

3.1 Introduction

This chapter is devoted to describing the fundamentals of true triaxial (cubical) testing, the main components of the newly developed cubical device, calibration of Linear Variable Displacement Transducers (LVDTs), and the step-by-step assembly process. Considerable attention is given to the fundamentals and description of the true triaxial testing technique.

From the 1960s, true triaxial devices became popular and have been refined and upgraded over the last four decades. The core system of the present device was manufactured at the University of Colorado-Boulder, under direct supervision of Professor Stein Sture, and was ultimately assembled at the University of Texas at Arlington, under direct supervision of Professor Laureano Hoyos. The device has the salient feature of enabling the application of matric suction via axis translation technique.

In the present work, however, a series of true triaxial tests have been performed along a variety of stress paths on pluviated silty sand with naturally occuring suction, since the purpose was to calibrate and check-out verify the correct functioning of each basic component without the controlled-suction capability.

3.2 True Triaxial Testing

3.2.1 Introduction

Cylindrical triaxial devices are able to generate only axisymmetric ($\sigma_2 = \sigma_3$) and hydrostatic ($\sigma_1 = \sigma_2 = \sigma_3$) stress states, as depicted in figure 3.1(a). However, true triaxial devices are capable of generating complete stress paths under a variety of stress states: (1) Axisymmetric ($\sigma_2 = \sigma_3$) stress states, (2) Hydrostatic ($\sigma_1 = \sigma_2 = \sigma_3$) stress states, and (3) True triaxial ($\sigma_1 \neq \sigma_2 \neq \sigma_3$) stress states, as shown in figure 3.1(b). In nature, soils, rocks, and other materials are subjected to three-dimensional stress gradients; therefore, tests based on true triaxial stress states are required to investigate the three dimensional behavior of soils, rocks, and other nature materials for accurate prediction purposes.

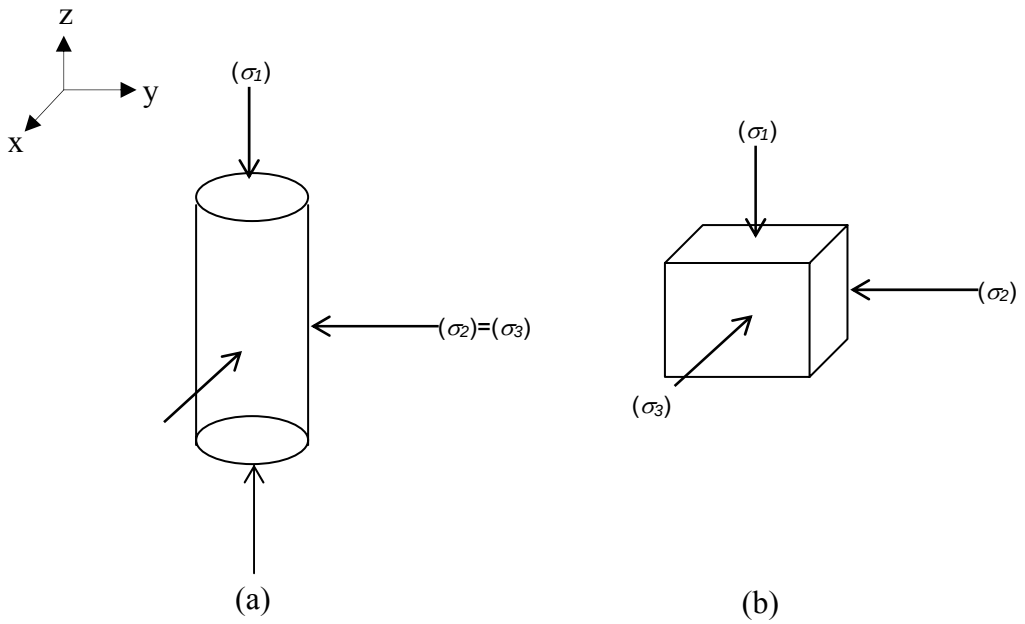

Figure 3.1 (a) Axisymmetric ($\sigma_2 = \sigma_3$) and Hydrostatic ($\sigma_1 = \sigma_2 = \sigma_3$) Stress States; (b) True Triaxial ($\sigma_1 \neq \sigma_2 \neq \sigma_3$) Stress States

The three-dimensional state of stress can be expressed in terms of the normal and tangential components of stresses acting on the octahedral plane defined by $\sigma_x+\sigma_y+\sigma_z$ = const, as shown in figure 3.2. The normal component, σ_{oct}, and the tangential component, τ_{oct}, are generally called "mean principal stress" and "octahedral shear stress", respectively, and are calculated as (Yamada and Ishihara, 1982):

$$\sigma_{oct} = \frac{\sigma_1 + \sigma_2 + \sigma_3}{3} \tag{3.1}$$

$$\tau_{oct} = \frac{1}{3}\sqrt{(\sigma_1 - \sigma_2)^2 + (\sigma_2 - \sigma_3)^2 + (\sigma_3 - \sigma_1)^2} \tag{3.2}$$

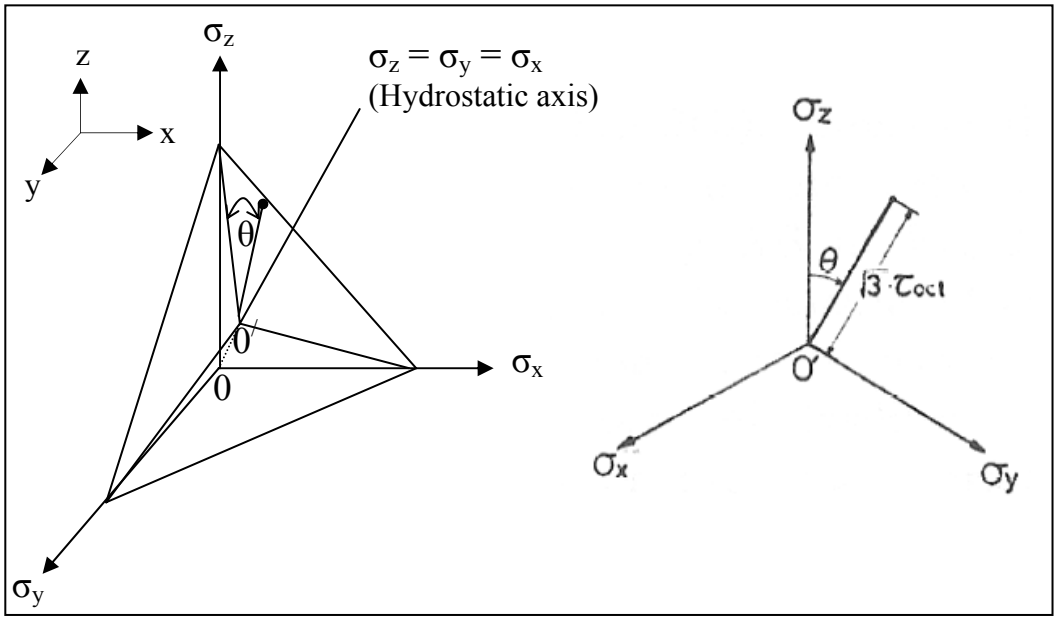

Figure 3.2 Representation of Stress Conditions in the Octahedral Plane (Yamada and Ishihara, 1982)

In order to specify three-dimensional stress conditions, it is necessary to adopt another independent variable, θ, which determines the direction of the shear stress on the octahedral plane, as shown in figure 3.2. This variable may be given by (Yamada and Ishihara, 1982):

$$\tan\theta = \frac{\sqrt{3}(\sigma_y - \sigma_x)}{2\sigma_z - \sigma_x - \sigma_y} \tag{3.3}$$

Volumetric strain, ε_v, is defined as follows,

$$\varepsilon_v = 1/3(\varepsilon_x+\varepsilon_y+\varepsilon_z) \tag{3.4}$$

3.2.2 Stress Paths

Hydrostatic ($\sigma_1 = \sigma_2 = \sigma_3$) Stress Path

Hydrostatic stress path is expressed in the following manner

$$\begin{aligned} &\delta\sigma_r \uparrow \\ &\delta q = 0 \\ &\delta p = \delta\sigma_r \end{aligned} \tag{3.5}$$

Where; σ_a = axial stress, σ_r = radial stress

p (net mean stress) = $\frac{\sigma_a + 2\sigma_r}{3}$, q (deviatoric stress) = $\sigma_a - \sigma_r$

$\sigma_a = \sigma_1$, $\sigma_r = \sigma_2 = \sigma_3$, σ_a and σ_r = stresses generated by cylindrical triaxial device

σ_1, σ_2, and σ_3 = stresses generated by true triaxial device

Hydrostatic stress path can be generated by both cylindrical and true triaxial devices, and is also plotted in figure 3.3.

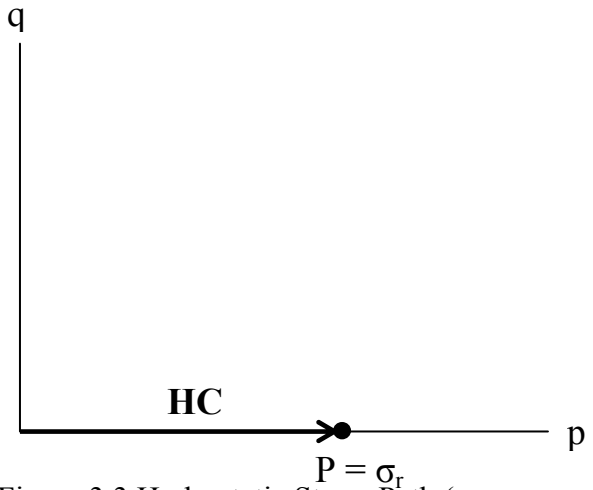

Figure 3.3 Hydrostatic Stress Path ($\sigma_1 = \sigma_2 = \sigma_3$)

Conventional Triaxial Compression ($\sigma_2 = \sigma_3$) Stress Path

In the case of true triaixal device, the intermediate (σ_2) and minor (σ_3) principal stresses are maintained constant while increasing the major (σ_1) principal stress. In the case of cylindrical triaxial device, radial (σ_r) stress is constant while increasing the axial (σ_a) stress. Conventional stress path is given by

$$\begin{aligned} &\delta\sigma_r = 0 \\ &\delta\sigma_a \uparrow \\ &\delta q > 0 \\ &\delta p = \frac{1}{3}\,\delta q \end{aligned} \qquad (3.6)$$

Where; σ_a = axial stress, σ_r = radial stress

p (net mean stress) = $\frac{\sigma_a + 2\sigma_r}{3}$, q (deviatoric stress) = $\sigma_a - \sigma_r$

$\sigma_a = \sigma_1$, $\sigma_r = \sigma_2 = \sigma_3$, σ_a and σ_r = stresses generated by cylindrical triaxial device

σ_1, σ_2, and σ_3 = stresses generated by true triaxial device

Conventional triaxial compression stress path can be generated by both cylindrical and true triaxial devices, and is also plotted in figure 3.4.

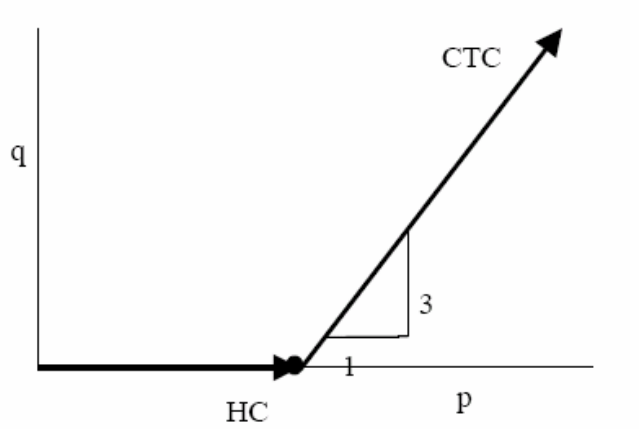

Figure 3.4 Conventional Triaxial Compression ($\sigma_2 = \sigma_3$)

Triaxial Compression ($\sigma_2 = \sigma_3$) Stress Path

During TC tests, the major (σ_1) principal stress is increased, whereas the intermediate (σ_2) and minor (σ_3) principal stress are equally reduced (i.e., $\Delta\sigma_2 = \Delta\sigma_3 = -\Delta\sigma_1/2$) in true triaxial devices. In cylindrical triaxial devices, axial (σ_a) stress is increased while decreasing radial (σ_r) stress. Triaxial compression stress path is expressed as

$$\delta p = 0$$
$$\delta\sigma_a \uparrow$$
$$\delta q > 0$$
$$\delta\sigma_r = -\frac{1}{2}\,\delta\sigma_a = -\frac{1}{3}\,\delta q \qquad (3.7)$$

Where; σ_a = axial stress, σ_r = radial stress

p (net mean stress) = $\frac{\sigma_a + 2\sigma_r}{3}$, q (deviatoric stress) = $\sigma_a - \sigma_r$

$\sigma_a = \sigma_1$, $\sigma_r = \sigma_2 = \sigma_3$, σ_a and σ_r = stresses generated by cylindrical triaxial device

σ_1, σ_2, and σ_3 = stresses generated by true triaxial device

Triaxial compression stress path can be generated by both cylindrical and true triaxial devices, and is also plotted in figure 3.5.

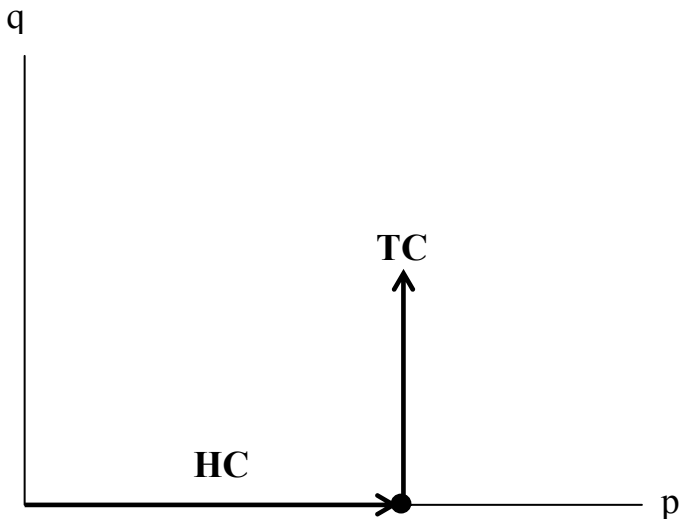

Figure 3.5 Triaxial Compression ($\Delta\sigma_2 = \Delta\ \sigma_3 = -\Delta\ \sigma_1/2$)

Triaxial Extension Stress Path

In TE tests, the intermediate (σ_2) and major (σ_1) principal stresses are equal and increased equally while the minor (σ_3) principal stress is decreased (i.e., $\Delta\ \sigma_3 = -2\Delta\ \sigma_2 = -2\Delta\ \sigma_1$) in true triaxial devices. In cylindrical triaxial devices, radial (σ_r) stress is increased, whereas axial (σ_a) stress is decreased. Triaxial extension stress path is given in the following manner.

$$\delta p = 0$$
$$\delta\sigma_r \uparrow$$
$$\delta q < 0$$
$$\delta\sigma_r = -\frac{1}{2}\,\delta\sigma_a = -\frac{1}{3}\,\delta q \qquad (3.8)$$

Where; σ_a = axial stress, σ_r = radial stress

p (net mean stress) = $\frac{\sigma_a + 2\sigma_r}{3}$, q (deviatoric stress) = $\sigma_a - \sigma_r$

$\sigma_a = \sigma_3$, $\sigma_r = \sigma_1 = \sigma_2$, σ_a and σ_r = stresses generated by cylindrical triaxial device

σ_1, σ_2, and σ_3 = stresses generated by true triaxial device

Triaxial extension stress path can be generated by both cylindrical and true triaxial devices, and is also plotted in figure 3.6.

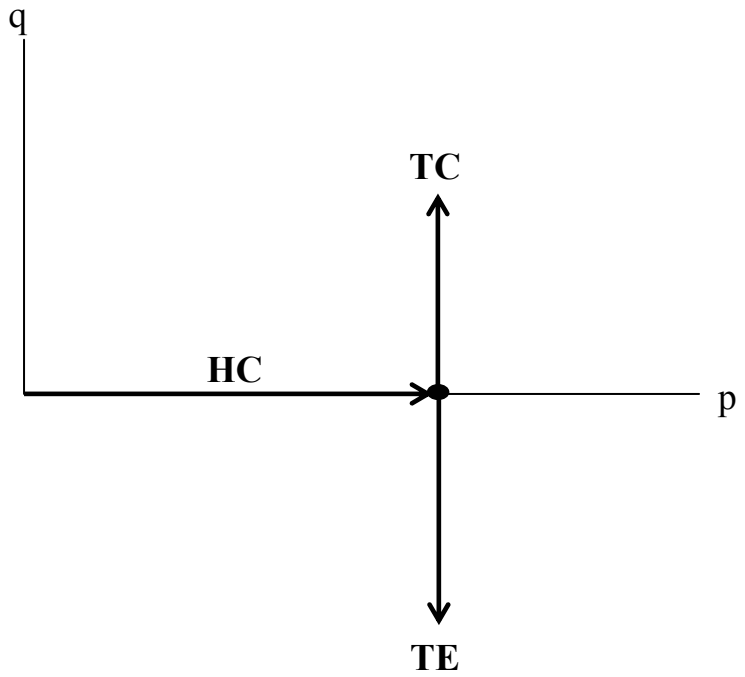

Figure 3.6 Triaxial Extension ($\Delta\sigma_3 = -2\Delta\sigma_2 = -2\Delta\sigma_1$)

Simple Shear Stress Path

During SS tests, the major (σ_1) principal stress is increased, and, simultaneously, the minor (σ_3) stress is decreased in the same magnitude (i.e., $\Delta\ \sigma_3 = -\Delta\ \sigma_1$), whereas the intermediate (σ_2) principal stress remains constant (i.e., $\Delta\ \sigma_2 = 0$) in true triaxial

devices. In the case of cylindrical triaxial devices, simple shear stress cannot be generated. The plot of SS stress path with other stress paths is shown in figure3.7.

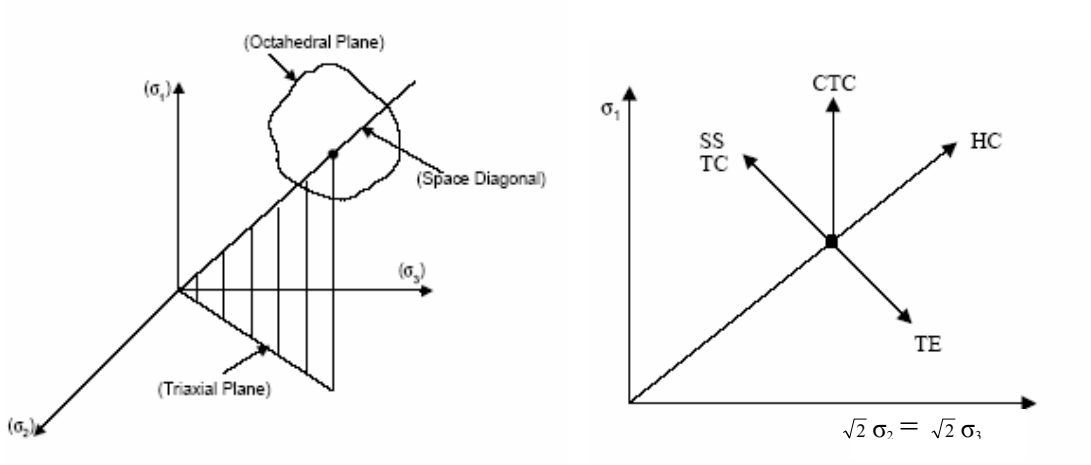

(a) (b)

Figure 3.7 (a) Principal Stress Space; (b) Projection of Stress Paths on Triaxial Plane

Stress Ratio

Stress ratio, b, is defined as $(\sigma_2 - \sigma_3) / (\sigma_1 - \sigma_3)$. Where σ_1, σ_2, and σ_3 are the major, intermediate, and minor principal stresses, respectively. Shear tests on octahedral planes can be performed with a variety of b values. In the previous chapters, TC, TE, and SS stress paths were mentioned, and the b values of these stress paths are corresponding to b = 0, b = 0.5, and b = 1, respectively. In the present work, TC, TE, and SS stress paths, which correspond to b = 0, b = 0.5, and b = 1, respectively, used as shear stress paths on octahedral plane as well (shown in figure 3.8). Therefore, the stress-strain-strength behavior of silty sand and the influence of total suction were investigated along the stress paths stated above.

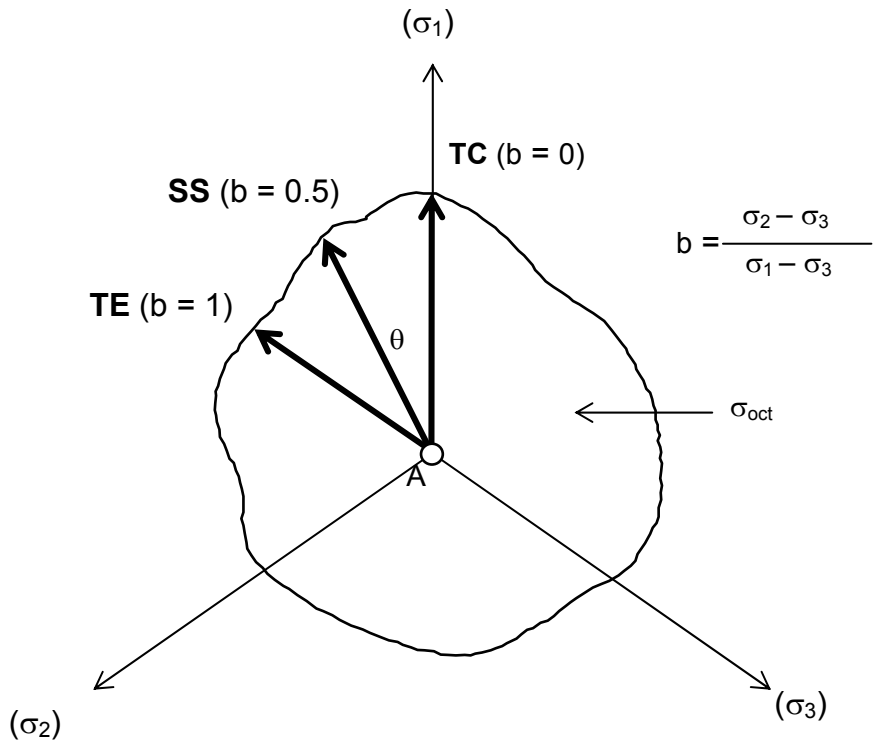

Figure 3.8 Representation of Shear Stress Paths on Octahedral Planes

3.3 Apparatus Description

The apparatus developed herein consists of six main components or modules: (1) a frame, (2) six wall assemblies, (3) a deformation measuring system, (4) a stress application and control system, (5) six membranes, and (6) a data acquisition system. A detailed, illustrated description of each of these components is provided below.

1. Frame: Two photographs of the frame are shown in figure 3.9 and 3.10, respectively. The frame was machined from solid aluminum. The frame supports top, bottom, lateral wall assemblies, and cubical specimen. The inner square cavities were machined into each of six faces of the frame to accommodate the membranes, and to

form pressure cavities. Connection bolts were provided on each face of the frame to fix the wall assemblies. Drainage pore were machined diagonally through the frame.

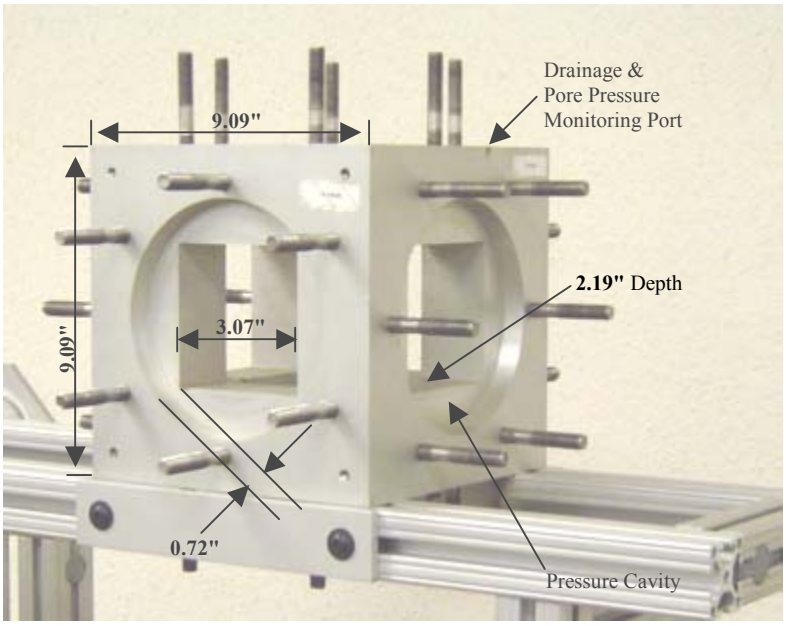

Figure 3.9 Close Photograph of Frame

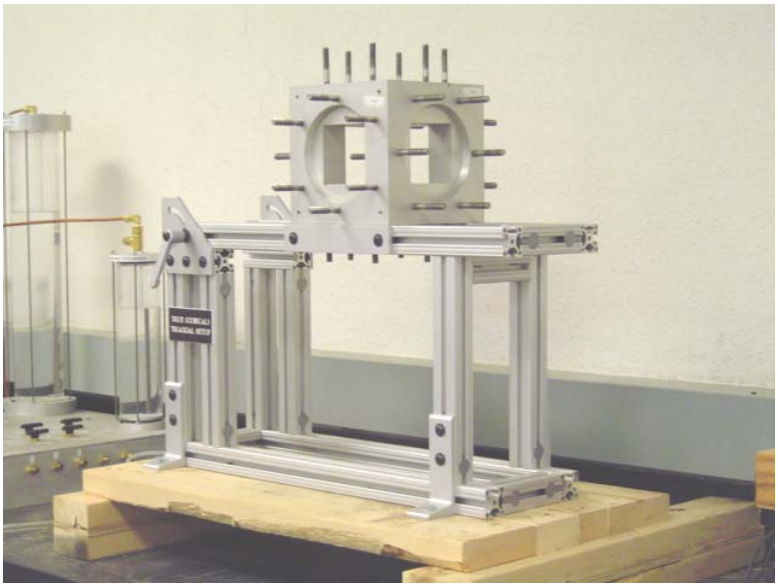

Figure 3.10 Photograph of Frame and Mounting Support

2. Wall Assemblies: Figure 3.11 shows a cross-sectional view of the complete wall assemblies. Six wall assemblies also were machined from aluminum.

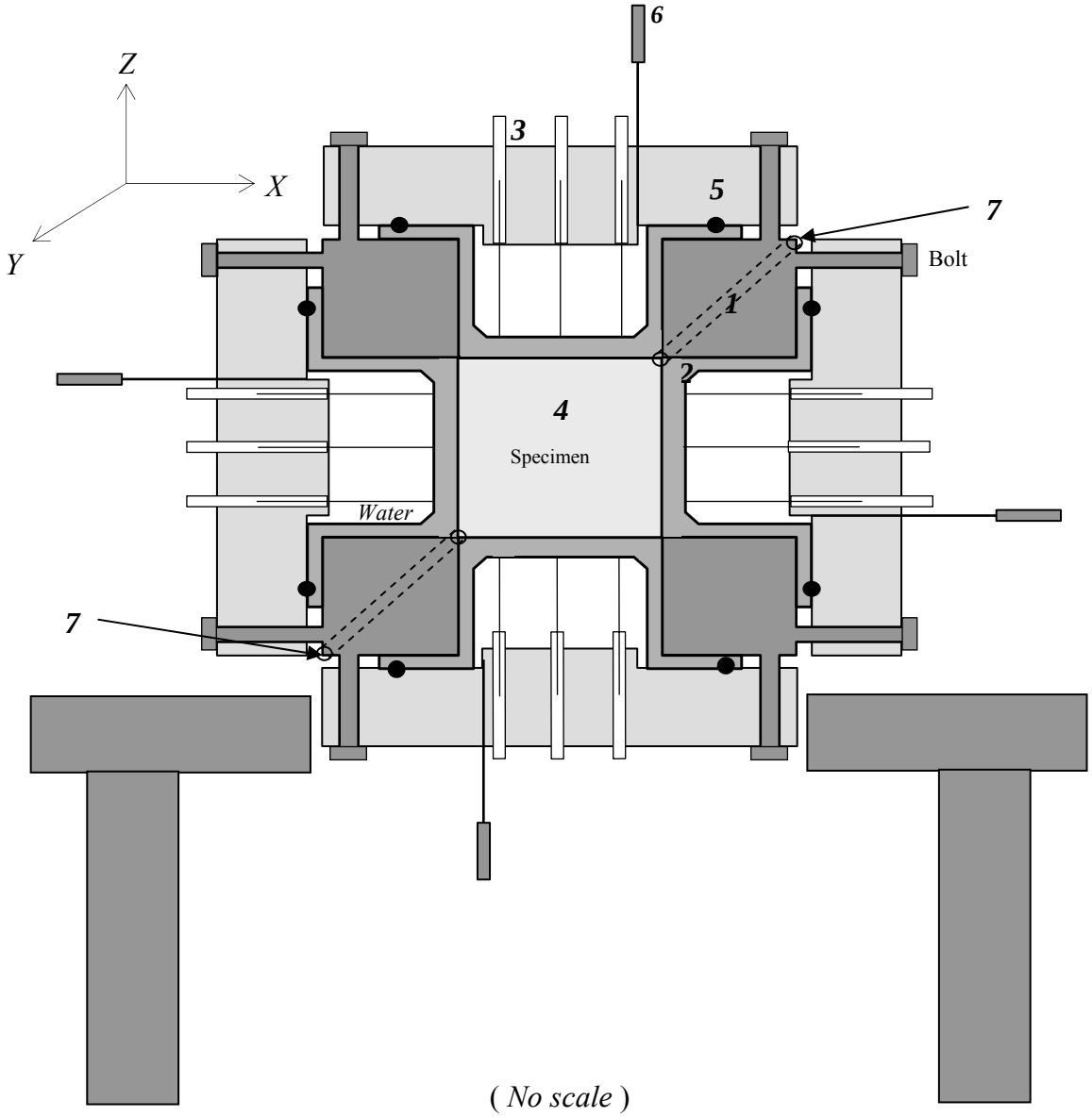

(*No scale*)

1. Cubical frame
2. LATEX
3. Schaevitz's LVDT
4. Specimen
5. Wall assembly
6. Pressure inlet
7. Drainage & pore pressure monitoring port

Figure 3.11 Cross-Sectional View of Complete Wall Assemblies

Each wall assembly is composed of: (1) a cover plate providing the wall seal for the interior pressure cavity, (2) a pressure inlet connection, and (3) three holes threaded to receive the stainless steel housing of three linear variable differential transformers (LVDT). Wall assembly of each face is same as that of a previous device (Reddy et al., 1992). The steel housings were inserted in the holes and sealed with epoxy as shown in figure 3.12. The outer ends of the housings were capped. The inside and outside diameters of each housing were machined to allow free movement of the core of a linear variable differential transformer (LVDT) within the housing, and allow the LVDT coil to slide over the housing. A photograph of the wall assembly is shown in figure 3.13. The pressure cavity and membranes were completely held by the inside projection of the wall.

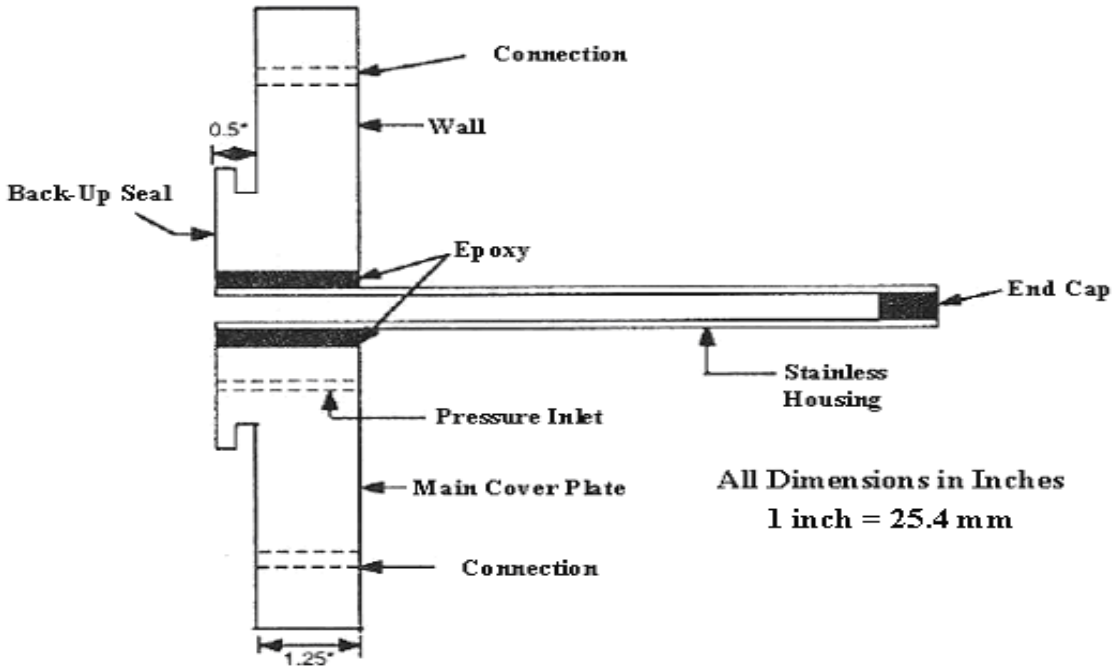

Figure 3.12 Wall Assembly

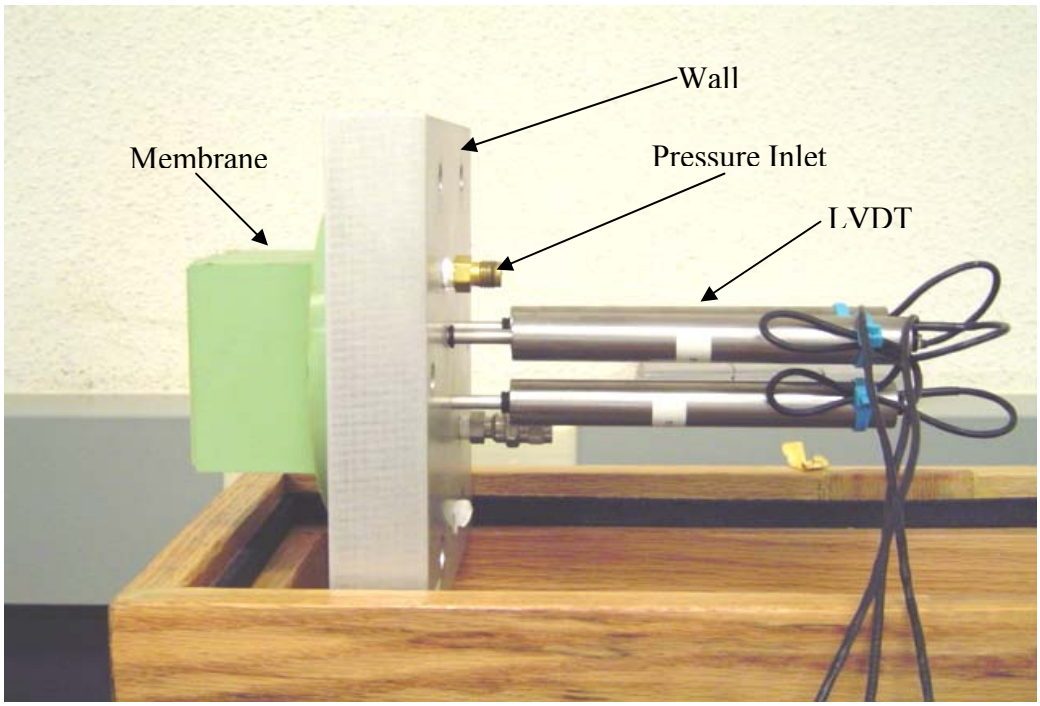

Figure 3.13 Photograph of the Wall Assembly

3. Deformation Measuring System: The deformation of the specimen is measured at three points on each of faces using 16 LVDTs (i.e., 3 LVDTs per face). The LVDTs (form Schaevitz Sensors Products, Inc.) are located at a120^{o} spacing on a 3.18-cm radius on each wall assembly. The core of each LVDT and its extension rod were thrust into contact with the flexible membranes by a spring as shown in figure 3.14. A data acquisition system controls and records the excitation and output of the LVDTs. As the core of LVDT move up and down within the housing, it causes change in the magnitude of voltage corresponding to the magnitude of deformation (i.e., measured in inches). Based on the above concept, calibration of each of LVDTs was performed by stacking up 0.1-inch aluminum stacks or taking out stacks one by one as shown in figure 3.15.

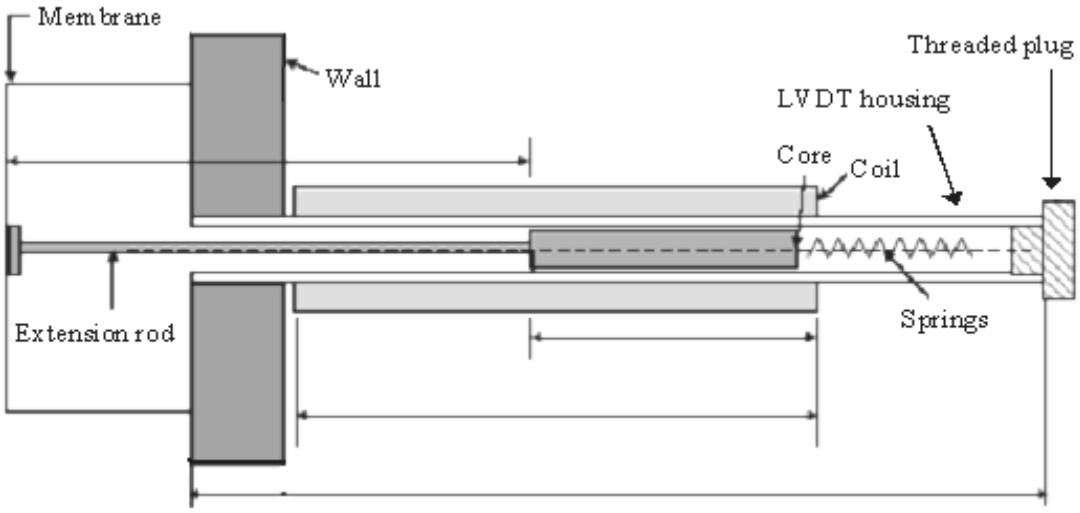

Figure 3.14 Deformation Measuring System

Approximately, 0.1-inch deformation is corresponding to 0.1-voltage reading; however, each of LVDTs has slightly different corresponding magnitude between voltage and deformation. In order to obtain precise corresponding magnitudes (i.e., slopes of calibration curve) from each of LVDTs, voltage versus inch responses were plotted. Figure 3.16 shows an example of the calibration curve and slope from X1(+) face. Table 3.1 is representing all of the slopes of calibration curves from all faces.

4. Stress Application and Control System: In this study, the stress control system consists of digital pressure gages, valves, and manual precision pressure regulators (shown in figure 3.17). It is possible to apply all three independent principal stresses to the specimen. A schematic of the stress control system is shown in figure 3.18. The three pressure regulators can be operated simultaneously, and allows achieving any stress path in the first octant. Three DPG 500 OM, absolute pressure transducers manufactured by Omega Engineering were used to measure the pressures

up to 200 psi (1378 kPa). Data and acquisition system can automatically record and store the transducer output.

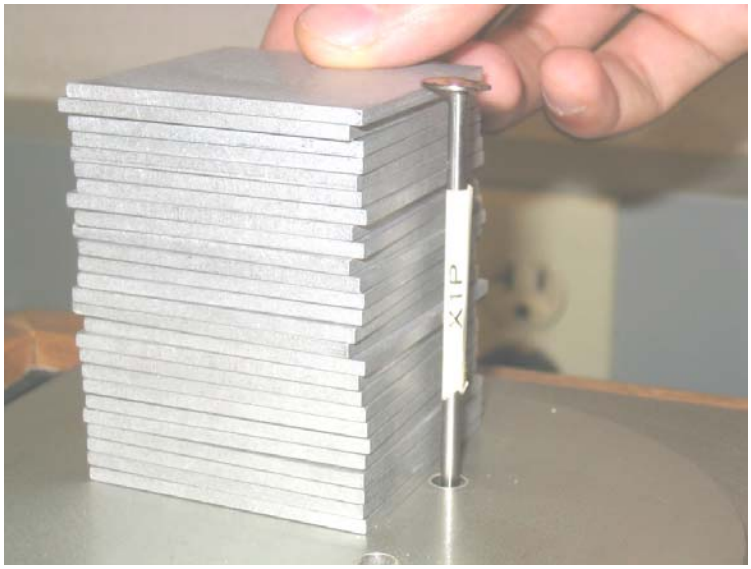

Figure 3.15 Photograph of Calibrating

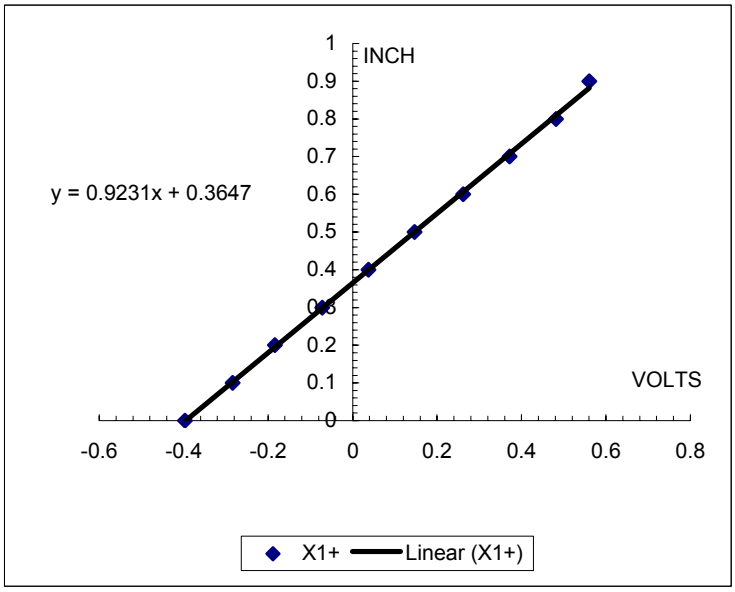

Figure 3.16 Example of Calibration Curve (X1(+) Face)

Table 3.1 Value of the Slope of Calibration Curve

SLOPE	X1+	X2+	X3+	X1-	X2-	X3-
slople (up)	0.9231	1.0395	1.0242	1.0366	1.0295	1.0479
slople (down)	0.9092	1.0136	1.0104	1.0261	1.0013	1.0483
average slope of X	0.9162	1.0266	1.0173	1.0314	1.0154	1.0481
SLOPE	Y1+	Y2+	Y3+	Y1-	Y2-	Y3-
slople (up)	1.0205	1.0287	0.9945	1.0706	1.0292	1.3391
slople (down)	1.0193	1.0238	1.0137	1.0509	1.0200	1.3604
average slope of Y	1.0199	1.0263	1.0041	1.0608	1.0246	1.3498
SLOPE	Z1+	Z2+	Z3+	Z1-	Z2-	Z3-
slople (up)	1.0286	0.9985	1.0216	0.9845	0.9905	0.9787
slople (down)	1.0178	0.9947	1.0138	0.9767	1.0041	0.9972
average slope of Z	1.0232	0.9966	1.0177	0.9806	0.9973	0.9880

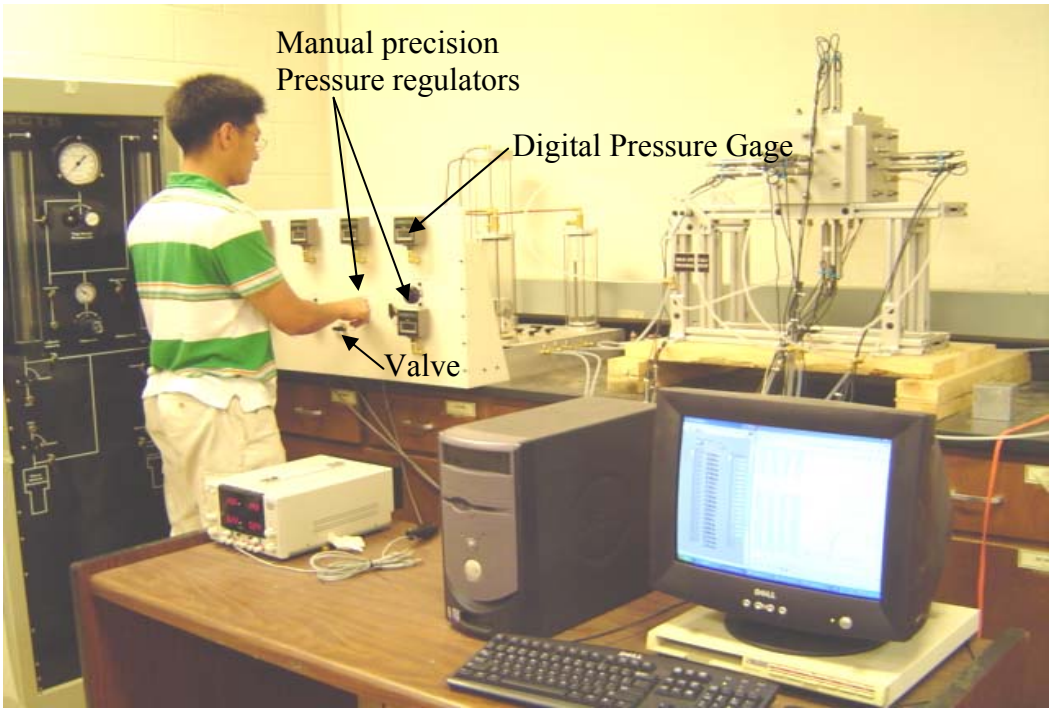

Figure 3.17 Pressure Application Process

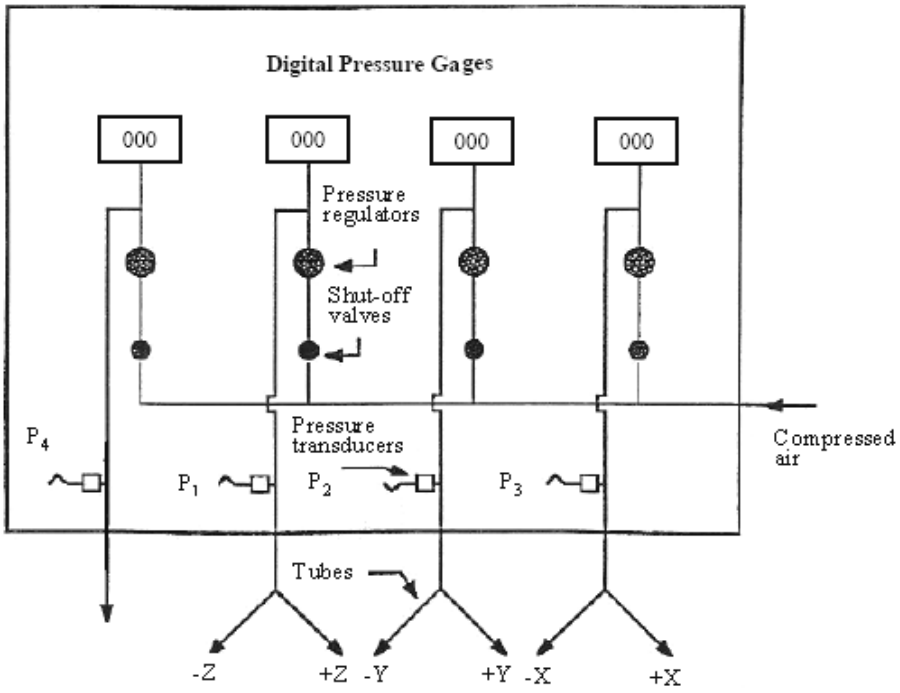

Figure 3.18 Schematic of Stress Application and Control System

5. Membrane: A silicone rubber possessing high tear strength and low stiffness were used to prepare the membranes in the laboratory. In this study, Dow Corning silicone rubber (i.e., Silastic J-RTV type) was used to make the membranes. An assembly consisting of top and bottom molds machined from aluminum was used to design dimensions of membranes. The silicone rubber and curing agent were deaired in a vacuum chamber (shown in figure 3.19) for about 30 minutes after being mixed to a uniform consistency. The mixture was then poured into the bottom mold, and was deaired in the vacuum chamber for another 30 minutes. After curing and deairing, the top mold was carefully bolted, and the mixture was allowed to cure for two days. The membrane was then removed from the mold and stored.

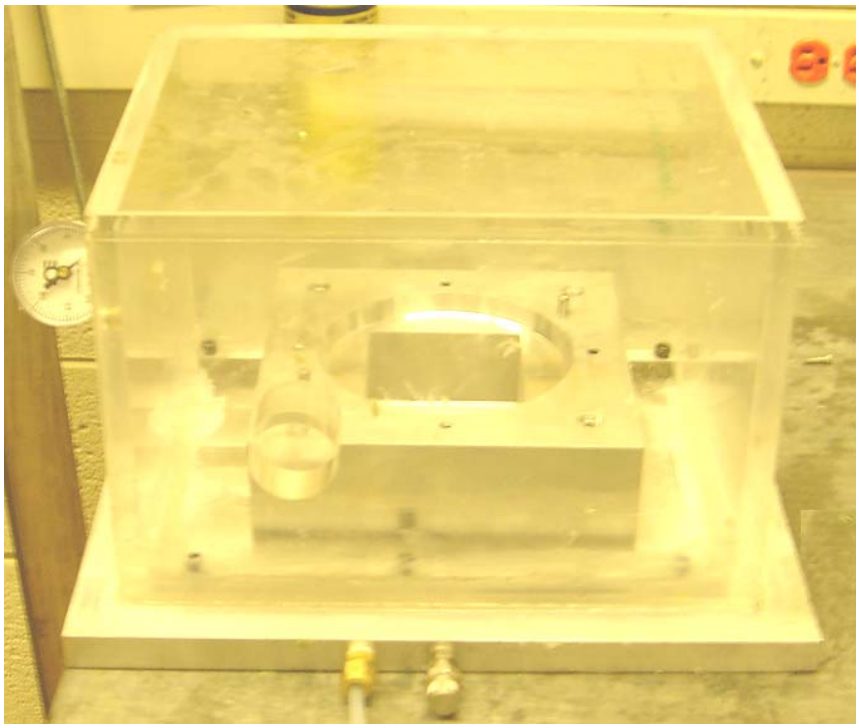

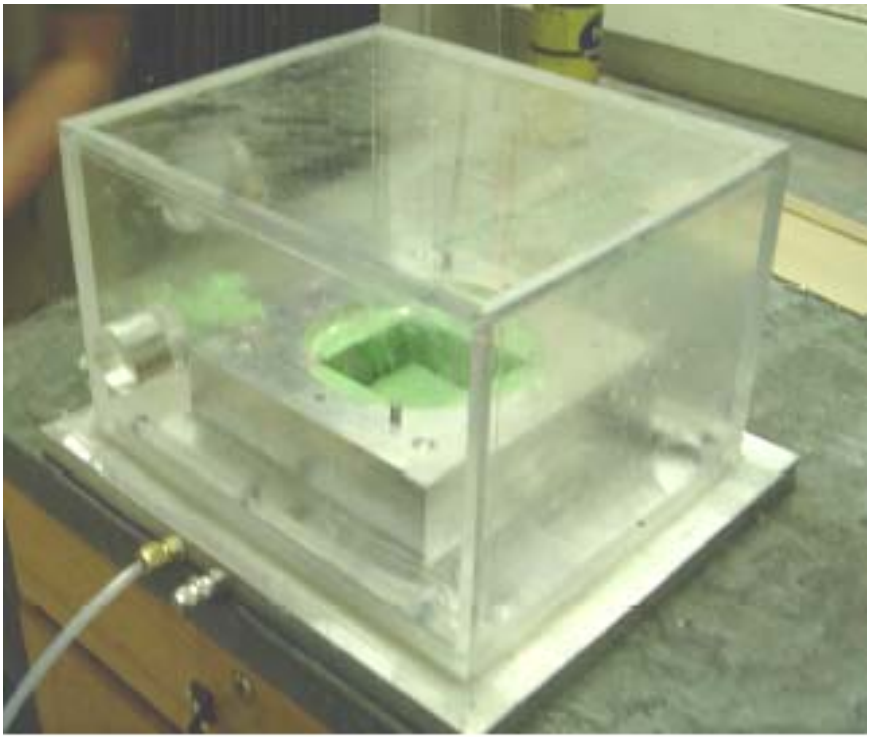

Figure 3.19 Photograph of Vacuum Chamber and Bottom Mold

6. Data Acquisition System: An automated data acquisition system was assembled to control the external pressures applied to the specimen and to monitor and store its resulting deformation. Figure 3.20 shows the schematic of the data acquisition system. A direct interface card (PCI-6603E from National Instruments) is plugged in the CPU of the PC-based computer (shown in figure 3.20).

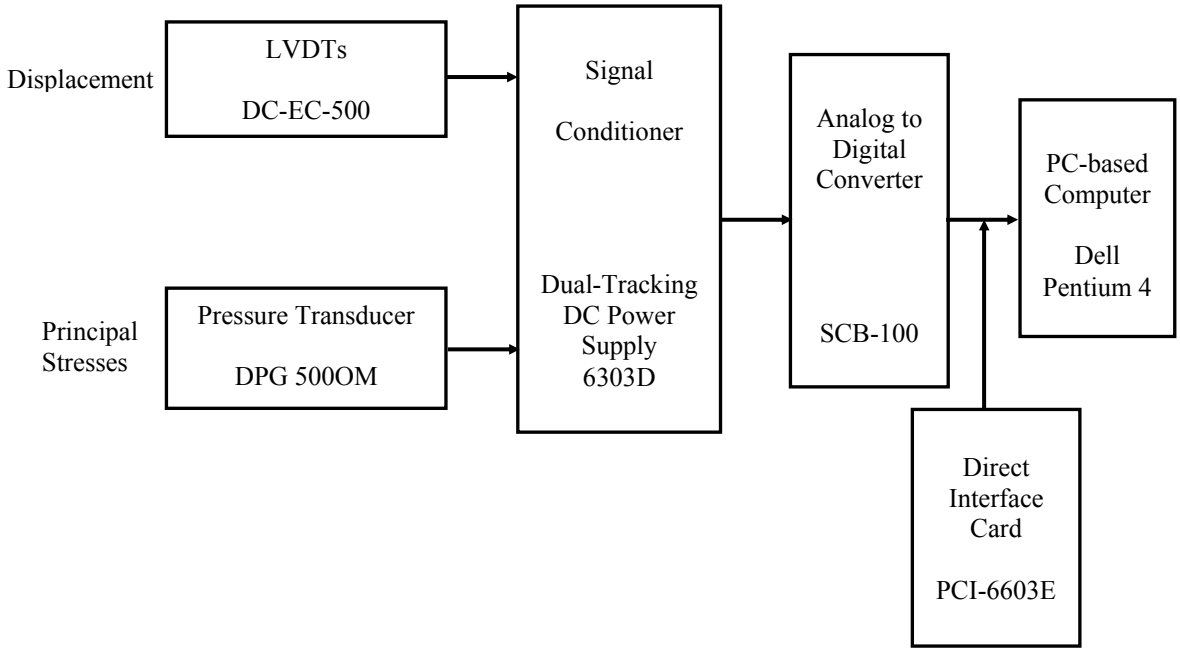

Figure 3.20 Schematic of Data Acquisition System

The analog input signals (Voltage) delivered by the LVDT are converted into digital signals by an analog-to-digital converter (SCB-100 from National Instruments) connected to the direct interface card (PCI-6603E from National Instruments). For signal conditioning, DC Power Supply (6303D from Topward) was used. The data acquisition can handle the 18 LVDTs for deformation and 3 pressure transducers for principal stresses. The raw data (output voltages) was calibrated by using computer

software (Labview 7.0 from National Instruments), and all details regarding calibration of LVDTs is previously mentioned.

3.4 Step-By-Step Assembling Process

Step-by-step procedure for the complete assemblage of the testing setup are summarized and illustrated in the followings: (1) the bottom wall assembly is assembled in figure 3.21; (2) after assembling the bottom wall, the specimen is placed on the bottom wall in figure 3.22; (3) the lateral wall assemblies are assembled in figure 3.23; (4) the top wall assembly is set into place in figure 3.24; and, finally (5) the inlet/outlet hoses of the pressure system are connected to the top, lateral, and bottom wall assemblies in figure 3.25.

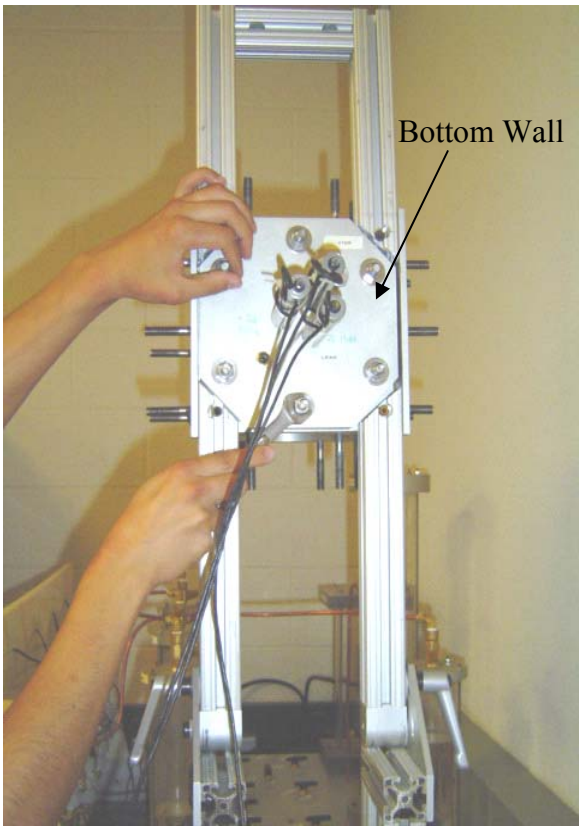

Figure 3.21 Photograph of Bottom Wall Assembling Process

Figure 3.26 shows a photograph of the complete laboratory testing setup. Chapter 4 presents the basic properties of the testing soil and a detailed description of all the experimental variables used in this thesis work.

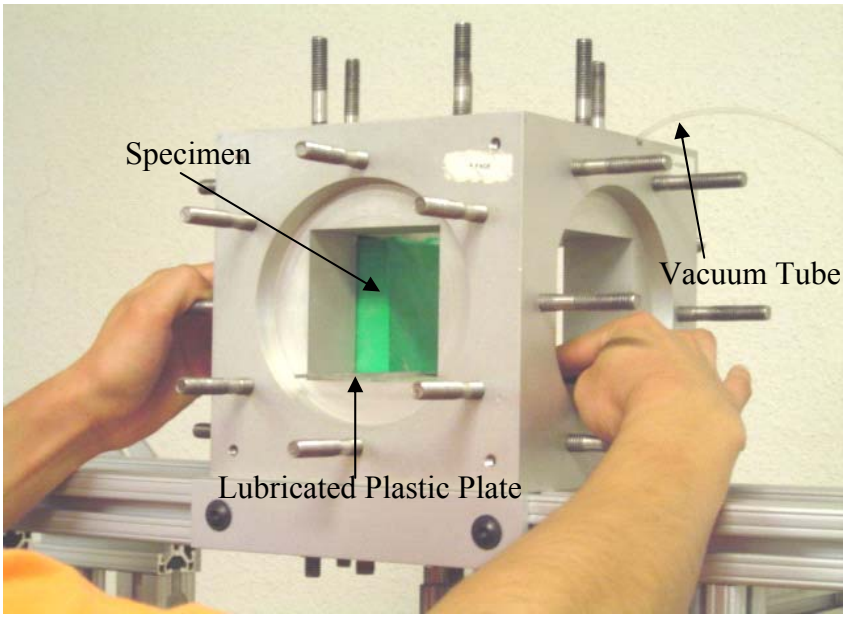

Figure 3.22 Photograph of Specimen Placement

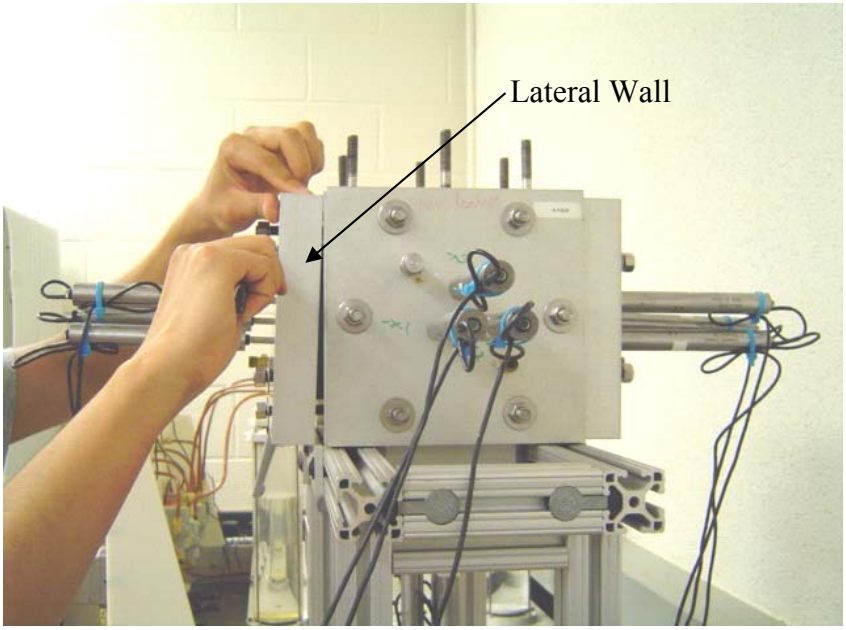

Figure 3.23 Photograph of Lateral Wall Assembling Process

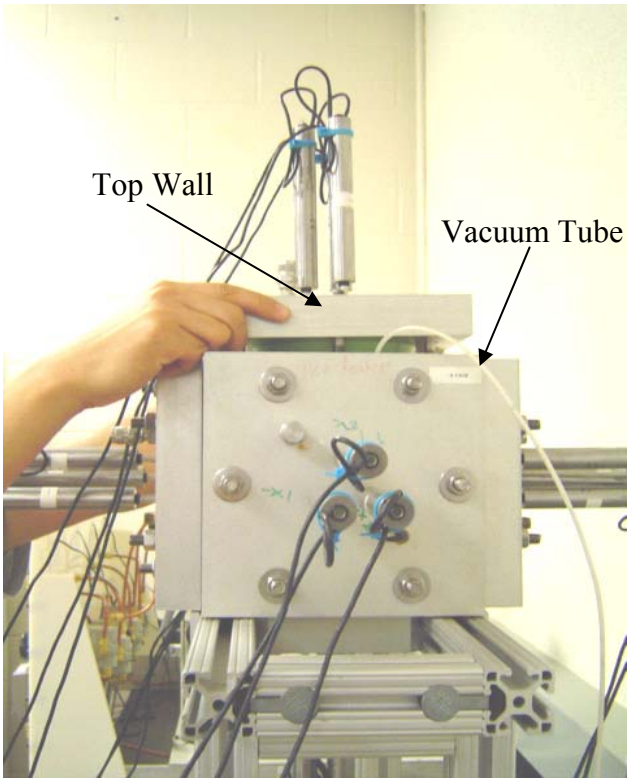

Figure 3.24 Photograph of Top Wall Assembling Process

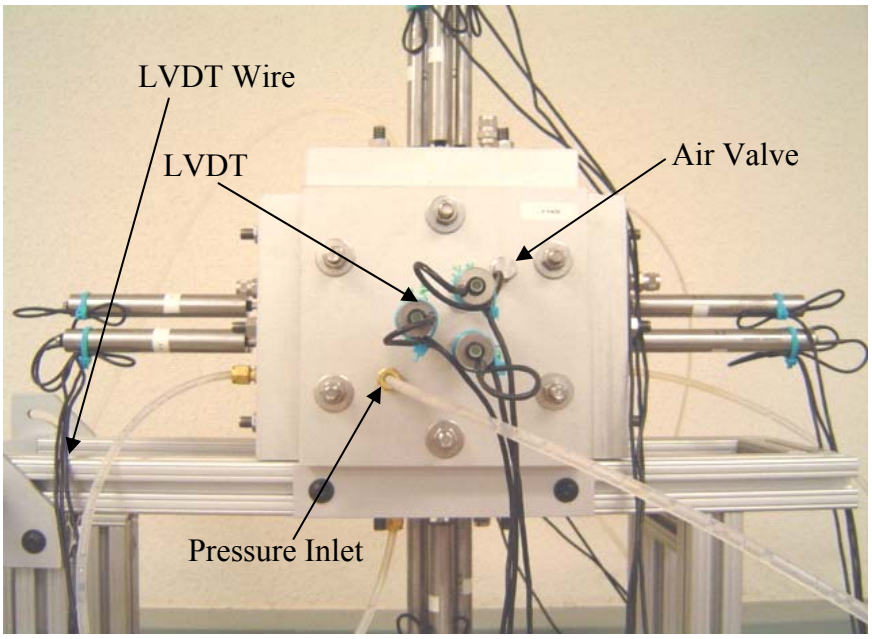

Figure 3.25 Photograph of Pressure inlet/outlet, LVDTs, and Air Valve

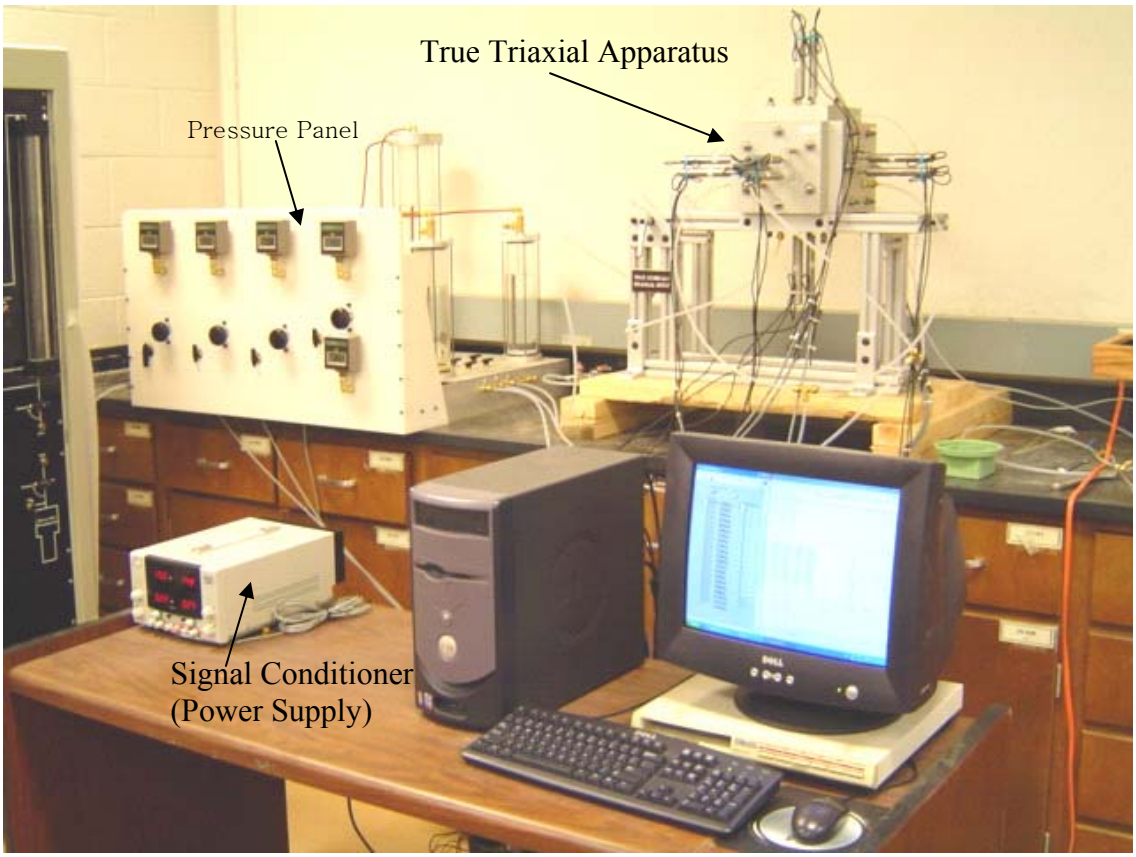

Figure 3.26 Photograph of Complete Laboratory Setup

CHAPTER 4

TESTING SOIL AND EXPERIMENTAL VARIABLES

4.1 Introduction

The experimental program in this thesis work was designed to study the stress-strain-strength behavior of partially saturated silty sand subjected to three-dimensional stress states along a variety of multiaxial stress paths. Partially saturated silty sand samples were artificially prepared at four different moisture contents corresponding to four different values of initial suction prior to testing: air-dried water content corresponding to soil suction of 800 psi (5516 kPa); w = 4.5% corresponding to soil suction of 365 psi (2514 kPa); w = 5.3% corresponding to soil suction of 237 psi (1632 kPa); and w = 6.1% corresponding to soil suction of 150 psi (1035 kPa).

The following sections describe the basic properties of the test soil, including SWCC via filter paper, specimen preparation method and design of pluviation frame, repeatability of specimen preparation process, and all experimental variables for true triaxial testing.

4.2 Testing Soil

The soil tested in this work was artificially prepared by mixing 30% of silt (from north Arlington, Texas) and 70% of clean sand (commercially supplied). The air-dried water content is 2.0% and the maximum dry unit weight attained via pluviation

technique is 14.9 kN/m^3, which corresponds to a moisture content of 5.3%. Sieve analysis (figure 4.1) shows an effective grain size (D_{10}) of 0.15-mm.

The soils classifies as SP-SM according to USCS. The basic engineering properties of the testing soil are summarized in table 4.1.

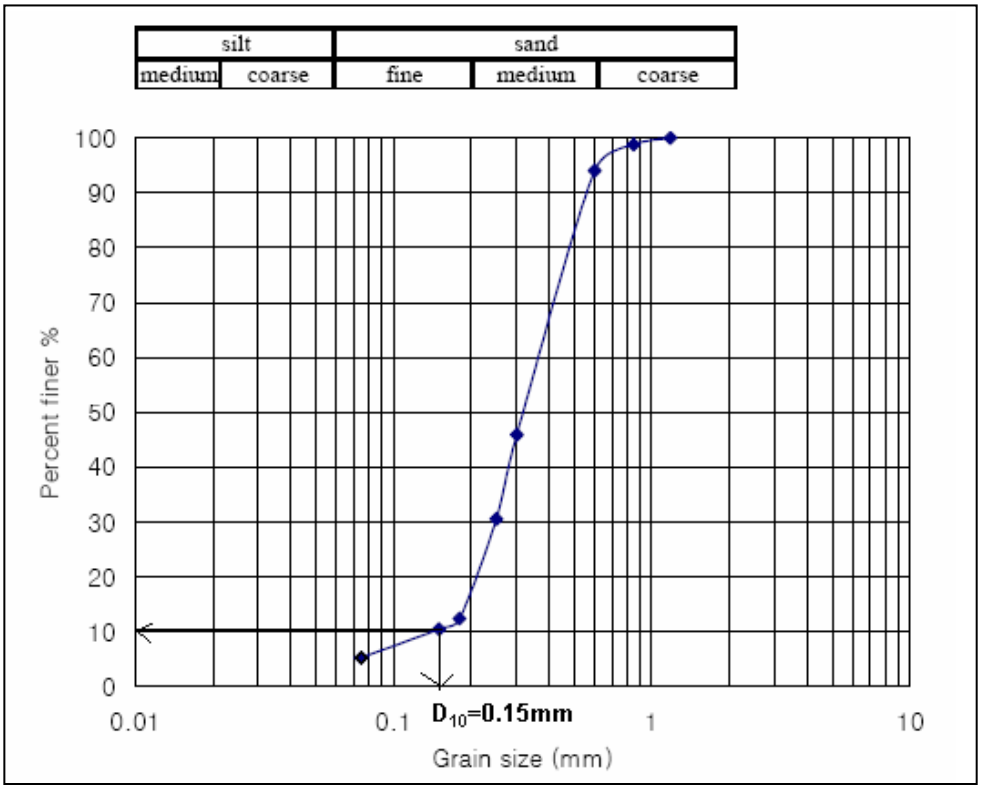

Figure 4.1 Particle Size Distribution of Artificially Prepared Silty Sand

Table 4.1 Basic Engineering Properties of Testing Soil

Property	**Magnitude**
Air-dried water content, w_a (%)	2.0
Air-dried suction, Ψ	800 psi (5516 kPa)
Pluviation optimum moisture content, w_{opt}(%)	5.3
Pluviation maximum dry unit weight, $\gamma_{d\text{-}max}$ (kN/m^3)	14.9
USCS Classification	SP-SM
D_{10} (mm)	0.15

4.3 Pluviation Induced Densities and Moisture Contents

The pluviation-based specimen preparation process with aim of reproducing specimens at extremely low preconsolidation pressure was conducted to prepare soil samples at different moisture contents in table 4.2. All three-inch soil specimens were pluviated in five layers using pluviation technique. Water was added to each layer to achieve target moisture content by spraying. After pluviating, moisture contents were measured and obtained, a series of measurements of suction were performed via filter paper method (refer to section 2.2.3). Soil Water Characteristic Curve (SWCC) was then obtained. This SWCC shows that each of water contents is corresponding to a value of suction as shown in figure 4.2.

Table 4.2 Initial Pluviation-Induced Soil Conditions

Soil Condition	Water Content (%)	Total Water Added (ml)	Dry Unit Weight (kN/m^3)	Void Ratio	Degree of Saturation (%)	Suction (kPa) from SWCC
Air-dried	2	Not Added	14.79	0.804	6.77	5516
85% (dry)	4.5	68.25	14.88	0.793	15.44	2514
Optimum	5.3	80.60	14.92	0.788	18.28	1632
85% (wet)	6.1	92.75	14.91	0.789	21.02	1035

4.4 Repeatability of Specimen Preparation

To verify consistency in the specimen preparation process, a series of repeated specimen preparation trials was first conducted to ensure reproducibility of specimens, prior to true triaxial testing, using a specially designed dual-mesh pluviation frame for 85% dry of optimum, optimum, and 85% wet of optimum moisture contents. All

specimens were identically prepared at different moisture contents via pluviation frame. Moisture content and dry unit weight were then measured. Table 4.3 shows the proof of repeatability during specimen preparation process.

Table 4.3 Proof of Repeatability of Specimen Preparation Process

Soil Condition	Sample	Water Content (%)	Average Water Content (%)	Dry Unit Weight (kN/m^3)	Standard Deviation (S)
85% (dry)	1	4.5	4.4	14.85	10.4
	2	4.1		14.94	
	3	4.5		14.90	
Optimum	1	5.3	5.4	14.92	2.33
	2	5.2		14.91	
	3	5.7		14.88	
85% (wet)	1	6.1	6.0	14.91	0.04
	2	5.9		14.91	
	3	5.8		14.90	

4.5 Experimental Variables

The corresponding value of total suction for a given moisture content was obtained from the soil water characteristic curve (SWCC) shown in figure 4.2.

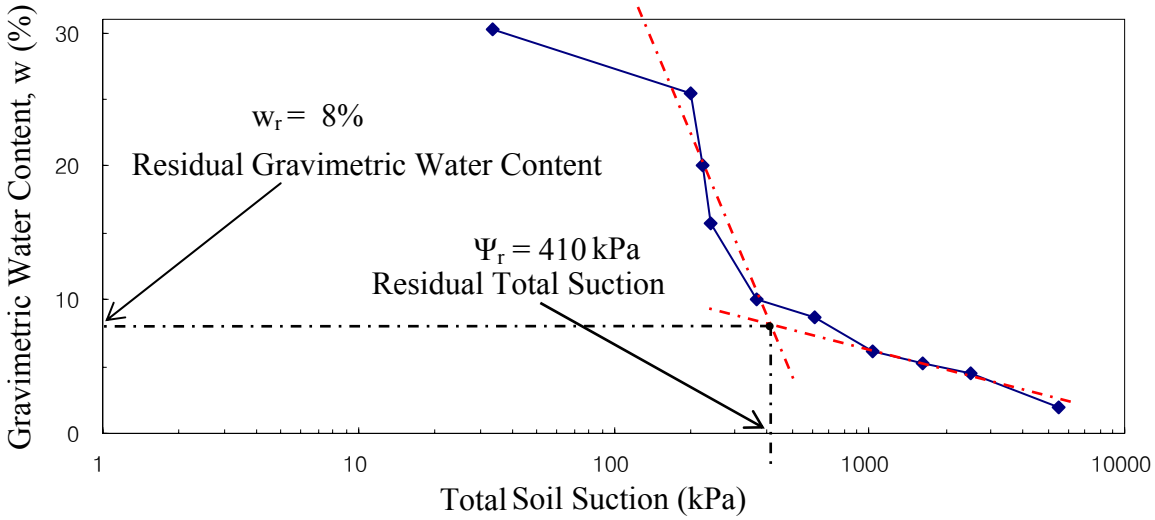

Figure 4.2 Soil Water Characteristic Curve (SWCC) of Silty Sand

Isotropic confining pressures during true triaxial testing ranged from 5 psi to 40 psi. Table 4.4 summarizes all the experimental variables used in this thesis work for true triaxial testing. The low range of moisture contents, from 2% to 6.1%, was selected to test soil at higher values of pluviation-induced total suctions, that is, for suction values beyond the residual total suction (Ψ_r), as shown in figure 4.2.

Table 4.4 Experimental Variables Used for True Triaxial Testing

Variable	**Number**	**Description**
Soil type	1	• Silty Sand (70% Sand and 30% Silt) • Pluviation optimum moisture content, w_{opt} = 5.3% • Pluviation maximum dry unit weight, $\gamma_{d\text{-}max}$ = 14.9 kN/m^3 • USCS Classification = SP-SM
Initial moisture content	3	• 85% dry of optimum, w = 4.5 % • Optimum, w = 5.3 % • 85% wet of optimum, w = 6.1 %
Suction	4	• Suction of air-dired, Ψ = 5516 kPa (800 psi) • Suction of 85% dry of optimum, Ψ = 2514 kPa (365 psi) • Suction of optimum, Ψ = 1632 kPa (237 psi) • Suction of 85% wet of optimum, Ψ = 1035 kPa (150 psi)
Confining pressure	5	• 5 psi • 10 psi • 20 psi • 30 psi • 40 psi
Stress path	5	• Hydrostatic compression (HC) • Conventional triaxial compression (CTC) • Triaxial compression (TC) • Triaxial extension (TE) • Simple shear (SS)

4.6 Specimen Preparation Method and Placement

All lateral walls of the specimen preparation mold were assembled with the connection to outer vacuum in figure 4.3.

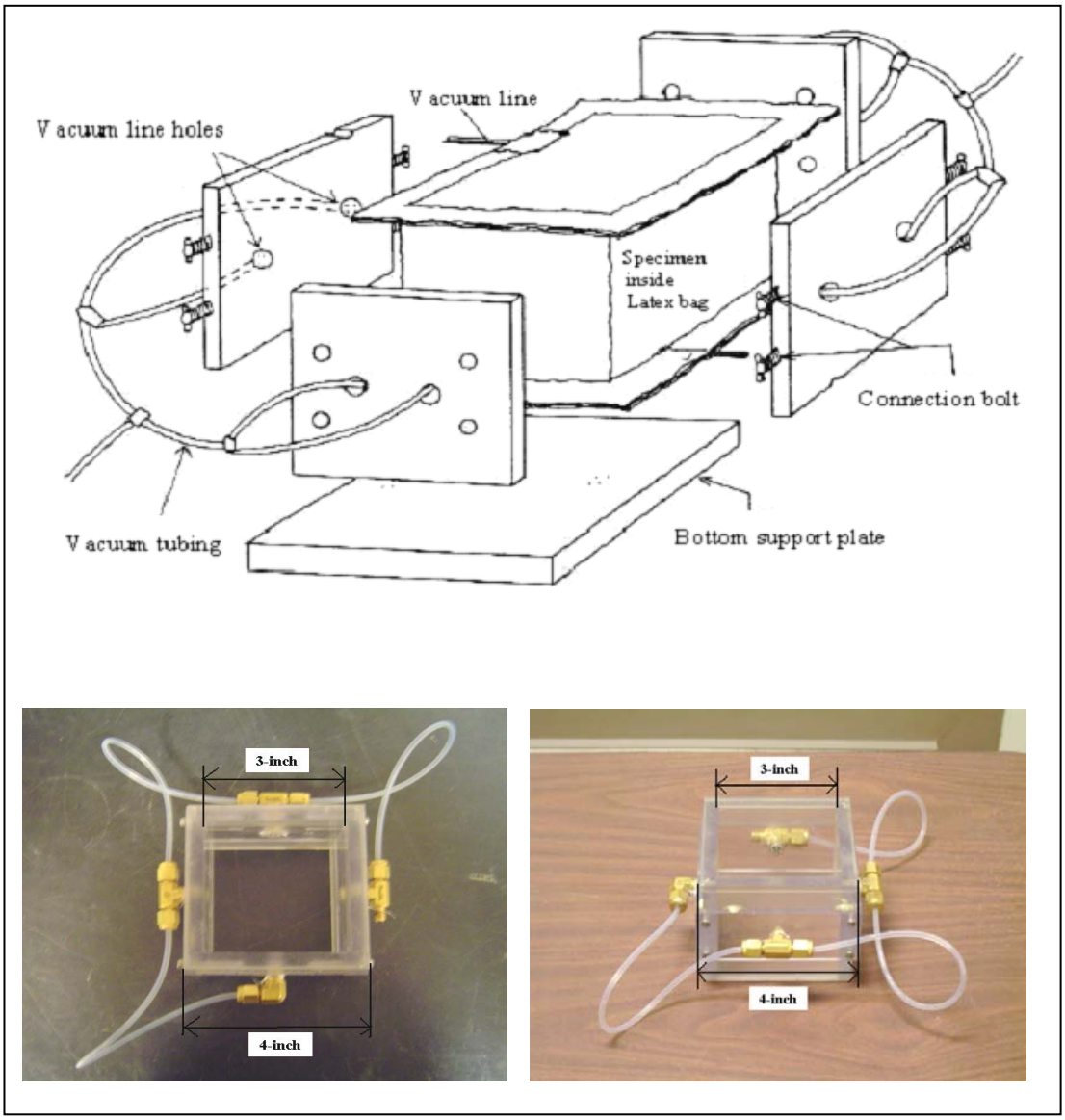

Figure 4.3 Schematic and Photograph of Specimen Preparation Mold

Pieces of latex rubber membrane for lateral walls were glued together and rolled onto insides of lateral walls. The bottom piece of latex rubber membrane placed on the

bottom support plate was glued to the lateral pieces of latex rubber. In order to hold the latex rubber membrane tight to the lateral walls of the mold without wrinkles and bubbles, suction was applied through vacuum ports. The artificially mixed soil (silt and sand) was then pluviated in five equal layers into a specially designed, 3-in by 3-in, 3-in in height, transparent specimen preparation mold (shown in figure 4.3) using a dual-mesh pluviation frame (shown in figure 4.4).

Each layer was provided with the necessary amount (ml) of water calculated from the desired moisture content in table 4.2. After pluviation was completed, a thin nylon tube was inserted through the top groove of the mold. The inside end of the tube was covered with filter paper. The top piece of latex rubber membrane was then placed and glued to the inside latex rubber to seal the specimen completely. Even during testing, specimens were covered with membranes. The grease was used to seal between groove and tube to prevent leakage of vacuum. After all process stated above, the specimen was allowed to seat for 24 hours to allow for uniform suction equalization throughout soil. Before the specimen was placed, a vacuum was applied for handling purpose. Apart from the vacuum, the surfaces of the membranes were lubricated with a thin film of grease to eliminate friction. A thin lubricated plastic plate was then placed on the Z(-) face (shown in figure 3.22) to slide and set in the cubical frame.

4.7 Pluviation Frame Design

The frame used for pluviation of specimens is shown in figure 4.4. Mixed soil (silt and sand) is delivered from funnel into two diffuser meshes along a wooden guide.

(a)

(b)

Figure 4.4 (a) Photograph of Pluviation Frame; (b) Photograph of Water Spraying

The normal procedure is to fill the specimen preparation mold to slightly above the rim prior to carefully scraping off. The principal features of the frame are: (1) the opening size of the diffuser meshes is 1.19-mm (equivalent to No. 16 sieve); (2) and,

mesh #2 at the top to break up initial flow and then mesh #1 below to ensure an even spread. In this study, two meshes were used. The specially designed, 20-cm by 20-cm, 58.5-cm in height, guide frame minimizes dispersion of the sand rain and ensures that the concentration is uniform across the specimen preparation mold. Pluviation frame shows higher density comparing to free-fall pouring as shown in table 4.5. Figure 4.5 shows a detailed schematic of the pluviation frame.

Table 4.5 Results of Density Tests of Clean Sand

Type	Weight (kg)			Unit Weight (kN/m^3)		
	1st	2nd	3rd	1st	2nd	3rd
Pluviation	0.74	0.74	0.74	16.51	16.51	16.51
Pouring	0.65	0.67	0.64	14.48	14.90	14.25

The following chapter presents a comprehensive analysis of all true triaxial test results.

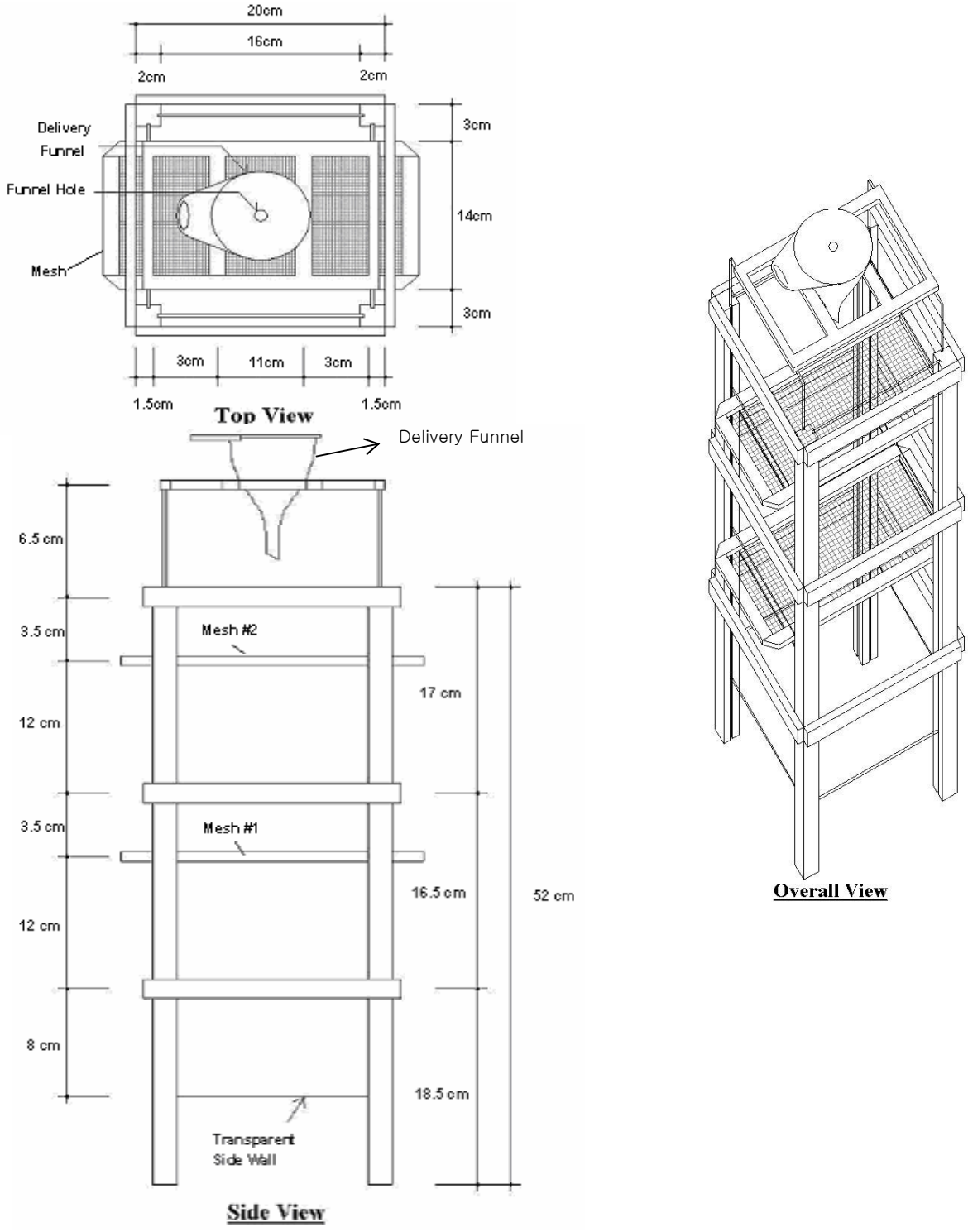

Figure 4.5 Schematic of Pluviation Frame Design

CHAPTER 5

ANALYSIS OF TEST RESULTS

5.1 Introduction

In this thesis work, a total of 56 true triaxial tests were performed on 56 specimens of artificially mixed silty sand, combining all the experimental variables described in chapter 4.

The present chapter presents a comprehensive analysis of all tests results, focusing on stress-strain of data obtained in the new true triaxial device from silty sand pluviated at different moisture contents (w) corresponding to different suctions (s).

5.2 Specimen Notation

Table 5.1 shows the notation symbols used in this thesis work to facilitate the reading of all variables intervening in the stress-strain-strength behavior of a given specimen, particularly those variables referred to stresses, strains, and stress paths.

5.3 Hydrostatic Compression (HC) Test

A series of 4 HC tests were successfully conducted in the new cubical setup on 4 specimens of artificially prepared silty sand at different moisture contents referring to the values of initial suction, Ψ = 5516 kPa (800 psi), 2514 kPa (365 psi), 1632 kPa (237 psi), 1035 kPa (150 psi). HC test results are presented in figure 5.1. The three principal strains measured are plotted against mean pressure in figure 5.1, as well. Figure 5.2

shows the total volumetric strain response. It can be noted that as the initial total suction increases, the volumetric stiffness of the silty sand also increases.

Table 5.1 Notation Symbols Used for True Triaxial Test

Symbol	Description
CTC	Conventional Triaxial Compression
HC	Hydrostatic Compression
SS	Simple Shear
TC	Triaxial Compression
TE	Triaxial Extension
p	Net Mean Stress = $(1/3)(\sigma_1 + \sigma_2 + \sigma_3)$
q	Deviatoric Stress = $(\sigma_1 - \sigma_2)$
ϵ_1	Major Principal Strain
ϵ_2	Intermediate Principal Strain
ϵ_3	Minor Principal Strain
ϵ_v	Volumetric Strain = $(1/3)(\epsilon_1 + \epsilon_2 + \epsilon_3)$
ϵ_{ij}	Strain Tensor
σ_1	Major Principal Stress
σ_2	Intermediate Principal Stress
σ_3	Minor Principal Stress
σ_{ij}	Stress Tensor
σ_{oct}	Octahedral Normal Stress = $\frac{\sigma_1 + \sigma_2 + \sigma_3}{3}$
τ_{oct}	Octahedral Shear Stress = $\frac{1}{3}\sqrt{(\sigma_1 - \sigma_2)^2 + (\sigma_2 - \sigma_3)^2 + (\sigma_3 - \sigma_1)^2}$
b	Stress Ratio = $(\sigma_2 - \sigma_3) / (\sigma_1 - \sigma_3)$

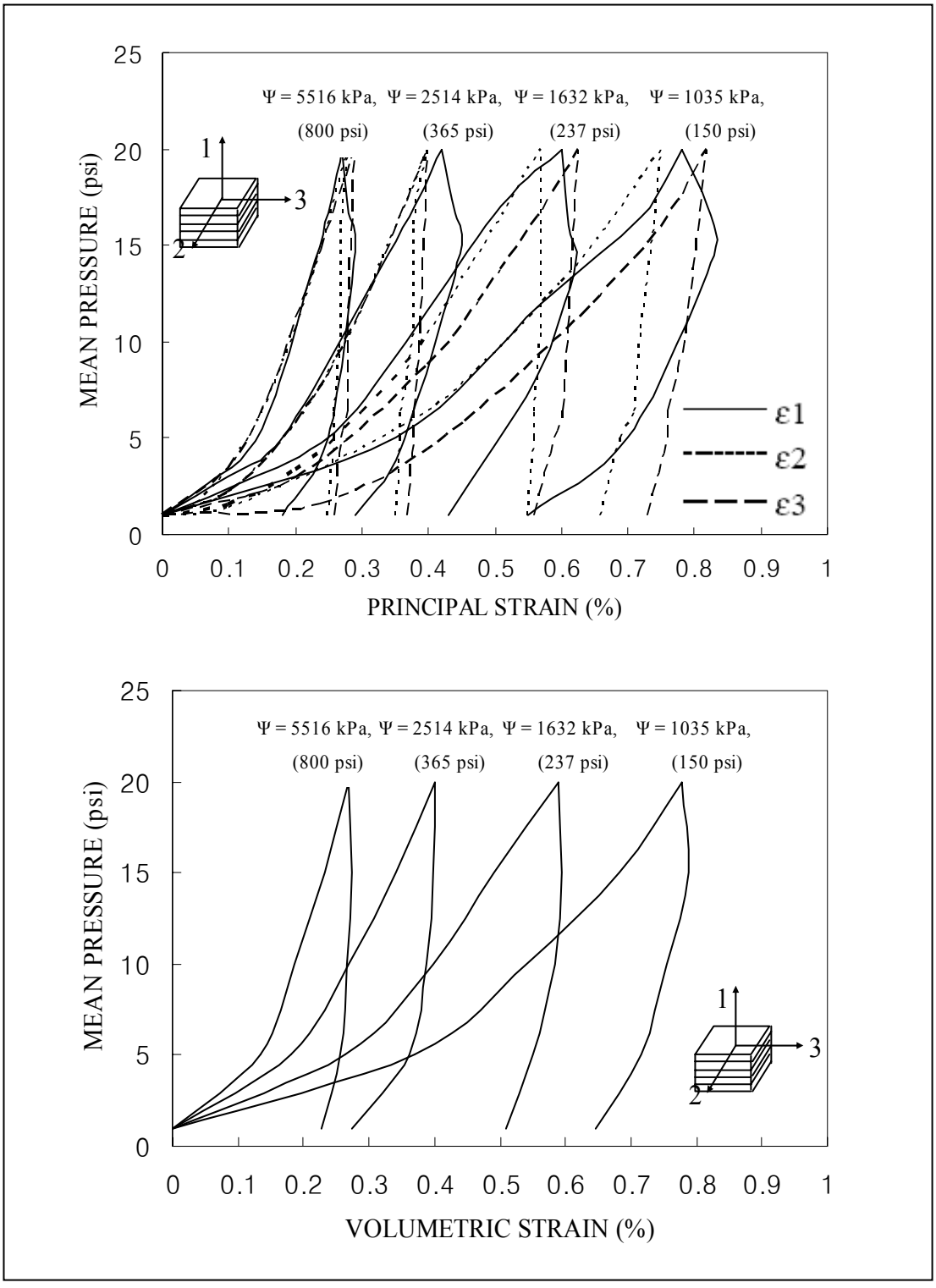

Figure 5.1 Hydrostatic Compression Test Results (p = 0 - 20 psi)

5.4 Repeatability of HC Tests

To establish the new true triaxial testing equipment functionality and repeatability of test results, a series of 4 additional HC tests were performed on four specimens of silty sand at different moisture contents referring to the values of suction of Ψ = 5516 kPa (800 psi), 2514 kPa (365 psi), 1632 kPa (237 psi), and 1035 kPa (150 psi) after first four HC tests.

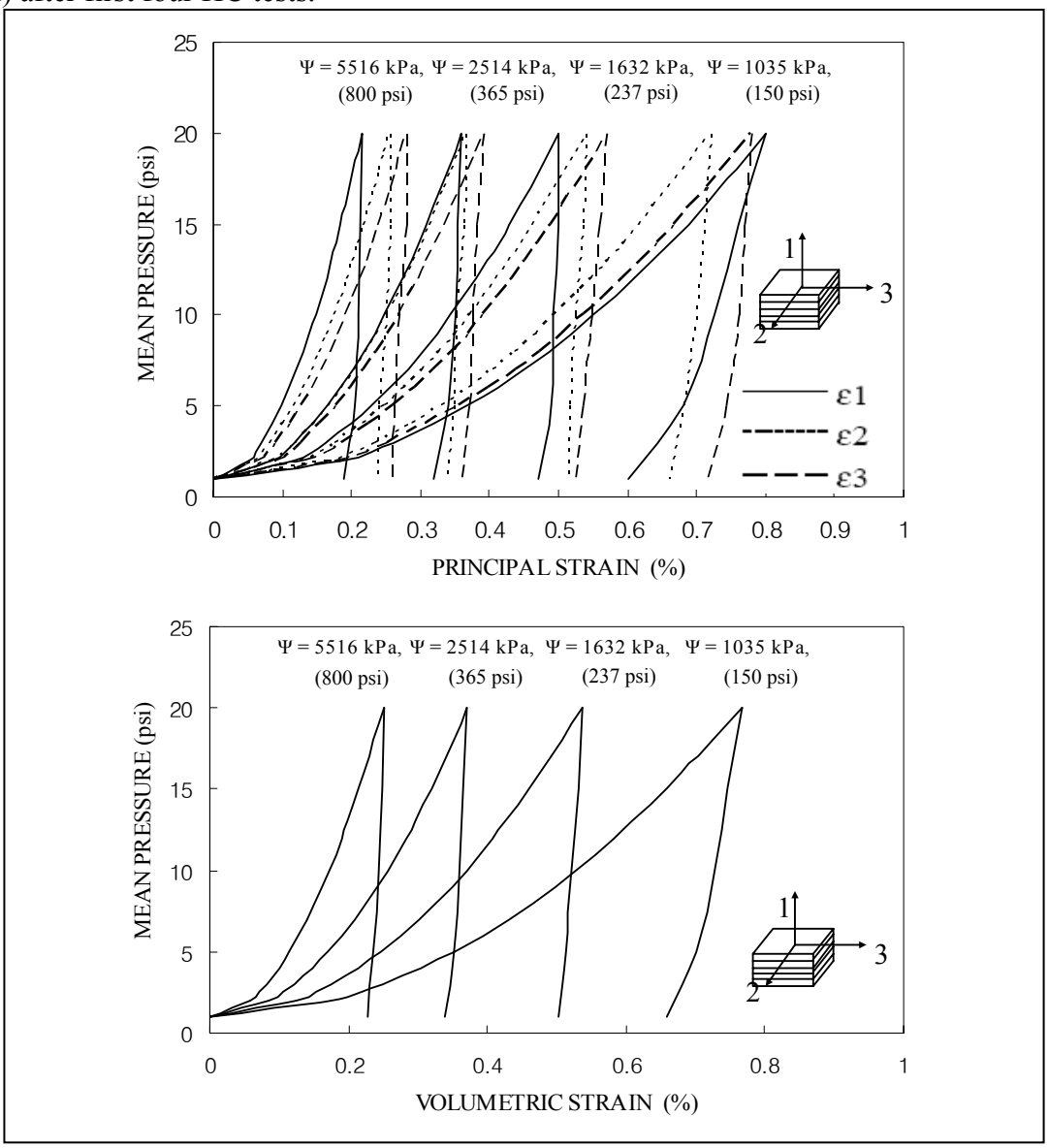

Figure 5.2 Hydrostatic Compression Test for repeatability (p = 0 - 20 psi)

In each test, stress increment ($\Delta\sigma$) was 1 psi/hr, and the maximum hydrostatic pressure was 20 psi. Figure 5.2 shows similar trend to figure 5.1. Apart from similar trends of pressure versus strain plots in figure 5.1, figure 5.2 also shows the influence of initial total suction, increasing the volumetric stiffness along with an increase in suction. As shown in figure 5.2, plots and results from these quality control tests proved reasonably repeatable. In figure 5.3, bulk modulus, K, was obtained from figure 5.2 and found as function of total suction (Ψ). As value of total suction increases, value of bulk modulus increases. The increase in bulk modulus to total suction presents stiffer volumetric strain.

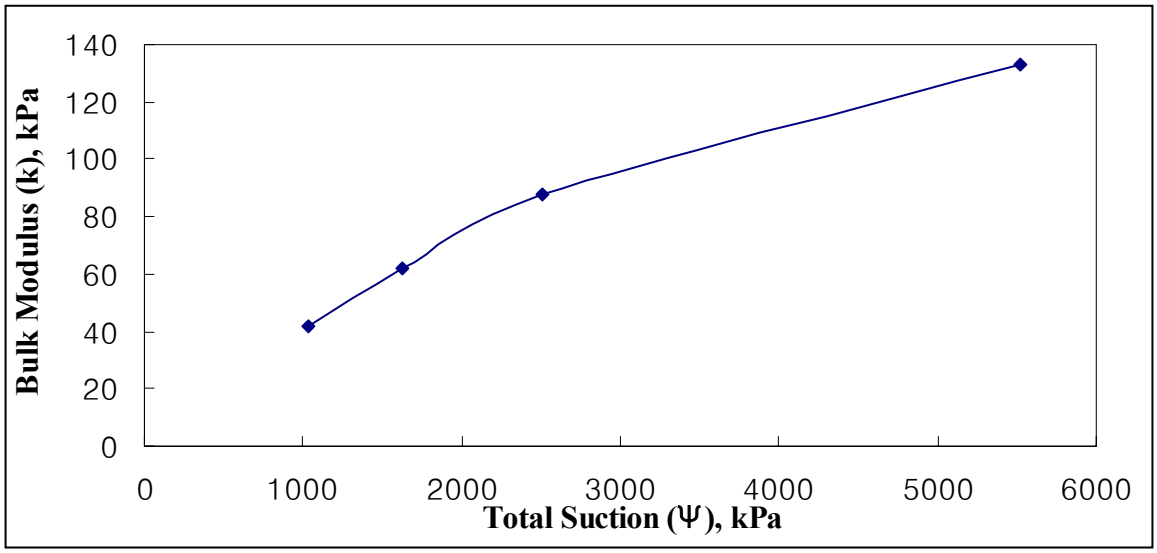

Figure 5.3 Bulk Modulus as Function of Total Suction

5.5 Influence of Octahedral Stress (σ_{oct})

5.5.1 Conventional Triaxial Compression (CTC) Tests

A series of 12 CTC tests were successfully conducted in the new cubical setup on 12 specimens of artificially prepared silty sand at different moisture contents referring to the values of suction, Ψ = 5516 kPa (800 psi), 2514 kPa (365 psi), 1632 kPa (237 psi), and 1035 kPa (150 psi). Figures 5.4 to 5.7 show deviatoric stress versus principal strain response and volumetric strain versus major principal strain response from the twelve tests. The CTC tests were performed under effective confining pressures of 5, 10, and 20 psi. In these tests, the intermediate and minor principal stresses were maintained constant while increasing the major principal stress. It can be observed from figure 5.4 to 5.7 that the principal strains in x and y direction are slightly expansive while the stress in z direction is compressive. The results from the twelve tests show no significant variation of the intermediate (ϵ_2) and minor principal strain (ϵ_3) while the major principal strain (ϵ_1) is significantly compressive. Figure 5.4 shows the volumetric strains (σ_{oct} = 10 and 20 psi) are dilative while the volumetric strain (σ_{oct} = 5 psi) is reflecting the loose nature of the pluviated specimen. In figure 5.5, the volumetric strains (σ_{oct} = 5 and 20 psi) are dilative while the volumetric strain (σ_{oct} = 10) is reflecting the loose nature of the pluviated specimen. In figure 5.6, all the volumetric strains (σ_{oct} = 5, 10, 20 psi) are reflecting the loose nature of the pluviated specimen. In general, the volumetric strains (= 5 and 10 psi) are reflecting the loose nature of the pluviated specimen in figure 5.7, whereas the volumetric strain (σ_{oct} = 20 psi) is predominantly dilative.

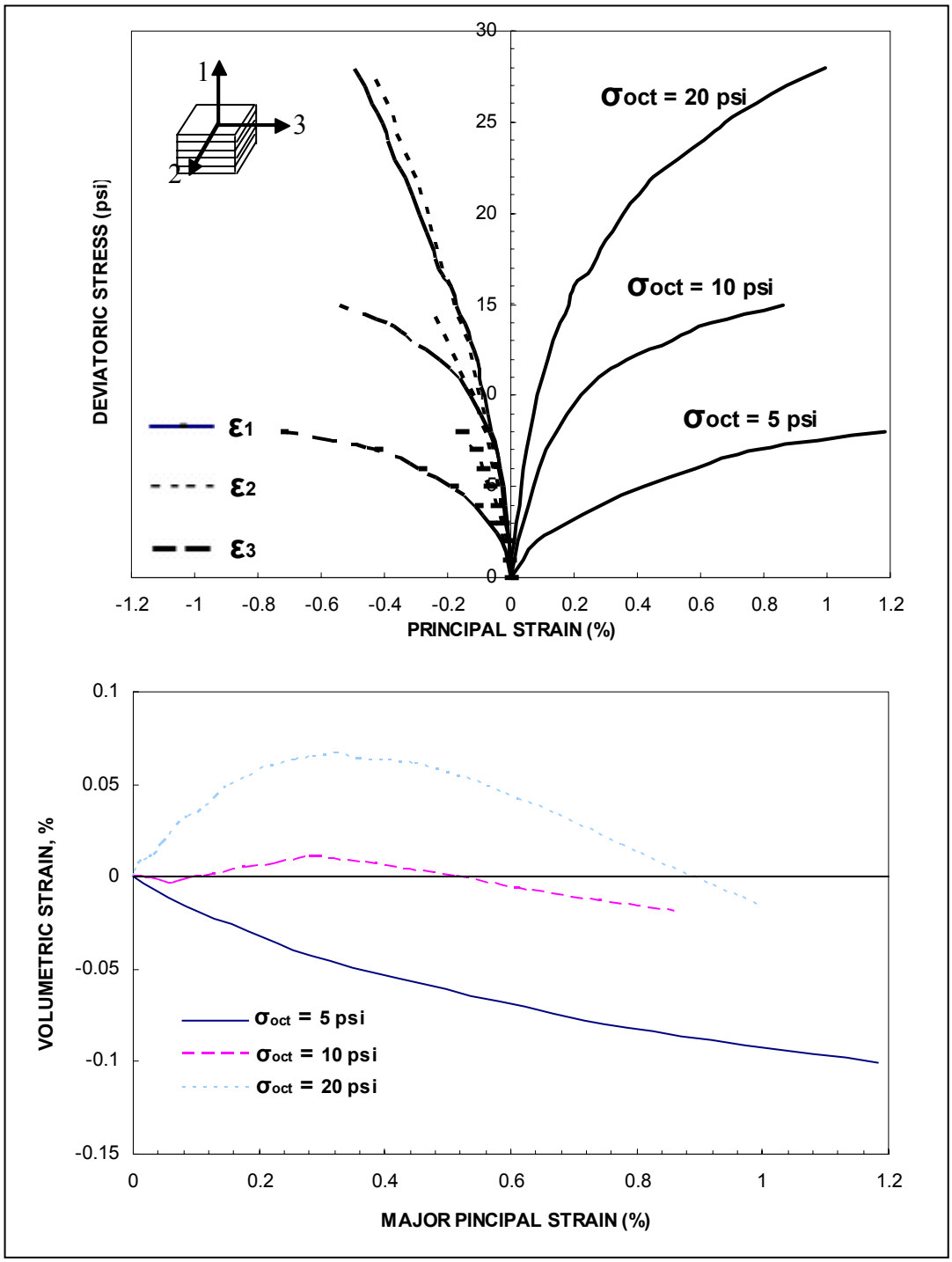

Figure 5.4 CTC Results for Air-Dried Silty Sand (Ψ = 800 psi, w = 2.0%)

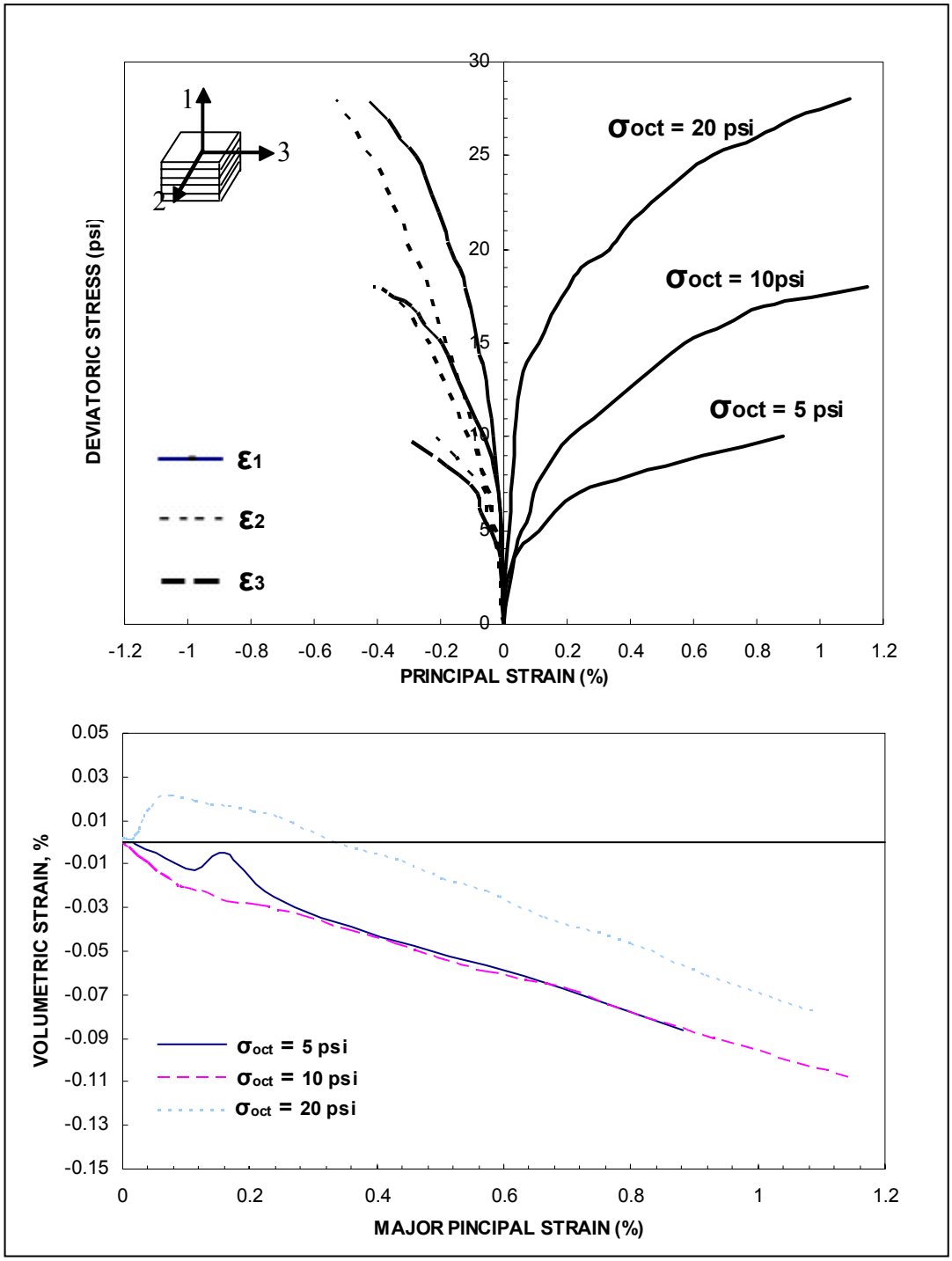

Figure 5.5 CTC Results of 85% Dry for Optimum Silty Sand (Ψ = 365 psi, w = 4.5%)

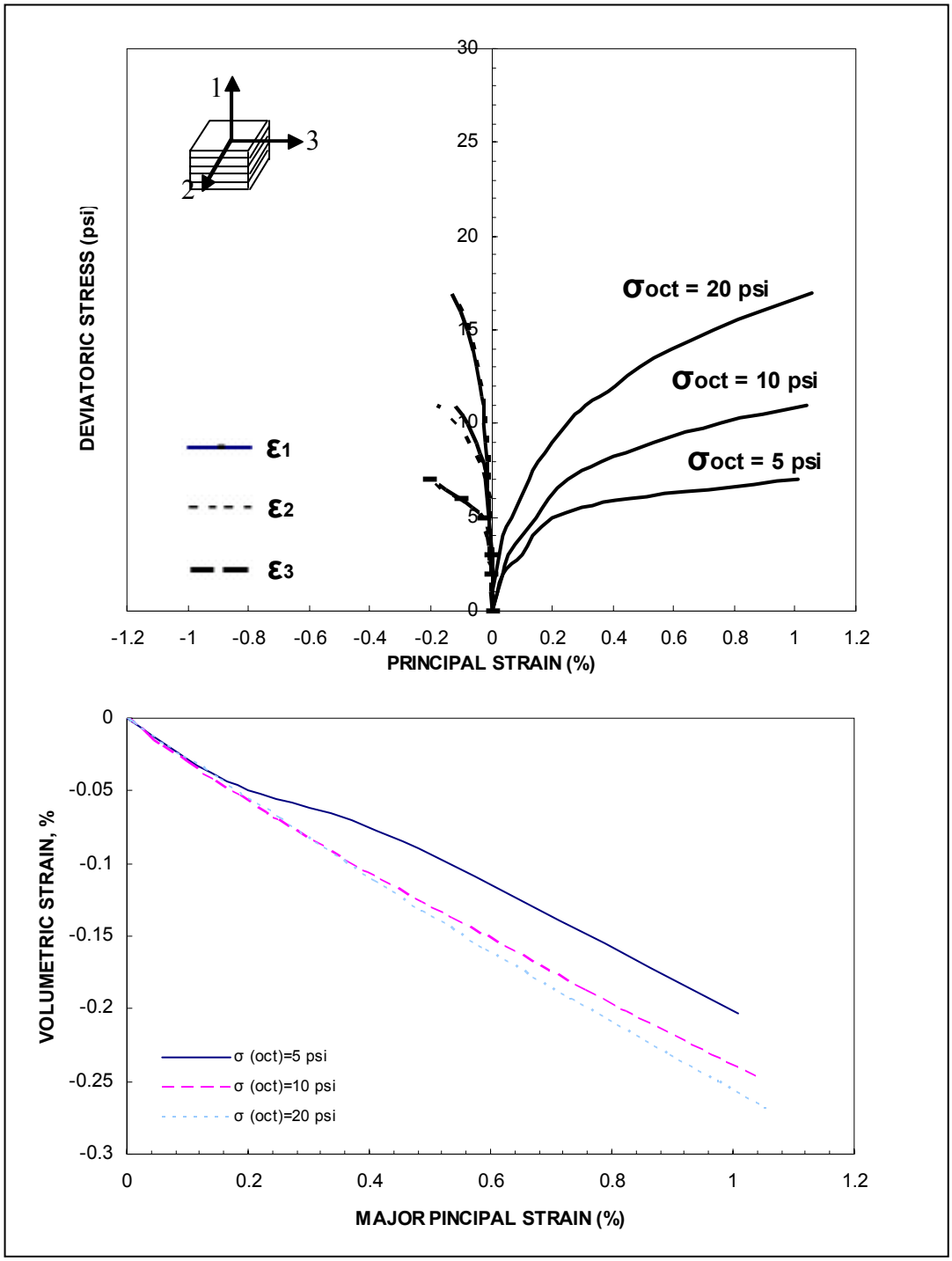

Figure 5.6 CTC Results for Optimum Silty Sand (Ψ = 237 psi, w = 5.3%)

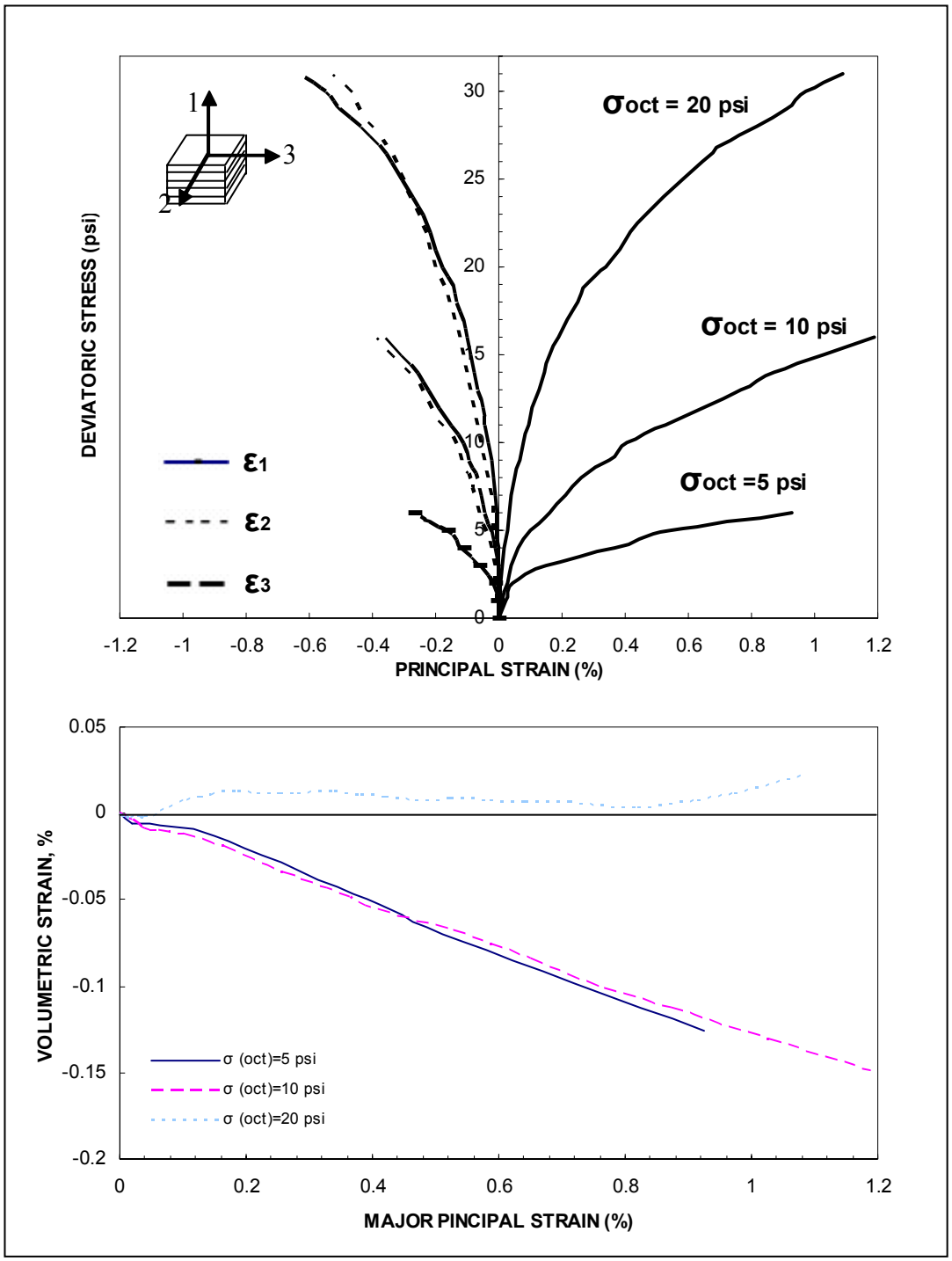

Figure 5.7 CTC Results of 85% Wet for Optimum Silty Sand (Ψ = 150 psi, w = 6.1%)

5.5.2 Triaxial Compression (TC) Tests

A series of 12 TC tests were successfully performed in the new cubical setup on 12 specimens of artificially prepared silty sand at different moisture contents, referring to the initial values of suction of Ψ = 5516 kPa (800 psi), 2514 kPa (365 psi), 1632 kPa (237 psi), and 1035 kPa (150 psi) under effective confining pressures of 20, 30, and 40 psi.

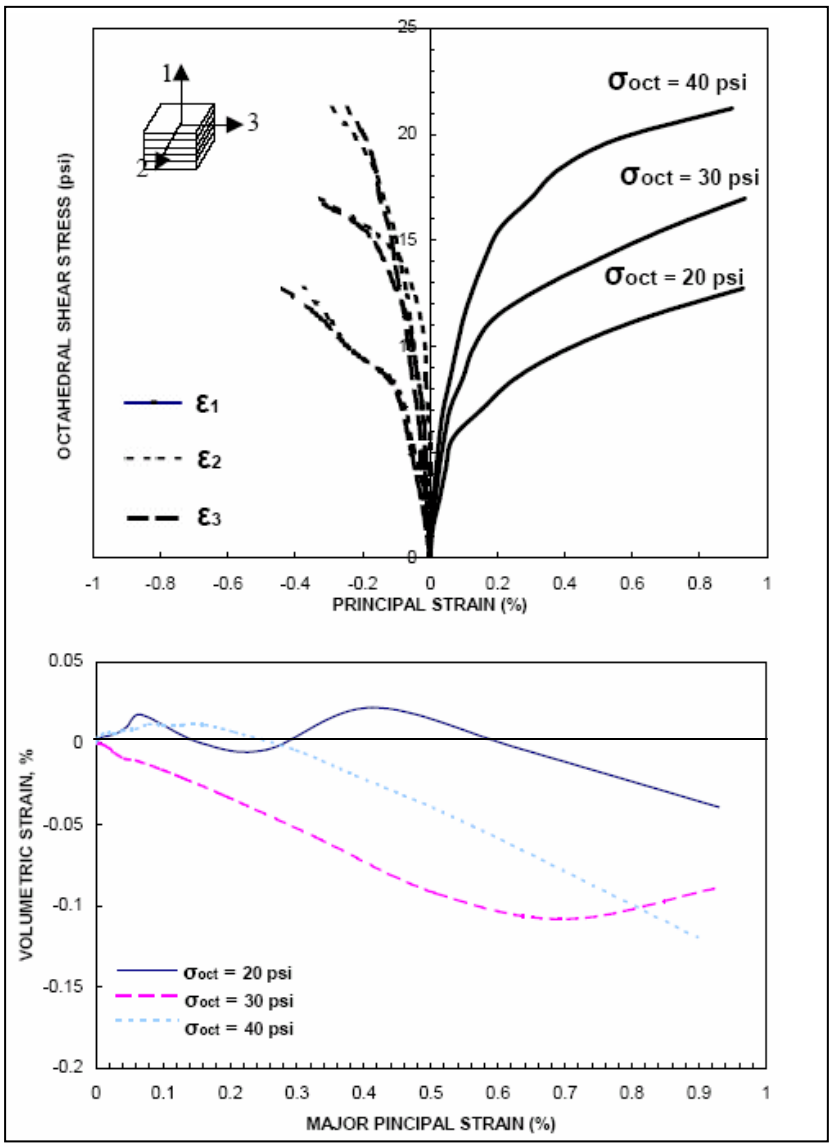

Figure 5.8 TC Results for Air-Dried Silty Sand (Ψ = 800 psi, w = 2.0%)

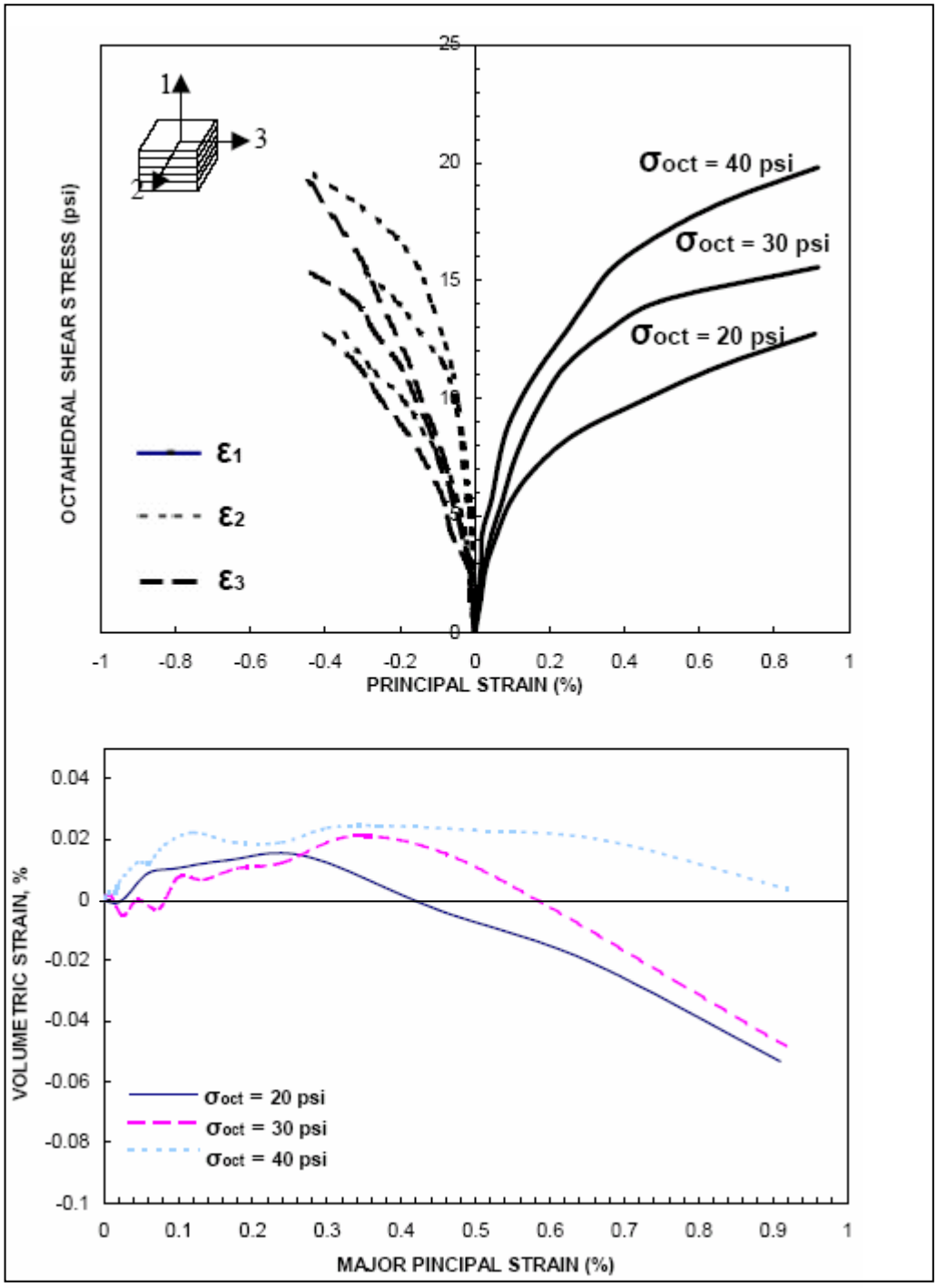

Figure 5.9 TC Results for 85% Dry of Optimum Silty Sand (Ψ = 365 psi, w = 4.5%)

In these tests, values of two principal stresses equally decreased (i.e., $\Delta\sigma_2 = \Delta\ \sigma_3 = -\Delta\sigma_1/2$) while the other stress was increased, such that σ_{oct} remained constant. As the minor (σ_3) and intermediate (σ_2) stresses were decreased equally, the corresponding strains (ϵ_3, ϵ_2) were found expansive, indicating isotropic behavior.

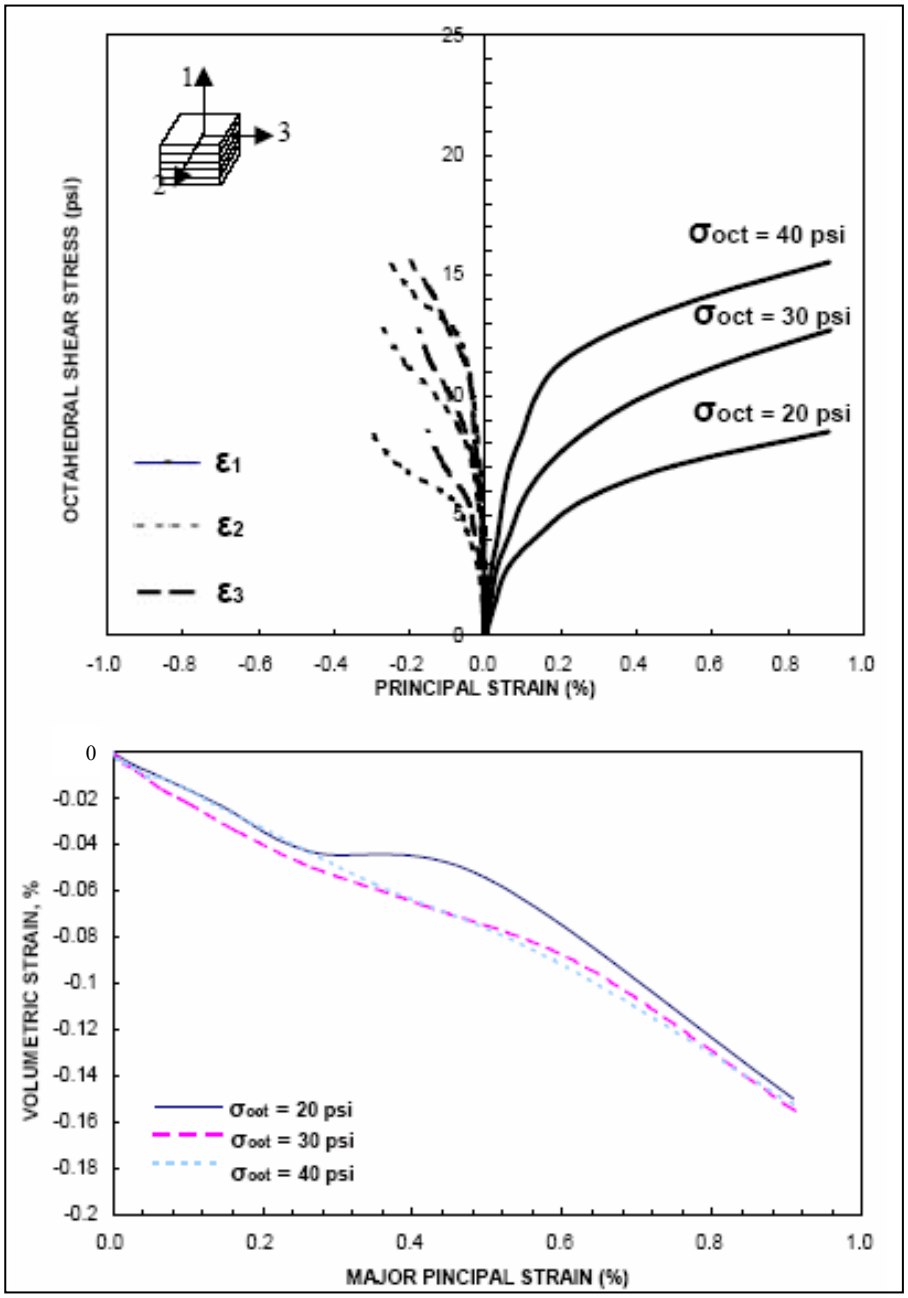

Figure 5.10 TC Results for Optimum Silty Sand (Ψ = 237 psi, w =5.3 %)

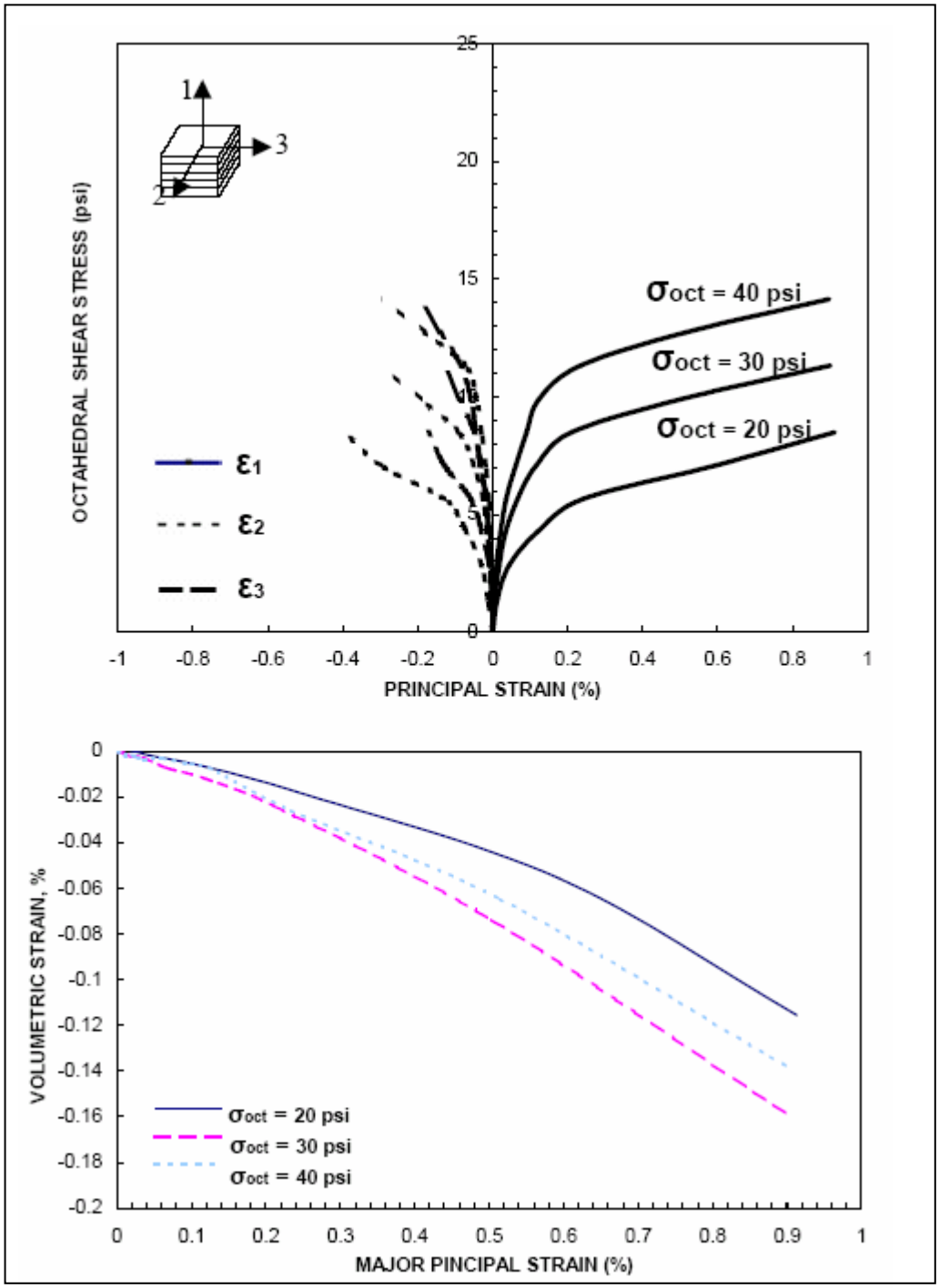

Figure 5.11 TC Test Results of 85% Wet for Optimum Silty Sand (Ψ = 150 psi, w = 6.1%)

The major (σ_1) principal stress was increased during testing; consequently, its corresponding major principal strain was compressive (+). Figures 5.8 to 5.11 show the stress-strain behavior stated above. In figure 5.8, the volumetric strains (σ_{oct} = 20 and 40 psi) are dilative while the volumetric strain (σ_{oct} = 30 psi) is reflecting the loose nature of the pluviated specimen. In figure 5.9, all the volumetric strains (σ_{oct} = 20, 30, and 40 psi) are predominantly dilative. Figure 5.10 shows all the volumetric strains (σ_{oct} = 20, 30, and 40 psi) are generally reflecting the loose nature of the pluviated specimen; however, the volumetric strain (σ_{oct} = 20 psi) slightly dilated between the major principal strains of 0.28% to 0.7%. In figure 5.11, all the principal strains (σ_{oct} = 20, 30, and 40 psi) are predominantly reflecting the loose nature of the pluviated specimen.

5.5.3 Triaxial Extension (TE) Tests

A series of 12 TE tests were successfully conducted in the new cubical set up on 12 specimens of artificially prepared silty sand at different moisture contents referring to the values of suction, Ψ = 5516 kPa (800 psi), 2514 kPa (365 psi), 1632 kPa (237 psi), and 1035 kPa (150 psi). The TE tests were performed under effective confining pressures of 20, 30, and 40 psi. Figures 5.12 to 5.15 present the octahedral shear stress (τ_{oct}) versus principal strain response from the series of twelve tests. In TE tests, the intermediate (σ_2) and major (σ_1) principal stresses were equally increased (i.e., $\Delta\sigma_2 = \Delta\sigma_3$), whereas the minor ($\sigma_3$) principal stress was decreased (i.e., $\Delta\sigma_3 = -2\Delta\sigma_2 = -2\Delta\sigma_1$). Thus, the intermediate (ϵ_2) and major (ϵ_1) principal strains were found to be compressive (+), and the minor (ϵ_3) principal strain was expansive (-).

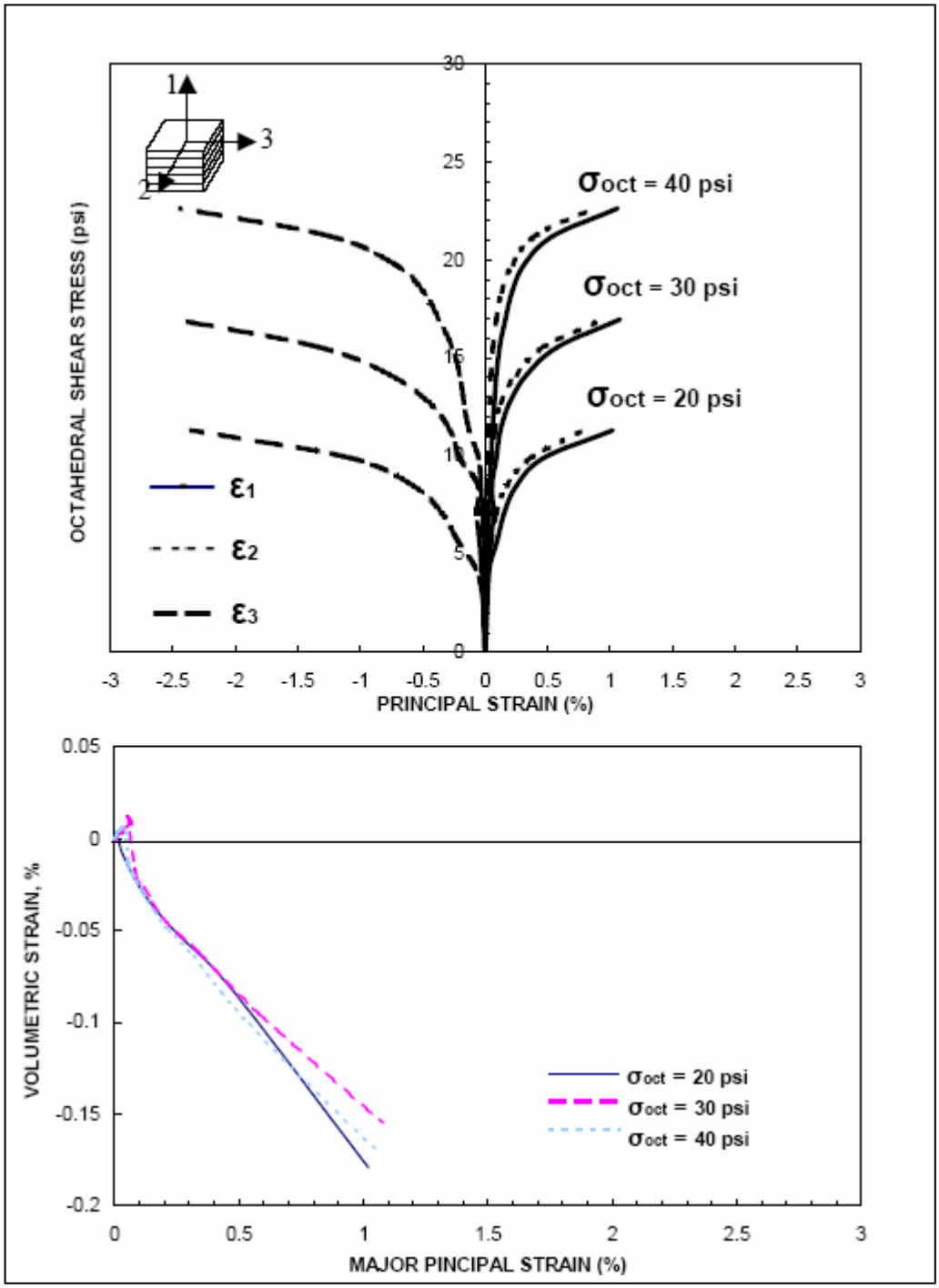

Figure 5.12 TE Test Results for Air-Dried Silty Sand (Ψ = 800 psi, w = 2.0%)

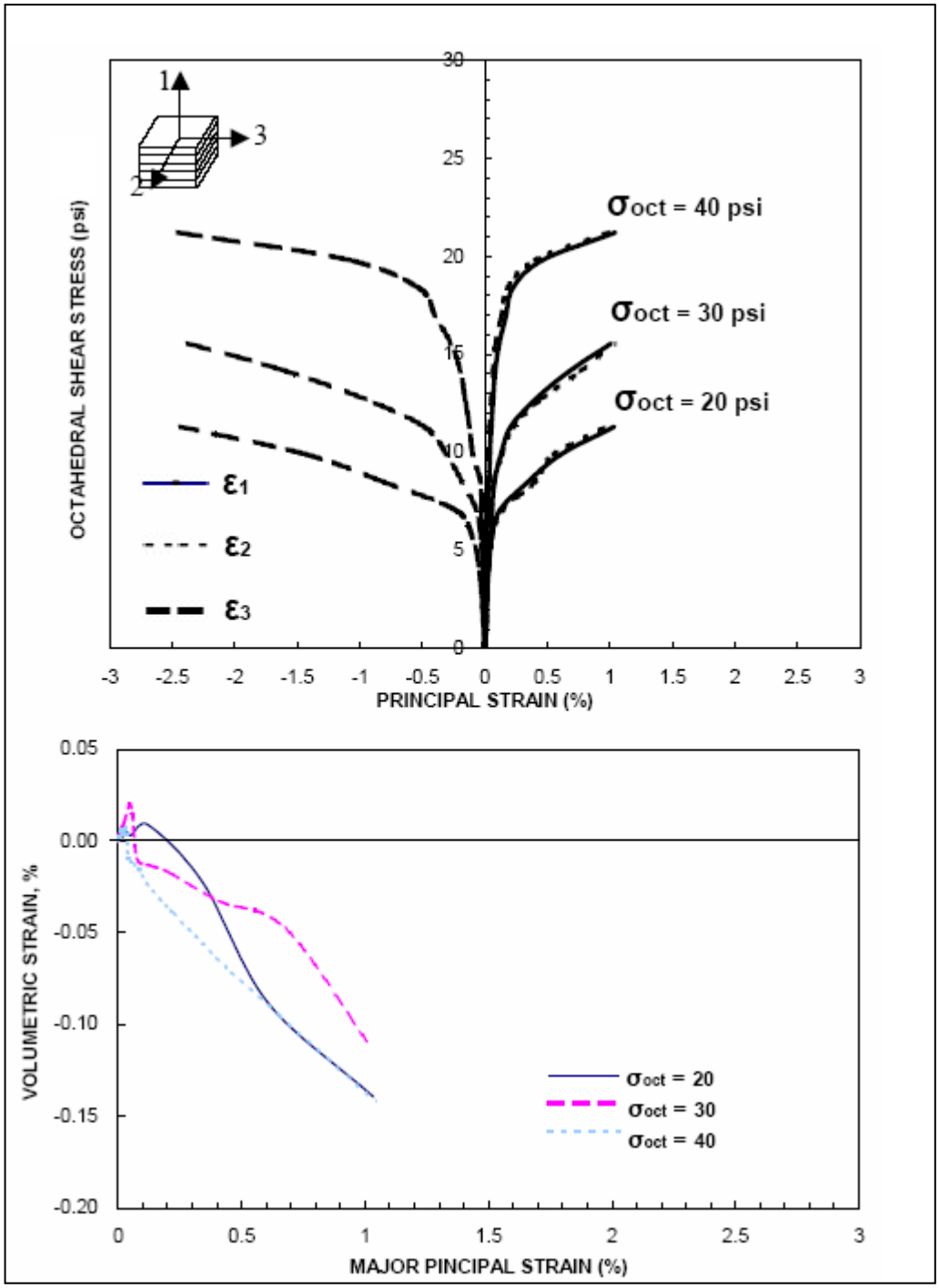

Figure 5.13 TE Test Results for 85% Dry of Optimum Silty Sand (Ψ = 365 psi, w = 4.5%)

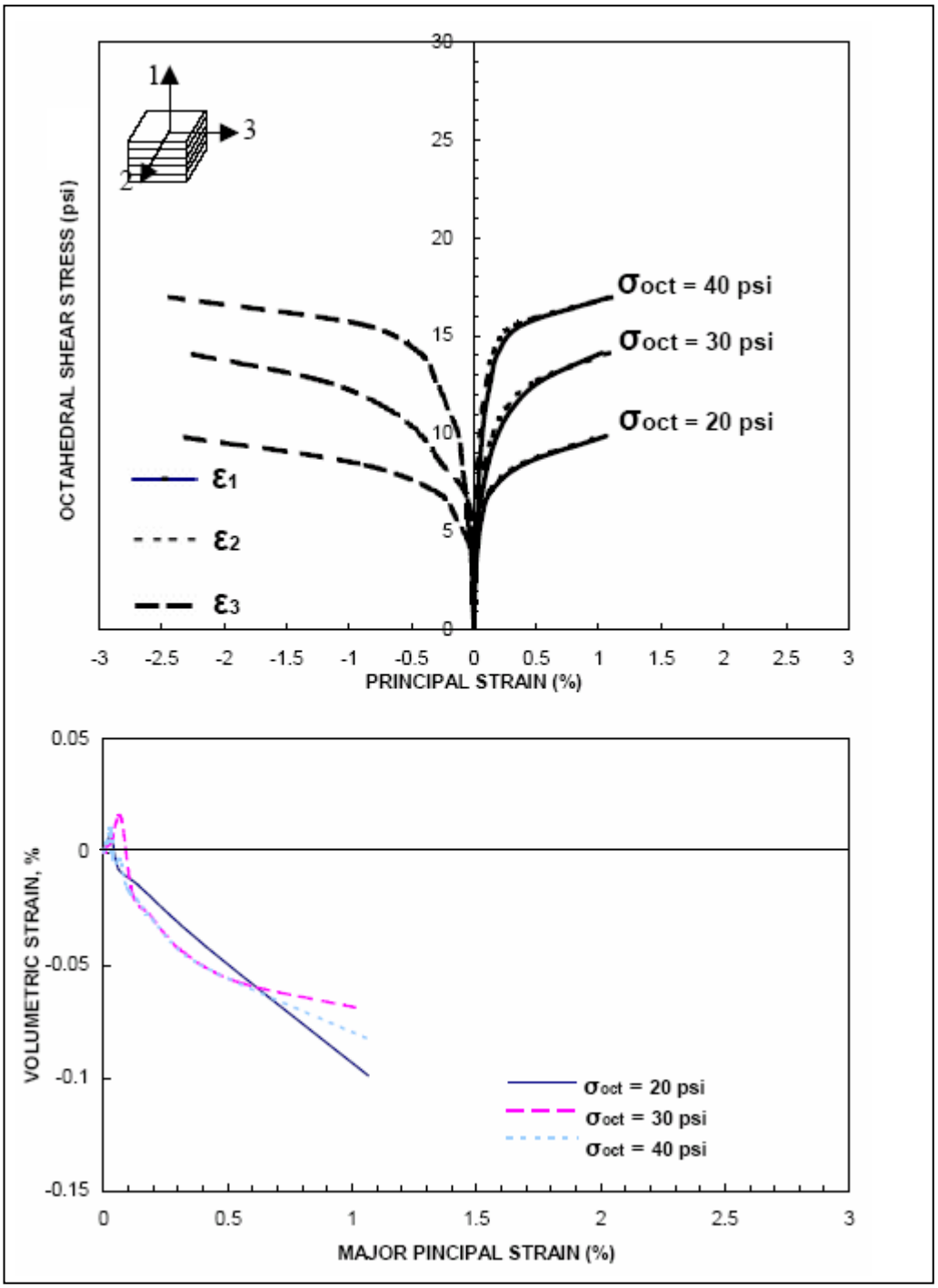

Figure 5.14 TE Test Results for Optimum Silty Sand (Ψ = 237 psi, w = 5.3%)

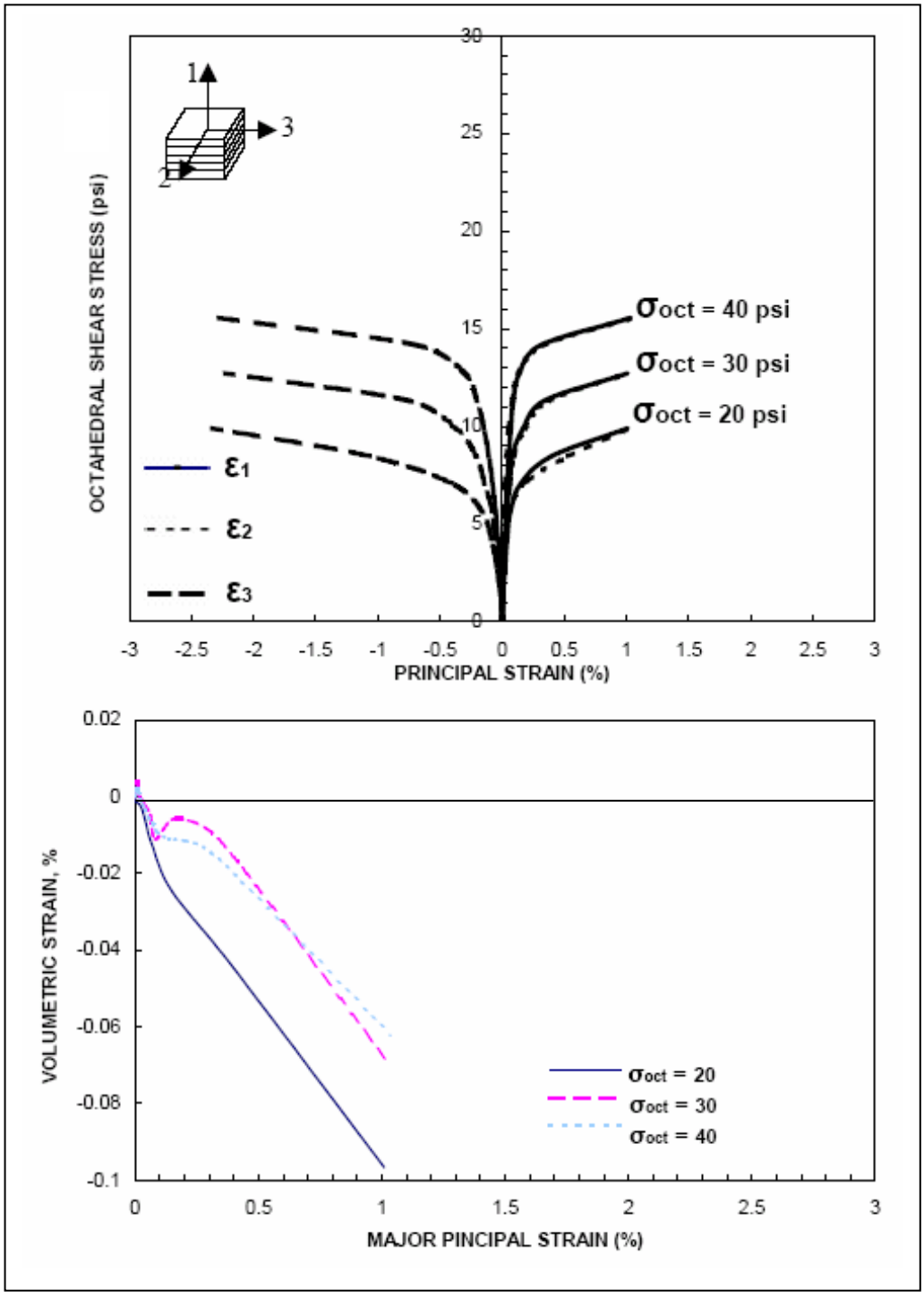

Figure 5.15 TE Test Results for 85% Wet of Optimum Silty Sand (Ψ = 150 psi, w = 6.1%)

In figure 5.12, the volumetric strains (σ_{oct} = 30 and 40 psi) are dilative while the volumetric strain (σ_{oct} = 20 psi) is reflecting the loose nature of pluviated specimen. Figure 5.13 shows all the volumetric strains (σ_{oct} = 20, 30, and 40 psi) are dilative. Figure 5.14 shows all the volumetric strains (σ_{oct} = 20, 30, and 40 psi) are predominantly dilative. In figure 5.15, all the volumetric strains are slightly dilative.

5.5.4 Simple Shear

A series of 12 SS tests were successfully conducted in the new cubical set up on 12 specimens of artificially prepared silty sand at different moisture contents corresponding to the values of suction, Ψ = 5516 kPa (800 psi), 2514 kPa (365 psi), and 1632 kPa (237 psi), 1035 kPa (150 psi). The TE tests were performed with σ_{oct} = 20, 30, and 40 psi, and results obtained are shown in figure 5.16 to 5.19. During SS testing, the major principal stress (σ_1) was increased and at the same time the minor principal stress (σ_3) was decreased in the same magnitude (i.e., $\Delta\sigma_3 = -\Delta\sigma_1$), while the intermediate (σ_2) principal stress was maintained constant (i.e., $\Delta\sigma_2 = 0$). Accordingly, the major (ϵ_1) principal strain was compressive (+), and the minor (ϵ_3) principal strain was expansive (-). As the intermediate (ϵ_2) principal strain was very small, this type of test condition closely corresponds to a plane strain condition.

In general, all the volumetric strains are initially reflecting the loose nature of pluviated specimen from figure 5.16 to 5.19. In figure 5.16, the volumetric strain (σ_{oct} = 40 psi) is dilative around major principal strain of 0.6%. All the volumetric strains in figure 5.17 are slightly dilative around major principal strain of 0.5%. Figure 5.18 also shows dilatancy of volumetric strains (σ_{oct} = 20 and 40 psi) after major strain of 0.5%

while the volumetric strain (σ_{oct} = 30 psi) is reflecting the loose nature of pluviated specimen after major strain of 0.5%. In figure 5.19, the volumetric strains (σ_{oct} = 30 and 40 psi) slightly contract while the volumetric strain (σ_{oct} = 20 psi) is dilative around major strain of 0.6%.

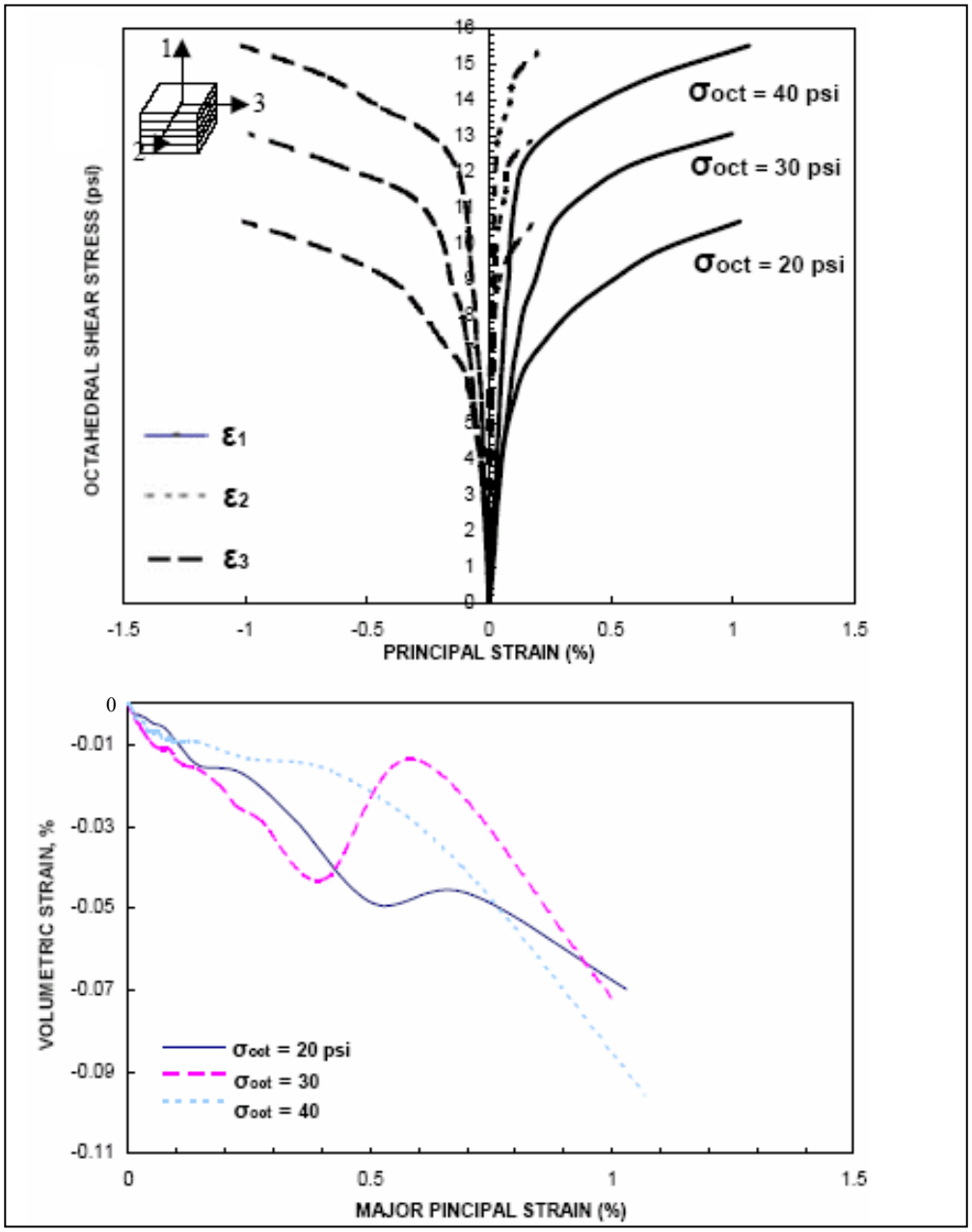

Figure 5.16 SS Test Results for Air-Dried Silty Sand (Ψ = 800 psi, w = 2.0%)

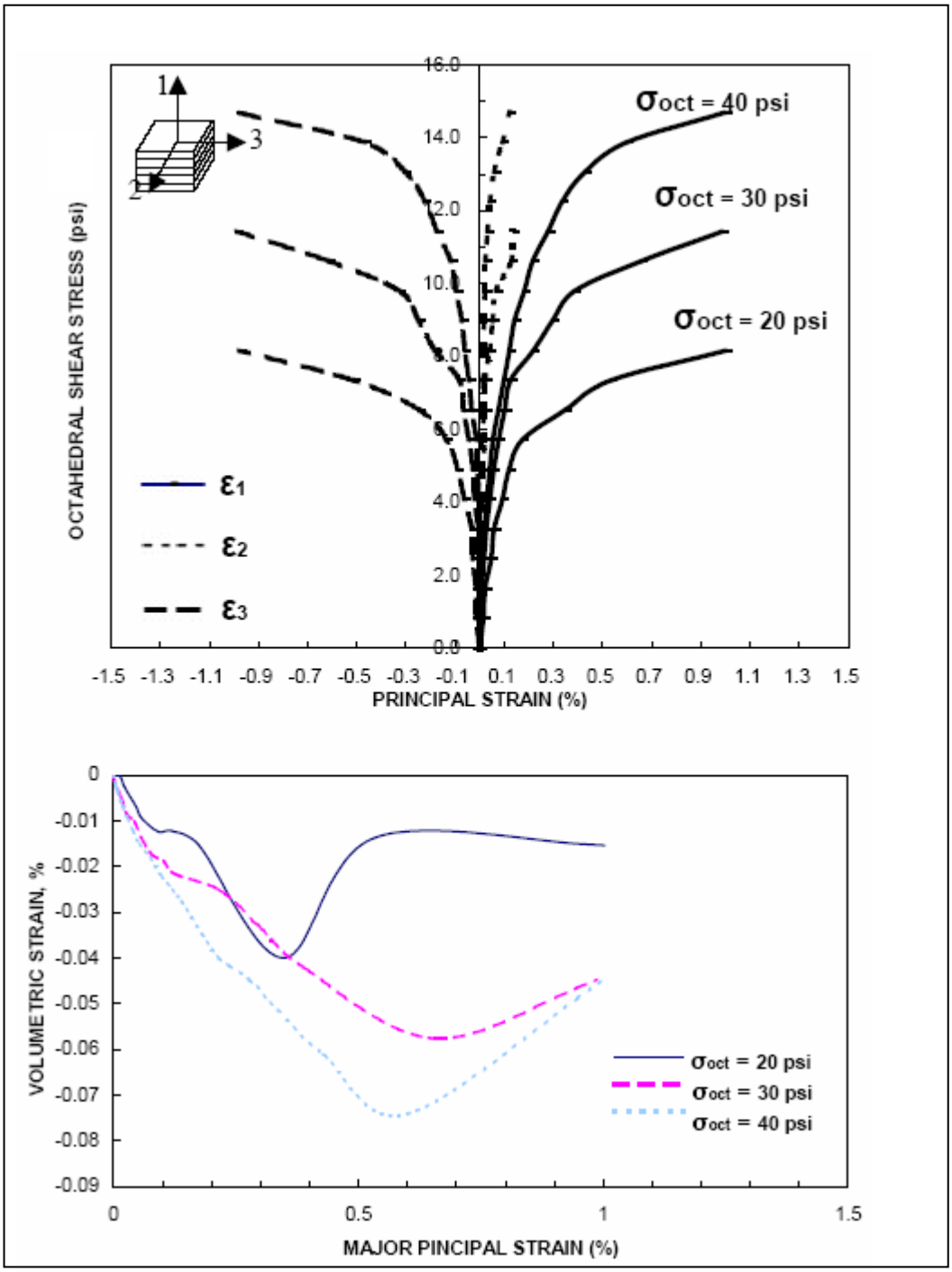

Figure 5.17 SS Test Results for 85% Dry of Optimum Silty Sand (Ψ = 365 psi, w = 4.5%)

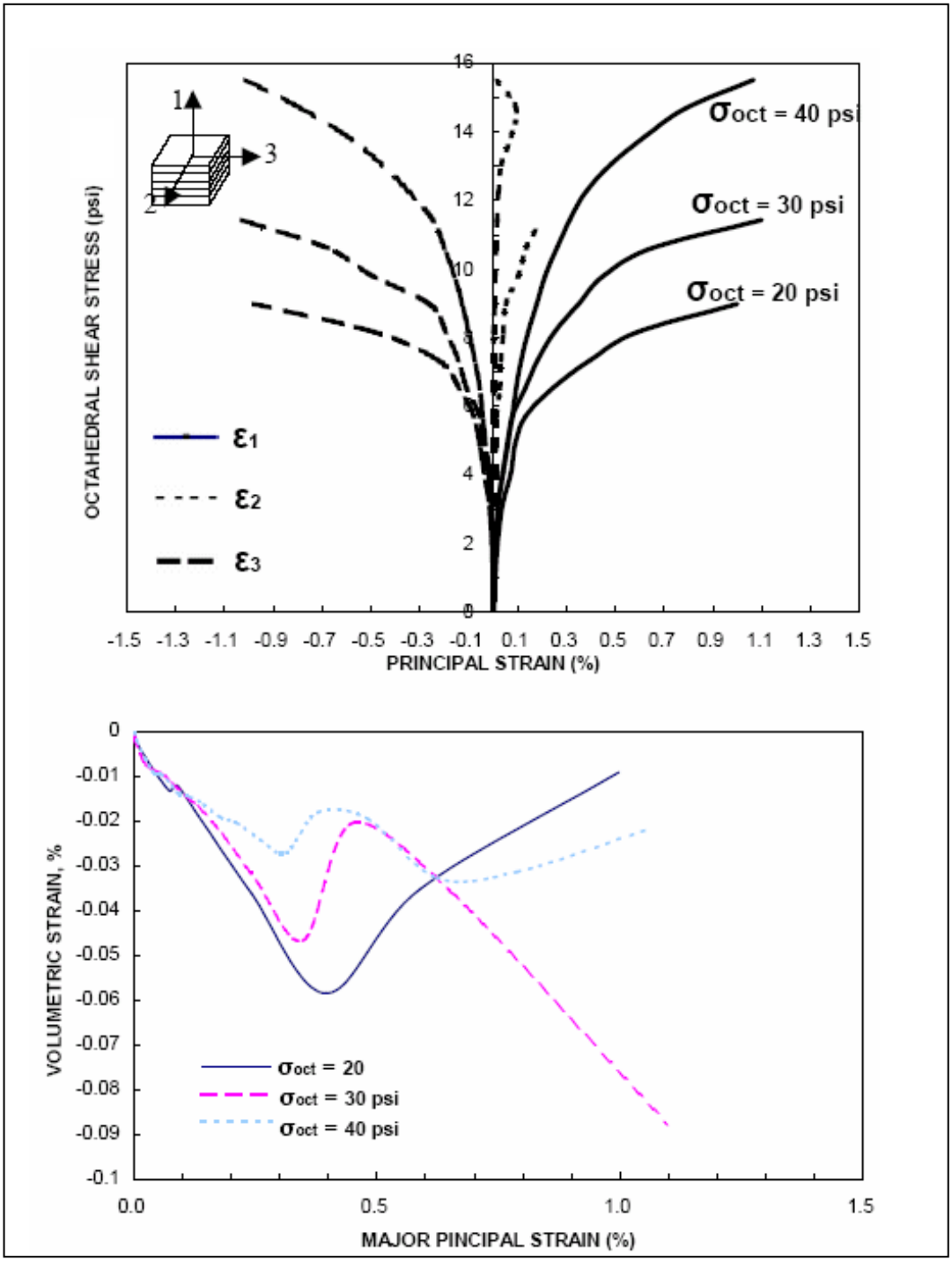

Figure 5.18 SS Test Results for Optimum Silty Sand (Ψ = 237 psi, w = 5.3%)

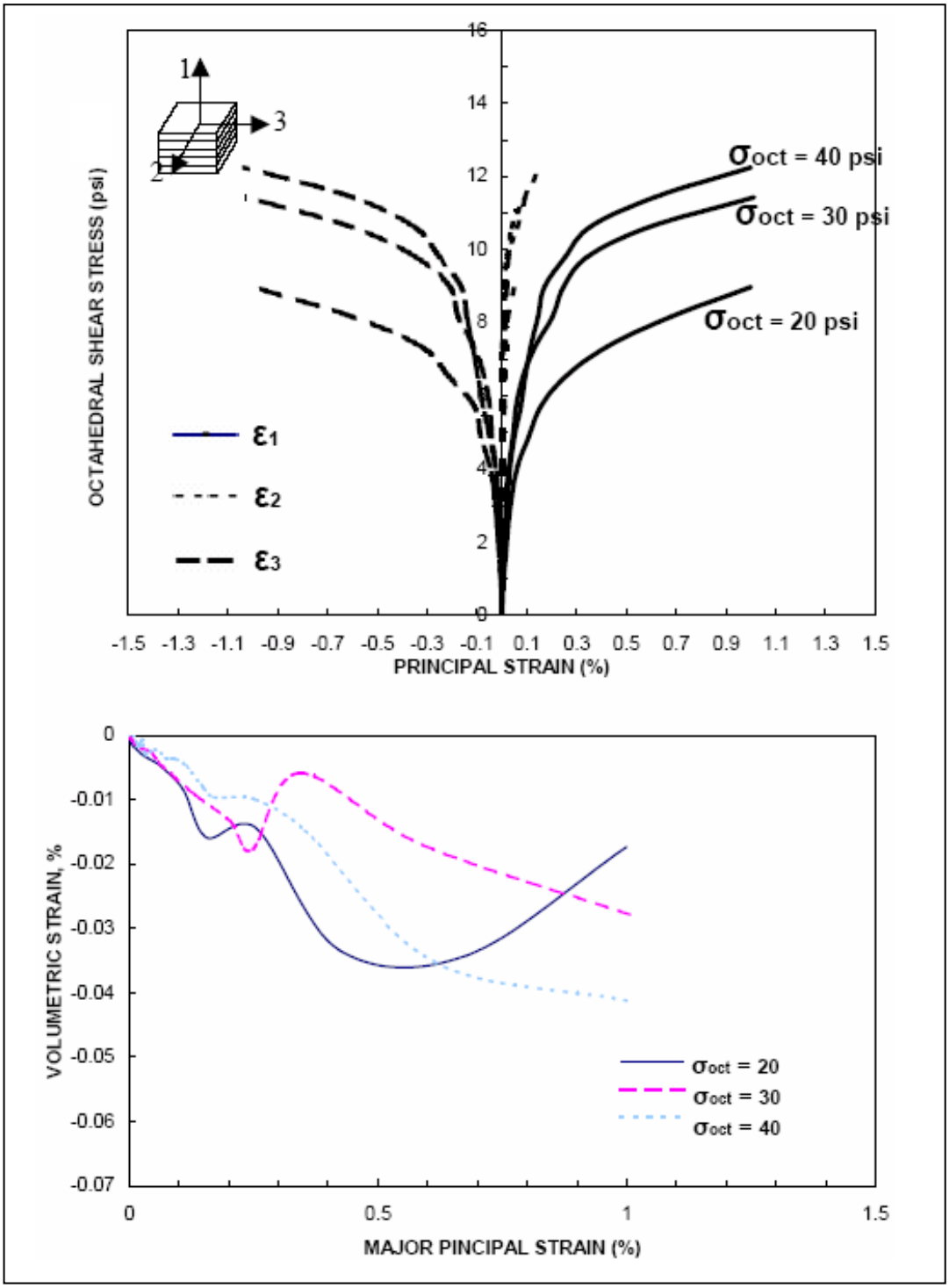

Figure 5.19 SS Test Results for 85% Wet of Optimum Silty Sand (Ψ = 150 psi, w = 6.1%)

5.6 Influence of Initial Total Suction

The influence of initial suction can be confirmed through figures 5.20 to 5.27. As the magnitude of suction increased, in general, the peak values were increased. This is an evidence of the contribution of suction to increase in soil strength. However, the suction induced in the present thesis work was not kept constant throughout the tests. At a certain stress or time, therefore, suction may dissipate as menisci are broken. Accurate assessment of influence of suction on soil behavior is hence difficult. In order to accurately predict soil response, suction-controlled true triaxial testing is required.

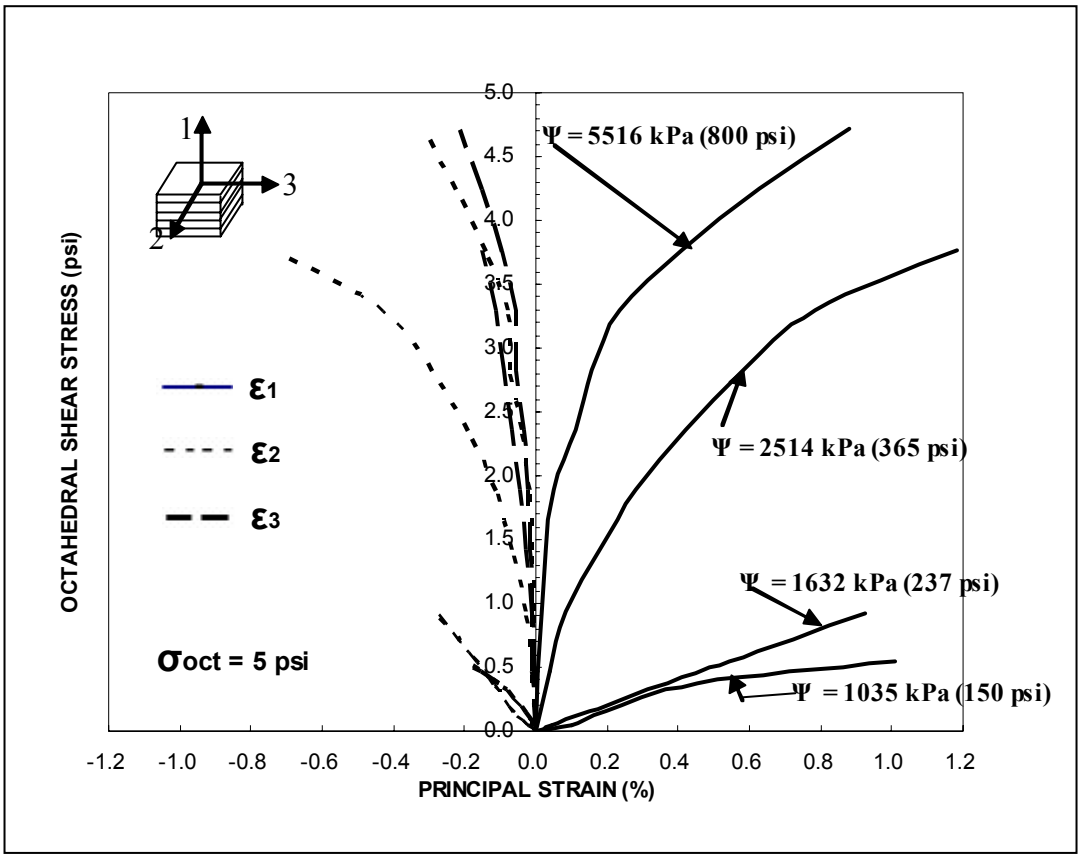

Figure 5.20 CTC Test Results with Different Suction (σ_{oct} = 5 psi)

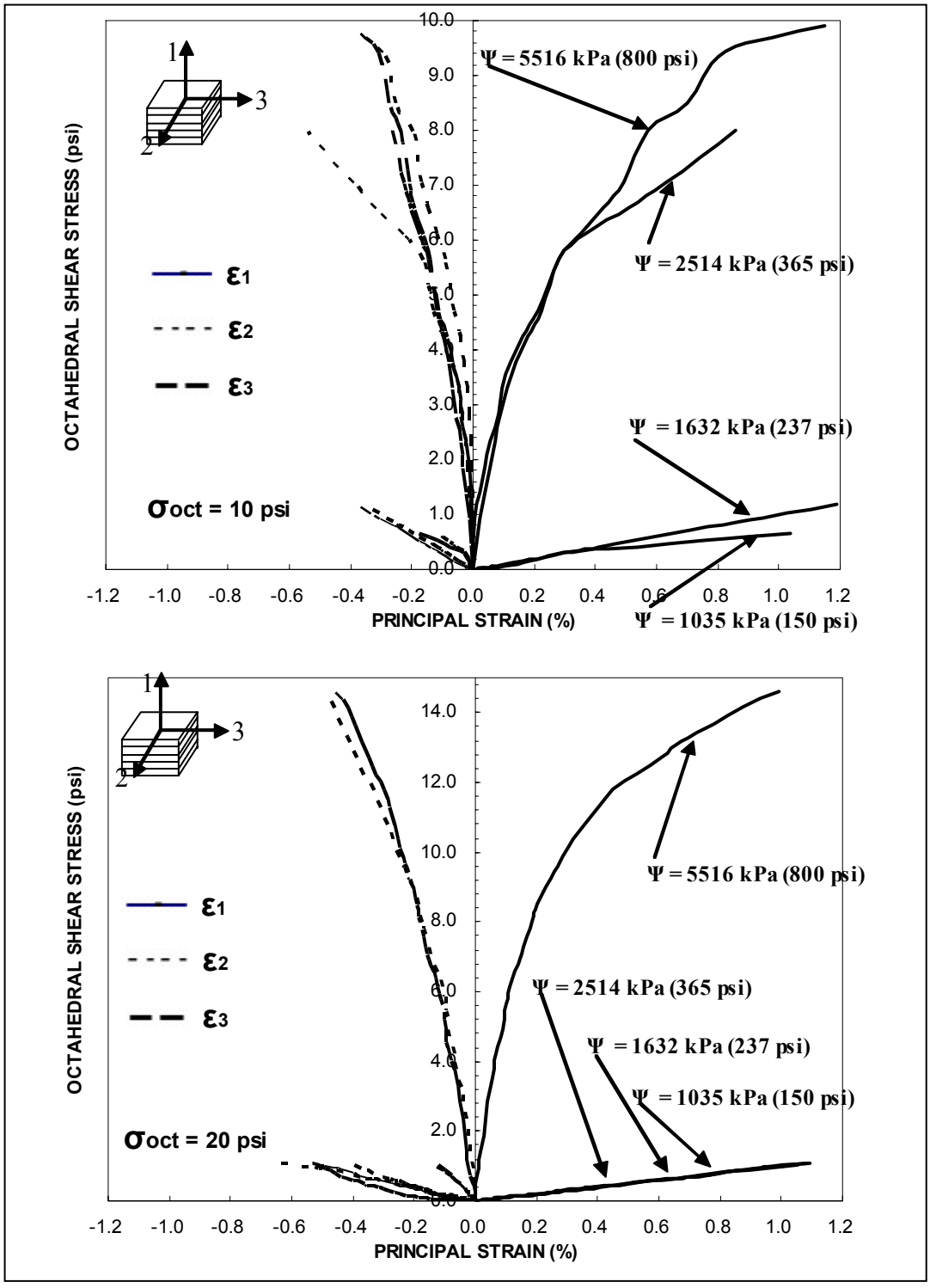

Figure 5.21 CTC Test Results with Different Suction (σ_{oct} = 10 psi, 20 psi)

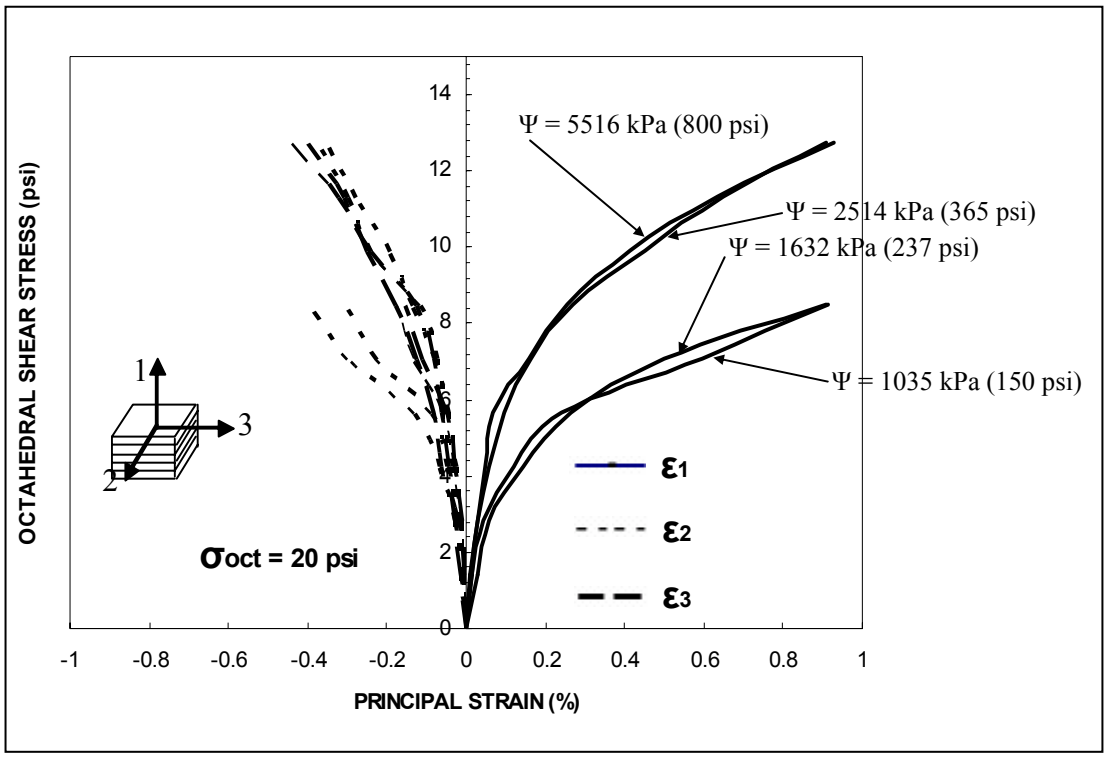

Figure 5.22 TC Test Results with Different Suction (σ_{oct} = 20 psi)

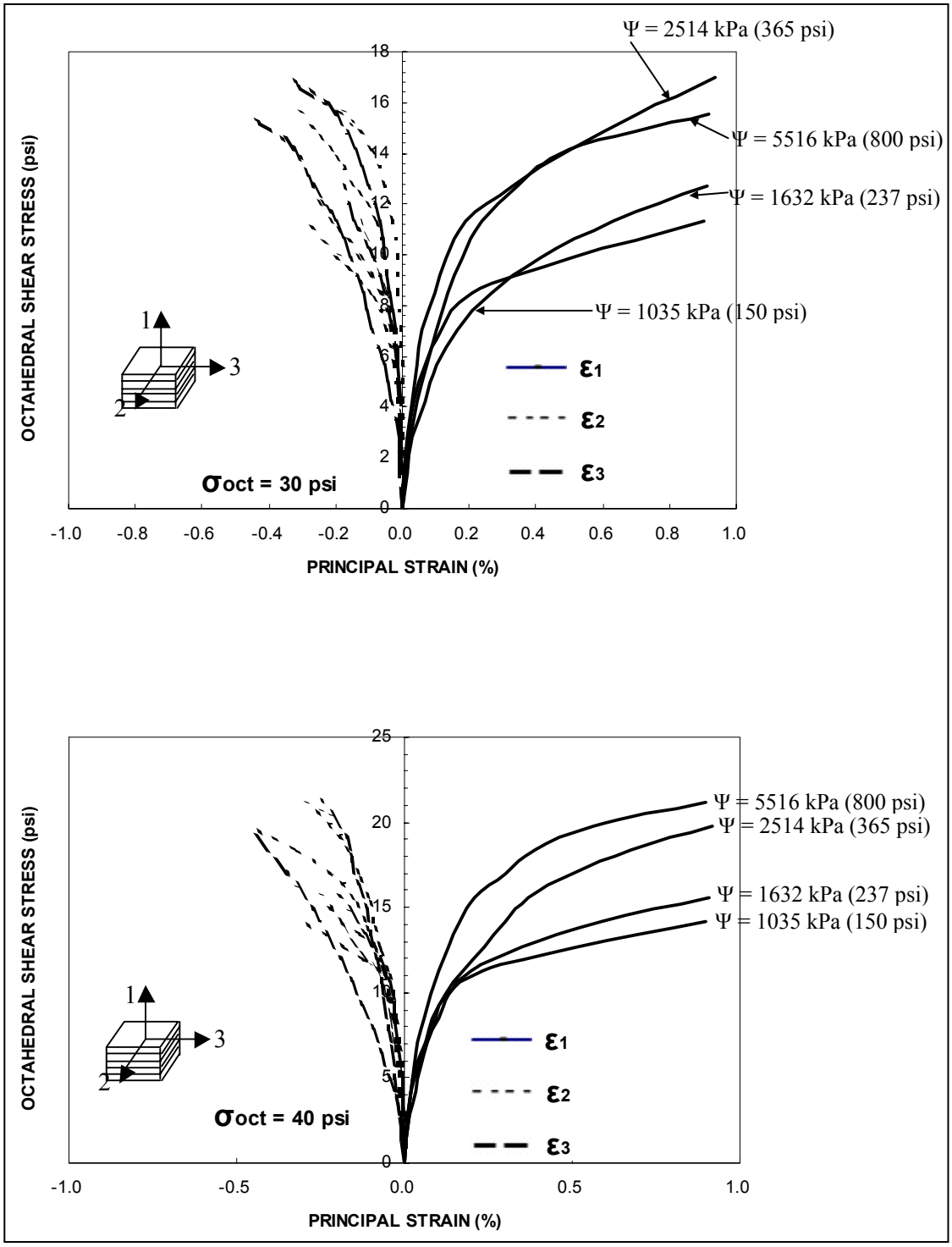

Figure 5.23 TC Test Results with Different Suction (σ_{oct} = 30 psi, 40 psi)

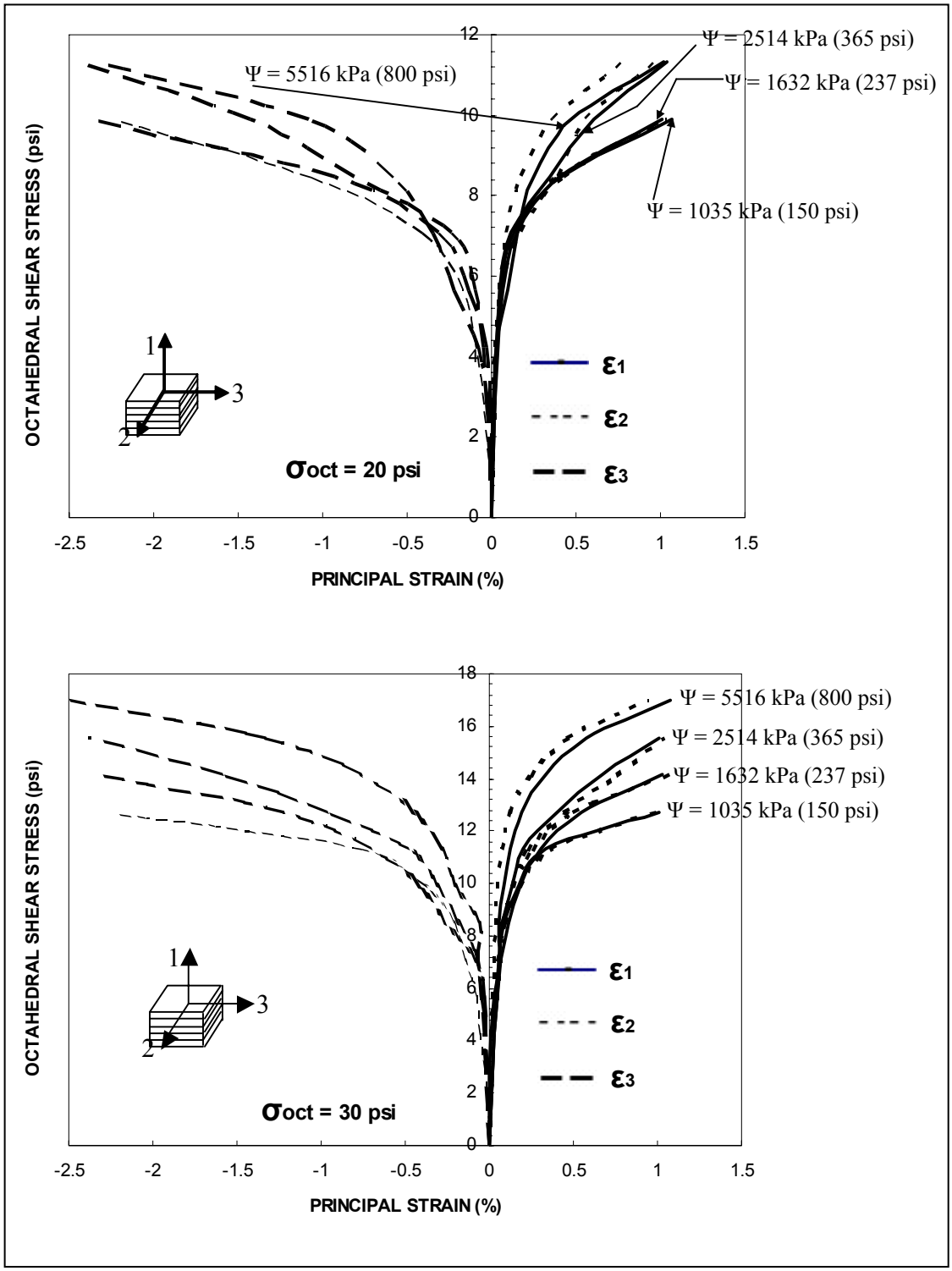

Figure 5.24 TE Test Results with Different Suction (σ_{oct} = 20 psi, 30 psi)

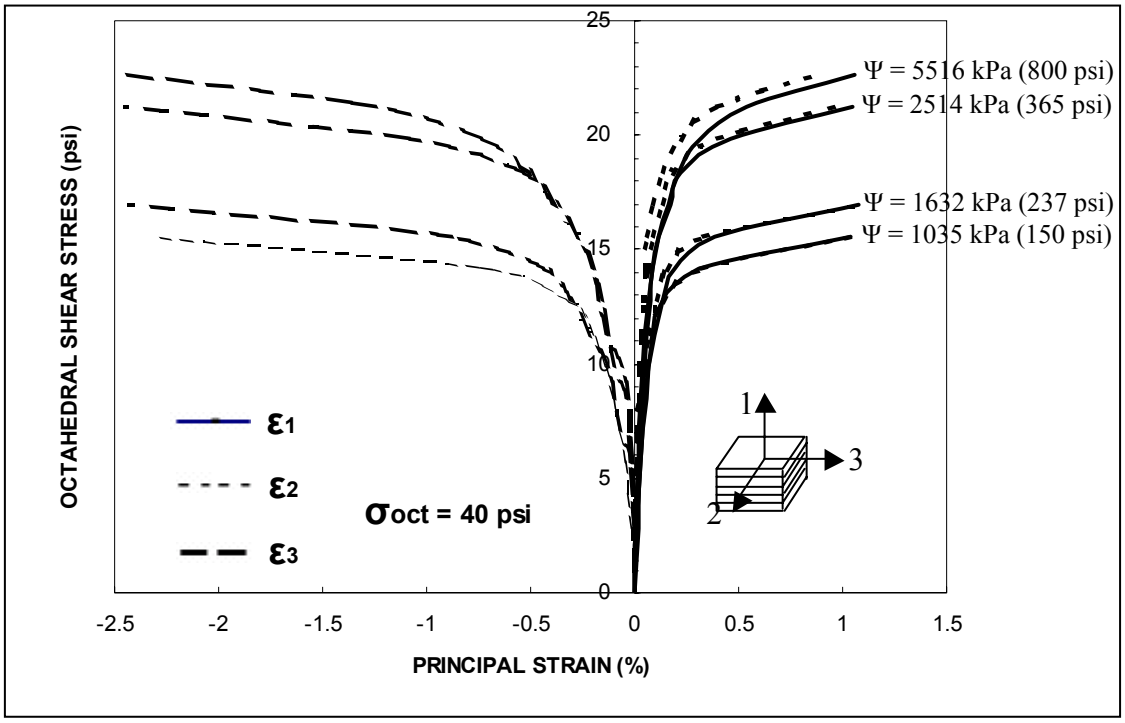

Figure 5.25 TE Test Results with Different Suction (σ_{oct} = 40 psi)

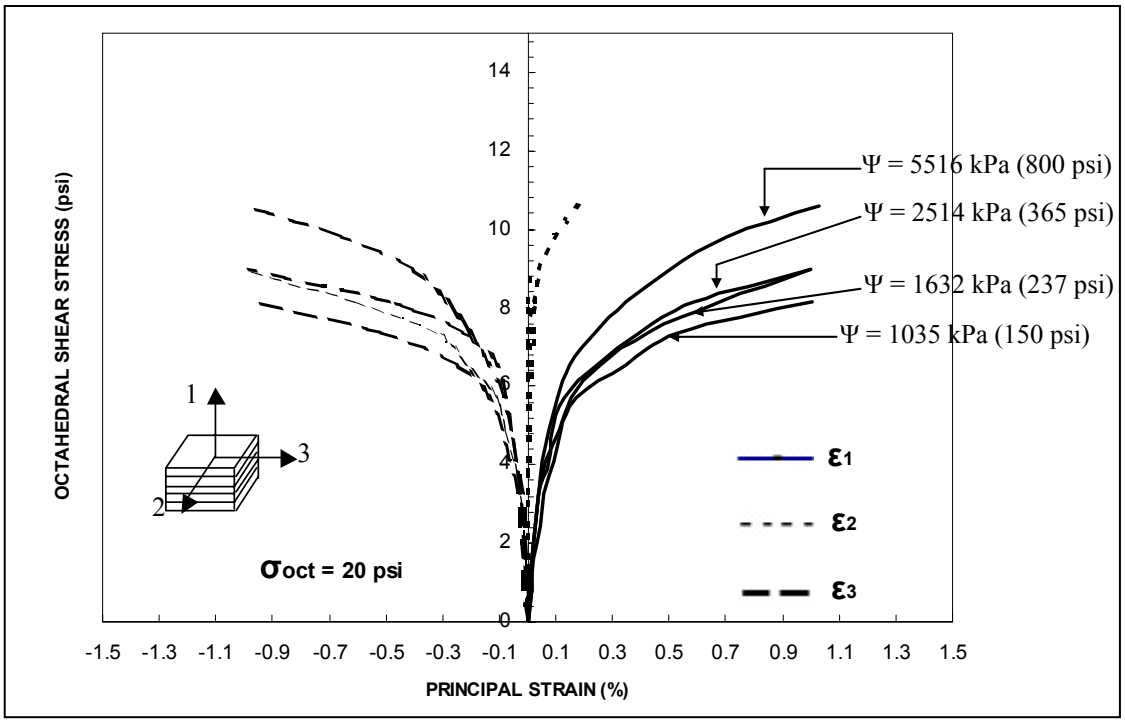

Figure 5.26 SS Test Results with Different Suction (σ_{oct} = 20 psi)

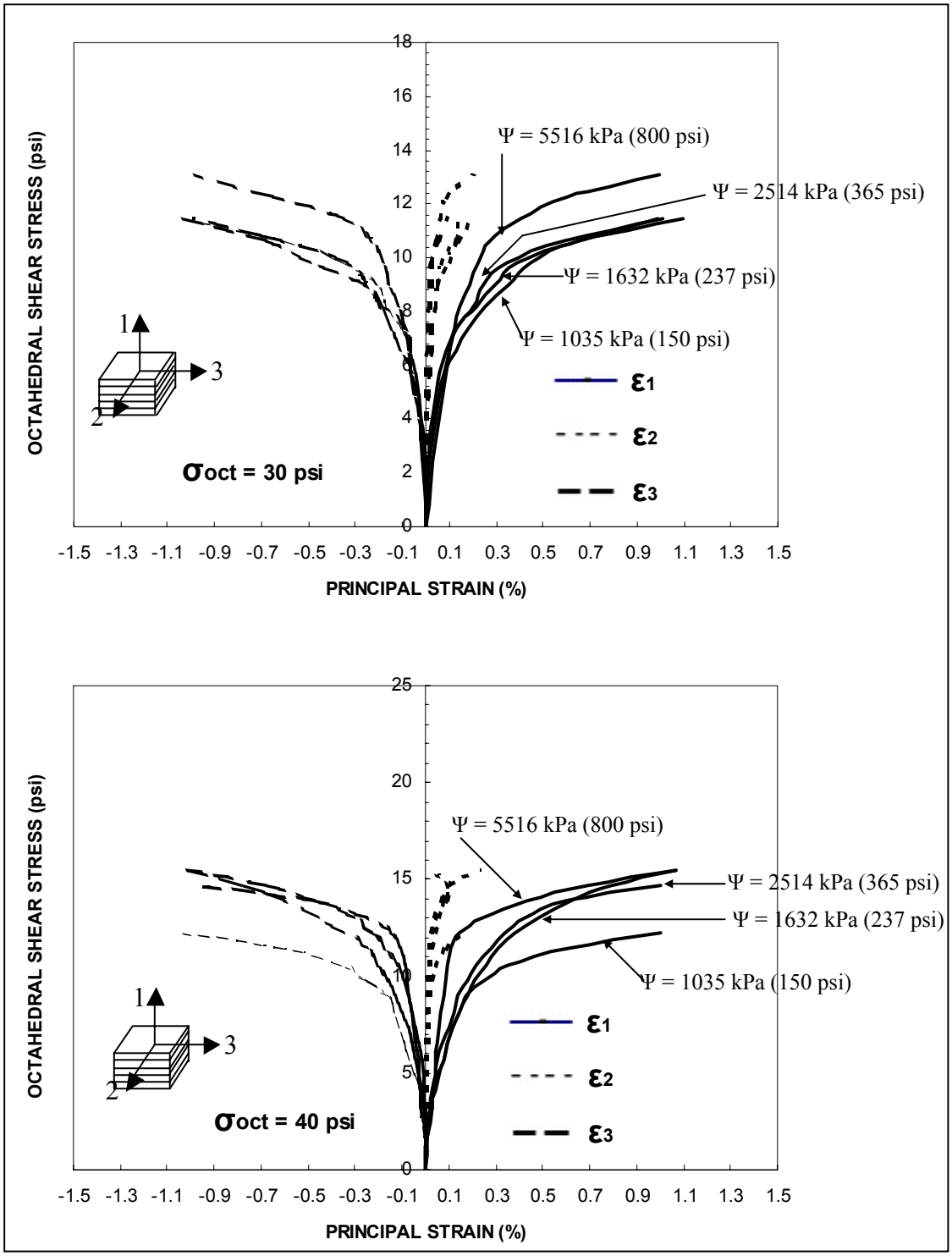

Figure 5.27 SS Test Results with Different Suction (σ_{oct} = 30 psi, 40 psi)

5.7 Incipient Failure Envelopes on Octahedral Plane

Figure 5.28 shows the projection of incipient failure envelopes from all true triaxial tests onto the octahedral plane (π-plane) on the basis of initial total suction (s) and octahedral stress (σ_{oct}) level.

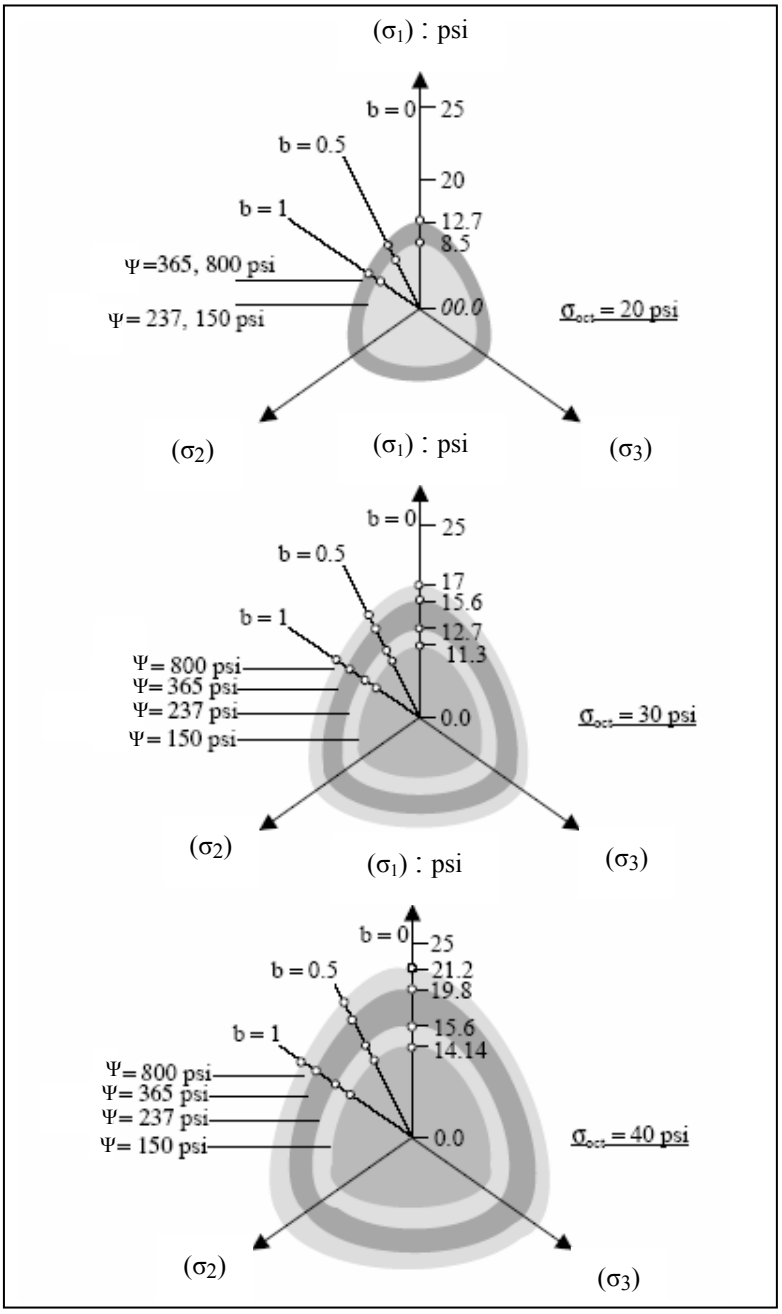

Figure 5.28 Projection of Incipient Failure Envelopes onto the Octahedral Stress Plane

Overall, figure 5.28 shows a significant influence of total suction on the size, position, and shape of the incipient failure envelopes, in accordance with results reported by Hoyos (1998). However, incipient failure envelopes based on σ_{oct} = 20 psi does not show significant influence of total suction on the size, position, and shape of the incipient failure envelopes as shown in figure 5.28.

CHAPTER 6

SUMMARY, CONCLUSIONS, AND RECOMMENDATIONS

6.1 Summary and Conclusions

A stress-controlled, flexible boundary, true triaxial (cubical) testing apparatus has been developed to test 3-inch cubical specimen of partially saturated soil under different moisture contents and for a wide range of multiaxial stress paths. A series of HC, CTC, TC, TE, and SS tests were conducted in order to perform a thorough performance and check-out verification testing of the newly developed device by investigating the multiaxial stress-strain response of partially saturated silty sand specimens artificially prepared in the laboratory. Imposed stress paths included an initial hydrostatic compression followed by conventional triaxial compression or any other path along different directions on the octahedral plane (π-plane). The development of the apparatus, including main device components, specimen preparation process, test procedure, and the corresponding validation of its suitability for testing partially saturated sandy soils are described.

In this work, specimens were prepared using a dual-mesh pluviation technique at four different moisture contents: w = 2.0, 4.5, 5.3, and 6.1%. The aim was to reproduce loose specimens at very low densities and with moisture contents lower than the residual gravimetric moisture content devised from the soil-water characteristic curve (SWCC). The SWCC was obtained via filter paper technique in order to assess

initial total suction in specimen prior to testing in the cubical cell. All tests were performed at a loading rate of 1 psi/hr, and results are presented in terms of octahedral stress – principal strain response of partially saturated silty sand. In all cases, initial soil suction was found to exert a paramount influence on the stress-strain-strength behavior of partially saturated silty sand.

The following main conclusions can be drawn from experimental findings of this thesis work:

1. The new true triaxial testing apparatus was successfully used to study multiaxial stress-strain behavior of partially saturated sand at high values of initial, pluviation-induced total suction (Ψ) according to SWCC data.

2. Initial total suction (Ψ) was found to exert a significant influence on stress-strain-strength behavior of artificially prepared silty sand along a wide range of stress paths.

3. In general, silty sand contracted in the direction of major principal stress, expanded in the direction of minor principal stress, and changed from expansive to compressive behavior during TC, TE, and SS tests.

4. The shape and size of incipient failure envelopes of silty sand on octahedral plane (π-plane) is similar to that reported on silty sand via suction-controlled testing by (Hoyos, 1998).

5. Bulk modulus, K, was obtained from HC (hydrostatic compression) tests and found as function of total suction (Ψ). As value of total suction increases, value of bulk

modulus increases. The increase in bulk modulus to total suction presents stiffer volumetric strain.

6.2 Future Research Recommendation

The present work was aimed at increasing the existing knowledge and understanding of stress-strain-strength behavior of partially saturated soils under true triaxial stress states. Key recommendations for future research are listed in the followings:

1. Suction-controlled testing on unsaturated soils via axis-translation technique.
2. Three-dimensional, multi-axial response of expansive soils.
3. Multi-axial testing on chemically/mechanically stabilized soils.

REFERENCES

Airey, D. W., & Wood, D. M. (1988). The Cambridge True Triaxail Apparatus. Advanced Triaixal Testing of Soil and Rock, STP 977, ASTM, Philadelpia, 796-805.

Arthur, J. R. F. (1988). Cubical Devices: Versatility and Constrains. Advanced Triaxial Testing of Soil and Rock, STP 977, ASTM, Philadelphia, 743-765.

Atkinson, R. H. (1972). A Cubical Test Cell for Mulaxial Testing of Materials. Ph.D. dissertation, University of Colorado at Boulder, Boulder, CO.

Callisto, L., and Calabresi, G. (1998). Mechanical Behaviour of a Natural Soft Clay. Gèotechnique 48 (4), 495-513.

Cresswell, A., Barton, M.E., & Brown, R. (1999). Determining the Maximum Density of Sands by Pluviation. Geotechnical Testing Journal, 22 (4), 324-328.

Fredlund, D. G., Morgenstern, N. R., & Widger, R. A. (1978). Shear Strength of Unsaturated Soils. Canadian Geotechnical Journal, 159 (3), 313-321.

Fredlund, D. G., & Rahardjo, H. (1993). Soil Mechanics for Unsaturated Soils. Wiley, New York.

Green, G. E. (1971). Strength and Deformation of Sand Measured in an Independent Stress Control Cell. Stress-Strain Behavior of Soils, Proceedings of the Roscoe Memorial Symposium, G. T. Foulis & Co. Ltd., Cambridge, England, 285-323.

Hambley, E. C. (1969). A New Triaxial Apparatus. Geotechnique, 19 (2), 307-309.

Ibsen, L, B., &Praastrup, U. (2002). The Danish Rigid Boundary True Triaxial Apparatus for Soil Testing. Geotechnical Testing Journal, 25 (3), 254-265.

Kamath, S., Puri, V. M., & Manbeck, H. B. (1994). Constitutive Model Development for Cohesive Powders Using Cubical Triaxial Cell. ASAE Paper No. 94-4027. June.

Kjellman, W. (1936). Report on an Apparatus for Consummate Investigation of the Mechanical Properties of Soils. Proc., 1st Int. Conf. on Soil Mechanics and Foundation Engineering, 2, 16-20.

Kamath, S., Puri, V. M., & Manbeck, H. B. (1994). Evaluation of Constitutive Model Parameters for Powder Flow Using Cubical Triaxial Tester. ASAE Paper No. 94-4508. December.

Ko, H. Y., & Scott, R. F. (1967). A New Soil Testing Apparatus. Geotechniuque, 17 (1), 40-57.

Lade, P. V., & Ducan, J. M. (1973). Cubical Triaxial Tests on Cohesionless Soil. Journal of the Soil Mechanic Foundation Division, ASCE, 99 (10), 793-812.

Li, F., & Puri, V. M. (1996). Measurements of Anisotropic Behavior of Dry Cohesive and Cohesionless Powders Using a Cubical Triaxial Tester. Powder Technology 89, 197-207.

Lu, N., and Likos W. J. (2004). Unsaturated Soil Mechanics.John Wiley & Sons, New York.

Matsuoka, H., Sun, D., Kogane, A., Fukuzawa, N., & Ichihara, W. (2002). Canadian Geotechnical Journal, 39, 608-619.

Sture, S., & Desai, C. S. (1979). Fluid Cushion Truly Traixial or Multiaxial Testing Device. Geotechnical Testing Journal, 2(1), 20-33.

Sture, S. (1979). Development of Multiaixial Cubical Test Device with Pore Water Pressure Monitoring Facilities. Report No. VPI-E-79.18, Deparment of Civil Engineering, Virginia Polytechnic Institute and State University, Blacksburg, VA.

Yamada, Y., & Ishihara, K. (1982). Yielding of Loose Sand in Three-Dimensional Stress Conditions. Japanese Society of Soil Mechanics and Foundation Engineering, 22 (3), 16-31.

BIOGRAPHICAL INFORMATION

Jae Hyun Park was born on January 26, 1976, at the City of Seoul, Korea. He received his bachelor's degree in Civil Engineering from Han Yang University, Korea, in Febuary 2002. During undergraduate school, he had the opportunity to be trained as a civil engineer at the Woo-Myun Mountain Tunnel project in Korea for 2 months. After graduation with B.S. degree, he decided to pursue graduate studies majoring in geotechnical engineering at The University of Texas at Arlington in 2004. During his studies, he had the opportunity to work as a graduate research assistant under supervision of Dr. Laureano R. Hoyos in the area of unsaturated soil mechanics. He received his Master of Science degree in Civil Engineering from The University of Texas at Arlington in August 2005.